The lithospheric structure at Japanese Islands: Integrated petrological and geophysical modeling

タメル, マハムウド, ラガブ, ファラグ

The lithospheric structure at Japanese Islands:
Integrated petrological and geophysical modeling

Tamer Mahmoud Ragab Farag

2022

The lithospheric structure at Japanese Islands: Integrated petrological and geophysical modeling

by

Tamer Mahmoud Ragab Farag

A Dissertation Submitted in Partial Fulfillment
of the Requirements for the degree of
Doctor of Engineering
(Earth Resources Engineering)

Academic Advisor:

Assoc. Prof. Hideki Mizunaga

KYUSHU UNIVERSITY

Laboratory of Exploration Geophysics

Department of Earth Resources Engineering

Graduate School of Engineering
Kyushu University

Japan

July 2022

Abstract

The scope of this work was to model the crustal thickness and the geometry of the Mohorovičić (Moho) discontinuity, the Lithosphere, and the upper mantle boundary at the Japanese archipelago from the sight of geophysics and petrology. For this purpose, I used the available receiver function results, seismic tomography models, global crustal thickness, and geological and tectonic information as constraints. The offshore areas are not well studied despite the seismometers spread around the Japanese Islands and several localized, small-scale seismic studies. The satellite data has a wide coverage, allowing us to explore rough terrain and the vast regions. It also enables the study of long-wavelength geological structures.

I used the latest satellite gravity model of Gravity Field and Steady-State Ocean Circulation Explorer (GOCE) GOCO06s with a spatial resolution of 80 km, which covers the study area. The study had three steps: the data corrections followed by the inversion and the modeling and comparing the estimated results with previous models and analyses. I used the previous seismic results in various positions to constrain my inversion algorithm results. I used the 3-D non-linear gravity inversion constrained by previous seismic data and geological information to model the 3-D crustal density variation, the crustal thickness, surface geometry of the Moho, and geometry of the stagnant slab in the Kuril Trench, Japan Trench, Nankai Trough, and Izu-Bonin Trough. This study used available receiver function results, seismic tomography models, global crustal thickness, and geological and tectonic information as constraints. Integration interpretation of various geophysical and geological data would constrain and minimize the interpretation uncertainty. The inversion algorithm used 34 km as a Moho reference depth and 600 kg/m^3 as a density contrast.

The resulting crustal thickness model and the depth to the Moho layer beneath the Japanese Islands and the area around were compared with the global thickness models and the Moho depths from global and localized seismic studies. The resulted model shows that crustal thickness ranges from 14 to 43 km, and the depth of Moho has a -0.78 mean misfit with previous Moho depths from seismic. The misfitting between the observed and calculated gravity data is 0.16 mGal. The normalized analytical signal helped delineate the different plates and their edges sharply. Three cross-sections were conducted to model the stagnant slab along the subduction zone of the Eastern Eurasian plate, western Pacific plate, Okhotsk Plate, and Philippine Sea plate. The eastern area of the entire region (Pacific plate) had a lower crust

thickness and high density than the western area (Eurasian plate), which had a high crust thickness and low density. The Moho depths model from gravity inversion can be used in the integrated geophysical and petrological inversion.

Mantle xenoliths of volcanic rocks appear for the compositional and thermal structure of the Lithospheric Mantle. Chemical and Petrological analysis shows the differences between the Northeast and Southwest of Japan. The published xenolith analysis results represent only localized areas, which may not constrain the composition and evolution of the Japanese Islands. Mantle petrology affects the density distribution and the geometry of the Lithosphere-Asthenosphere Boundary (LAB). I used the published petrology analysis of xenolith samples and tectono-thermal age of different domains to constrain my inversion algorithm. In this study, I applied the integrated inversion of geophysical observations and fields (elevation, crustal thickness, geoid height, gravity, and gravity gradients) with the Petrological analysis of Mantle xenoliths. The methodology depends on the chemical composition through self-consistent thermodynamic calculations to compute the seismic velocities and density at 400 km depth. To minimize the misfit between the calculated and observed data, the geometry of the crust and the lithosphere and mantle composition was modified within the uncertainty range. The output model is the variations in temperature, density, composition and the crustal and lithospheric thickness of the Lithosphere beneath the Japanese Islands.

Key Words: Moho, lithosphere- asthenosphere boundary, stagnantslabs, GOCE, Subduction zones, the Japanese Islands.

ACKNOWLEDGMENTS

Contents

List of Figures

List of Tables

Chapter 1

Introduction

Since the Pangea, The Japanese Islands have mainly taken place due to the subduction of the Eastern Eurasian plate, western Pacific Ocean plate, Okhotsk Plate, and the Philippine Sea plate. In the Quaternary, the Amur plate motion eastward has been triggered, which caused the strong east-west compression neotectonics regime (Taira, 2001). According to the Geological Survey of Japan, (1992), subduction zones and active faults are the main cause of seismicity in the Japanese Islands. Trenches regions are predominantly zones of major earthquakes with negative gravity and topography anomalies (Song, 2003).

This thesis uses interdisciplinary three-dimensional modeling the density, temperature, and seismic velocity using the integration between geophysical and field observations (gravity gradients, geoid, seismic tomography) and petrology (mantle xenoliths chemical analysis). Interpretation of high-resolution gravity field became highly important in the geophysical and geodynamic models of the Earth. Due to the poor coverage of terrestrial data, the need for gravity data from satellite gravity gradiometry enabled us to model the gravity potential at a regional scale. Another advantage is that fields are sensitive to long-wavelength structures.

The new model of Gravity Field and Steady-State Ocean Circulation Explorer (GOCE) GOCO06s was inverted to build an initial crustal thickness map. The three-dimensional detailed density model is constrained by the available seismic data results (receiver function, seismic tomography) and the geologic information. The high-resolution Moho depth map of the Northwest Pacific Ocean is critical for understanding subsurface geometrical structures and the evolution of study area geodynamics. As a result, it can be used to predict and study geohazards' migration, such as earthquakes. Furthermore, the crust thickness model can improve the ability to target and extract mineral resources and comprehend regional dynamics. A high-resolution model of deep surface structures would help with heat flow modeling, hydrocarbon accumulation, and rock maturity prediction (Allen and Allen, 2005; Hantschel and Kauerauf, 2009; Bouman et al., 2015).

It is critical in the potential geophysical method to constrain the interpretations to reduce ambiguity. Consequently, various data sets and global models were compiled in this study to constrain the interpretations of forward modeling and data inversion. The temperature and chemical composition of the lithosphere are important parameters in modern lithospheric modeling because the physical properties of the Earth (e.g., elasticity, rheology, density, etc.) controls its dynamics. The modeling approach used in this study is based on both static

interactive forward modeling and an integrated geophysical-petrological algorithm. Data sets such as (elevation, geoid, gravity, gravity gradients, surface heat flow, and seismic and upper mantle xenoliths petrological data) can be combined and interpreted concurrently and compared to published models. This study's model focuses on deep structures in the crust and upper mantle and the contribution of stagnant slabs of the Pacific Ocean plate and the Philippines sea plate beneath the Japanese Islands.

The Japanese islands are situated in a very active tectonic setting, with two oceanic (Pacific and the Philippine Sea) plates subducting beneath two continental (North American and Eurasian) plates, resulting in earthquakes and volcanism. These interactions result in the formation of the complex geometry of subducting slabs under the Japanese islands (Nakajima and Hasegawa, 2007b; Hirose et al., 2008). The Japanese islands are located on two continental plates (Eurasian and North American), which meet in central Japan in the Itoigawa Shizuoka Tectonic Line. Under this location, two oceanic plates (Pacific and the Philippine Sea) with different ages and subduction velocities subduct roughly from the east (Pacific plate) and the south (Philippine Sea plate). The Pacific plate subducts beneath the North American and Philippine Sea plates at the deepest Kuril–Japan–Izu-Bonin trench, which is 1500 km wide from north to south (Goudie, 2004), during the Philippine Sea plate subducts beneath the Eurasian plate at the Nankai Trough parallel to the Median Tectonic Line, which is one of Japan's largest fault systems. The subducted Pacific plate covers a large region beneath the Japanese islands, forming a stagnant slab that partially overlaps with the subducted Philippine Sea plate beneath Central to Southwest Japan. The growth of Japan arcs is primarily due to the complicated geometry of these plates, their interconnections, and the unstable torque balance around the triple junction (Takahashi, 2006b). Japan arcs have generally been split into six sections based on their tectonic setting: the Kuril, NE Japan, Central Japan, Izu-Bonin, SW Japan, and Ryukyu arcs (north to south). The Japanese Islands are divided into two primary tectonic blocks: northeastern (NE) Japan and southwest (SW) Japan. Recent research has discovered secular variations in the mode of magmatic activity, the magma plumbing system, erupted volumes, and magmatic composition associated with the evolution of crust-mantle structures related to the arc's tectonic history (Nakamura et al., 2019). The chemical composition, mineralogy, and Pressure-Temperature conditions of the lower crust and lithospheric mantle are all revealed by ultramafic xenoliths (Chattopadhaya et al., 2017; Kaczmarek et al., 2016; Maaløe and Aoki, 1977; Nixon, 1987; Perinelli et al., 2014; Satsukawa

et al., 2017). Mantle xenoliths are mantle material fragments carried to the Earth's surface by alkali basalt or kimberlite from the lithosphere or, perhaps, the asthenosphere (O'Reilly and Griffin, 2010). These xenoliths might be a valuable source of information on the lithosphere-asthenosphere boundary (LAB) zone.

The LAB is often identified by seismological measurements that show fast changes in shear wave velocity and attenuation. Temperature, water content, partial melting extent, chemical compositions, or grain size are all factors that contribute to LAB (O'Reilly and Griffin, 2006; Hirth and Kohlstedt, 1996; Green et al., 2010; Hirschmann, 2010; Karato, 2012). The LAB in the concept of plate tectonics indicates a border zone of a given thickness where heat, momentum, and materials are transferred between the conductive mantle (lithosphere) and the overlying convective mantle (asthenosphere) (O'Reilly and Griffin, 2006; Mckenzie and Bickle, 1988; Fischer et al., 2010; Anderson, 1995).

The following are the workflow and objectives of this thesis:

1- Study the tectonic setting of the Japanese Islands and their surroundings.

2- 2- Study the Subduction Zones and Stagnant Slabs' Nature.

3- Undertake studies on mantle xenoliths and petrology studies of the Northwest Pacific Ocean.

4- Evaluate previous seismic (receiver function analysis and seismic tomography).

5- Study gravity gradients data from the Gravity Field and Ocean Circulation Explorer (GOCE) satellite mission.

6- Conduct a 3-D gravity gradients inversion constrained by previous seismic studies to model crustal thickness and Moho depth in the study area.

7- Apply integrated 3-D inversion of geophysical observations and petrological analysis to model temperature, density, heat flow, and the chemical composition of the lithosphere and upper mantle in the Northwest Pacific Ocean area.

Thesis Structure

This thesis includes four chapters; two main chapters include a published or ready for submission manuscript in addition to the introduction and conclusion. The outline of each chapter is:

Chapter 1 focuses on the thesis' framework and objectives. It also includes the thesis structures.

Chapter 2 Discuss the 3-D density model, crustal thickness, and Moho depth map in the Northwestern Pacific Ocean area and the contribution of stagnant slabs in satellite gravity gradients data. The misfitting between the outcome model and the regional and global crustal thickness models is also included. Gravity data have been used to model the Moho geometry (petrological Moho) because the compositional transition between the lower crust mafic granulites and the mantle ultramafic peridotites produces gradients of seismic velocities. The Moho can be gradational and interlayered in non-cratonic regions (O'Reilly and Griffin, 2013). lithospheric modeling to study dynamic topography is one of the most effective applications of the Gravity Field and Ocean Circulation Explorer (GOCE) gravity gradients data. I used the non-linear 3-D gravity inversion (Uieda and Barbosa, 2016) to estimate Moho's depth. The method begins with correcting gravity data to remove the effects of topography and the effect of bathymetry. The remaining effect is considered reflective of the Moho and the upper mantle.

Chapter 3 Discuss the results of integrated inversion of a geophysical and petrological analysis of mantle xenolith samples. The models produced are for temperature, thermal heat flow, and density distribution in the study area. To reduce misfitting to an acceptable range, the calculated geophysical and potential fields are compared to the observed data (topography, geoid, gravity gradients, chemical composition) to reduce misfitting to an acceptable range.

Chapter 4 provides the dissertation's conclusion in addition to future research directions.

Chapter 2

Forward and inverse gravity modeling of the crust

2.1 Introduction

The Eastern Eurasian plate, western Pacific plate, Okhotsk Plate, and the Philippine Sea plate have experienced convoluted tectonic evolution since the breakup of Pangea. The growth of the Japanese island arc system, which has mainly taken place along the continental margin of Asia since the Permian, results from the subduction of the ancient Pacific Ocean floor. Backarc basin formation in the Tertiary shaped the present-day arc configuration. The neotectonics regime, characterized by strong east-west compression, has been triggered by the eastward motion of the Amur plate in the Quaternary (Taira, 2001). The tectonic evolution of the Japanese island arc system includes the formation of rock assemblages that are common in most orogenic belts. Because the origin and present-day tectonics of these assemblages are better defined in the case of the Japanese island arc system (and resulting Japan Islands), the study of the system provides useful insight into orogenesis and continental crust evolution. The seismicity of the Japan Islands is associated with subduction zones and active faults (Geological Survey of Japan, 1992). Since 1885, the Japan trench boundary has experienced more than 100 earthquakes than M6 (Taira, 2001). Trench regions with parallel negative gravity and topography anomalies are predominantly zones of major earthquakes (Song, 2003).

The Mohorovičić (Moho) discontinuity is generally considered to represent a compositional transition at the crust-mantle boundary between mafic granulites in the lower crust and ultramafic peridotites in the mantle. However, recent xenolith studies suggest that this petrological transition can be gradational, possibly interlayered, at 5–20 km in non-cratonic regions (O'Reilly and Griffin, 2013). Gravity data are typically used to model the mantle geometry because the density contrast between the mantle and the crust is strong. However, the mantle represents a narrow zone where the P-wave velocity changes rapidly in the lowermost crust/upper mantle, and hence it may be considered a Moho "proxy." P-wave velocity (Vp) is typically less than 7 km/s above the crust/uppermost mantle layer, while beneath this layer, Vp increases from 7.4 up to 8.0 km/s (Rabbel et al., 2013). That is consistent with a "petrological Moho" where interlaying of mafic and ultramafic rocks produces gradients of seismic velocities (O'Reilly and Griffin, 2013), giving some physical basis to our definition of the Moho as a velocity gradient. Iwasaki et al. (2002) noted that the Moho in some places under the Japanese island arc is not seismically sharp but appears to be transitional zones based on the reflected P-waves from the Moho discontinuity (PmP) observations. Identifying the

Earth's gravitational field is one of the Gravity Field and Ocean Circulation Explorer (GOCE). Using a spatial resolution of 80 km, lithospheric modeling to study dynamic topography is one of the most effective applications of GOCE data. Such GOCE data may be considered complementary to gravity and seismic tomography for modeling the density distribution and structure of the crust and upper mantle. Uieda and Barbosa (2016) presented a method for estimating the depth of the Moho using a constrained non-linear inversion of gravity. The method begins with correcting gravity data to remove the effects of topography and the effect of bathymetry. The remaining effect is considered reflective of the Moho and the upper mantle.

The scope of this work is to model the crustal structures and the density distribution of the subduction plates along the eastern side of the Japan Islands and the western edge of the Pacific and Philippine Sea plates, respectively. Despite the spread of earthquake monitoring networks such as the National Research Institute for Earth Science and Disaster Resilience, Japan Meteorological Agency, national universities and research institutes and the generation of many studies using onshore data from these networks, few offshore studies have been carried out. Previous seismic studies have covered only smaller local areas; thus, satellite gravity data have allowed us to study a wider regional area even without seismic data coverage.

Satellite gravity and topography data were obtained from the latest GOCE models (GOCO06s model of the Gravity Observation Combination (GOCO) project). The satellite data can be distinguished by their extensive coverage and ability to overcome natural and geopolitical barriers. In addition to wide satellite data coverage, the gravitational data can be characterized by high accuracy at shallow depths and across the horizontal extension. The geometry constrained the gravity inversion process and modeling and physical parameters obtained from multiple models, including the ETOPO1 Global Relief Model, CRUST1 model, seismic tomography models, and previous seismic studies. The results yielded a Moho depth model of crustal thickness, depth to the Moho boundary, subduction plates, and stagnant slabs at the eastern edge of the Japan Islands. The Moho depth model created a temperature distribution model for this complex tectonic region, part of the larger Ring of Fire.

2.2 Tectonic setting and previous studies

Since the Permian (i.e., the breakup of supercontinent "Rodinia"), the Japanese island arc system started to form along the Paleo-Asian continent margin as a consequence of the Paleo-

Pacific Ocean crust subduction. The Proto-Asian continental block was formed by accretion of rifted continental blocks (i.e., the South China, Sino-Korea, and Siberia blocks). The interplay between the Amur, Eurasia, Pacific, Okhotsk, and Philippine Sea plates (Wei and Seno, 1998) (Fig 2.1a).

Presently, Japan consists of four main islands: Hokkaido, Honshu, Shikoku, and Kyushu. At the western edge of the Pacific Ocean, the Japanese island arc system is an arc–trench system. The arc comprises two main island arcs, East Japan and West Japan Arc (Sugimura and Uyeda, 2013). Three subarcs (the Kuril, NE Japan (Honshu), and Izu-Bonin (Mariana)) form the arc of the East Japan arc. As a result of Pacific plate subduction, the East Japan arc system extends parallel to the Kuril, Japan, and Izu-Bonin trenches. The West Japan Arc is formed of two subarcs: the first being parallels to the South West trough and the second occurring along the northern boundary of the Philippine Sea Plate (Kaizuka, 1975). As a result of the oblique Pacific plate subduction at the Kuril arc, the Kuril forearc migrates westward, and the subduction of the Pacific plate then continues at the trenches of Izu-Bonin and Japan. In addition to the Pacific plate subduction in NE Honshu, the east-west convergence between the Okhotsk and Amur plates in northeastern Japan established a subduction zone on the eastern margin of the Japan Sea [i.e., (Nakamura, 1983; Tamaki and Honza, 1985)]. The Nankai forearc sliver migrates westward due to oblique northwestern subduction of the Philippine Sea plate to the Izu-Bonin collision zone and the Nankai trough (Fitch, 1972). The most critical tectonic activities and the formation of the majority of the basement rocks occurred from the Jurassic to the Paleogene. Figure (2.1b) shows an example of a cross-section perpendicular to the Nankai trough and shows rock formations in this area. The subduction of the Pacific plate began with the Asian continental margin in the Jurassic. At the east margin of Pangea, the Permo-Jurassic accretion of tectonic basement rocks took place (Isozaki, 1997). Following this, the collision of the Okhotsk plate began during the Paleogene, and Paleo-Bonin arc rifting and the Shikoku Basin spread took place around 25–15 Ma. That was followed by Japan Sea spreading, Paleo-Honshu continental spreading (22–15 Ma), and widespread igneous activity in SW Honshu (17–12 Ma).   At 15 Ma, the Philippine Sea plate subduction and the Izu-Bonin arc collision against Honshu began. The Kuril forearc sliver and the formation of the Hidaka mountain belt started to collide at 15 Ma, while the main phase of the Philippine Sea plate subductions began at 8 Ma.
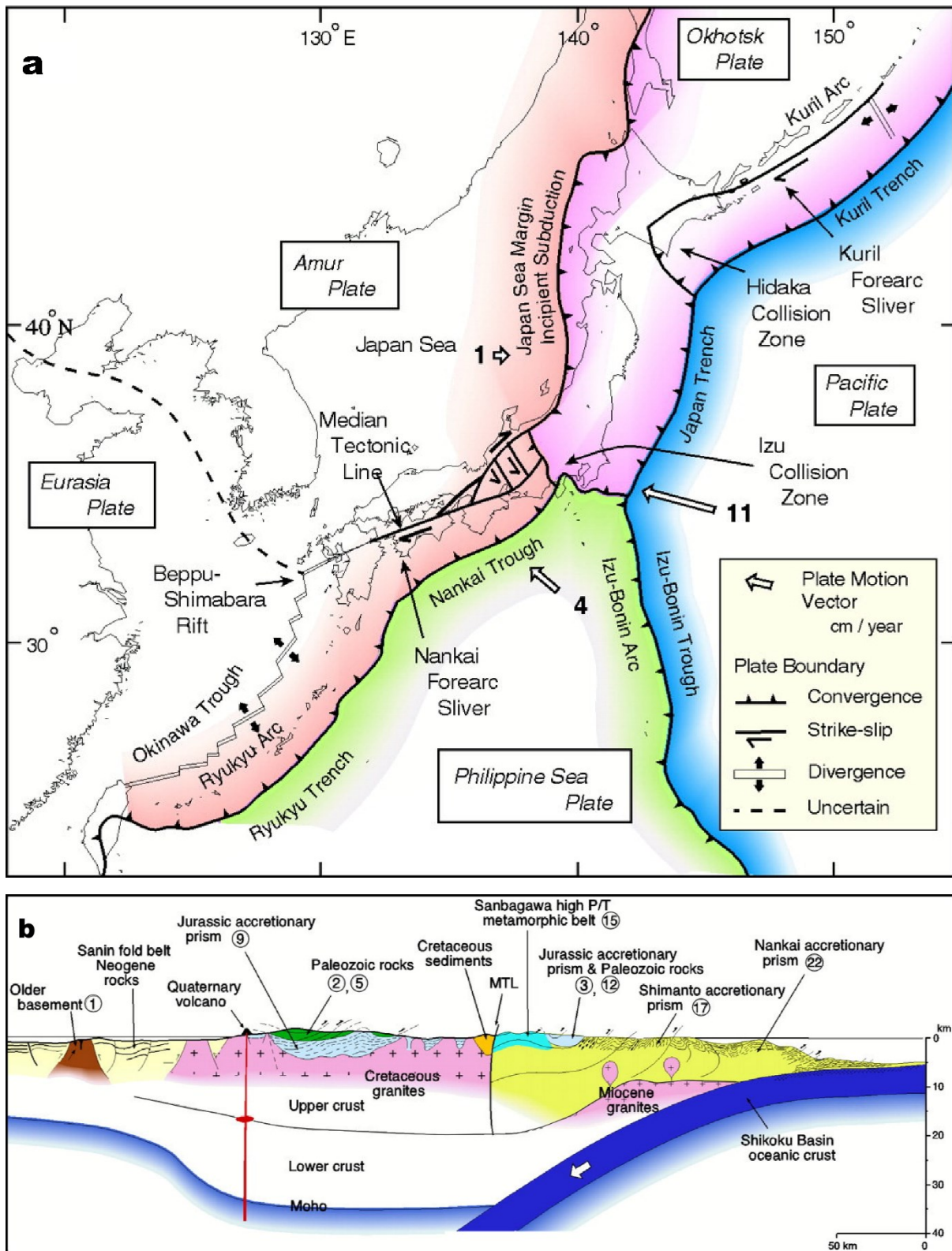
Figure 2.1: a) Plate tectonics of the Japanese island arc system, modified after (Van Horne et al., 2017). b) Cross-section in the Nankai trough area showing the distribution of different rock formations.

Simultaneously with the paleo-arc rifting and spreading of the Japan Sea, many phases of volcanic activity produced north-south horst and graben structures and the eruption of submarine volcanic rocks (green tuff) in NE Honshu. In SW Japan, high-magnesium andesite emplacement occurred due to the injection of hot asthenosphere, and the young Shikoku Basin seafloor first began subduction (Takahashi, 1999). From the late Pliocene to early Quaternary, east-west compression controlled the formation of the present arc system, and this was represented by the development of the fold belt and inversion of graben and horst structures in the NE of the Japan Sea (Okamura et al., 1995). Similarly, coarse clastic sediment accumulations in the Quaternary mark the deformation development of features in central Honshu and present-day faults (Huzita, 1968). The southern Kyushu counterclockwise rotation (Kodama et al., 1995) and rifting peak of the southern Okinawa Trough (Park et al., 1998) began in the Quaternary. The Japanese island arc system was initiated around 4–3 Ma and was developed at 2 Ma. It is probable that the eastward movement of the Amur plate then triggered neotectonics.

2.3 Database

This section describes the various datasets used in this study and the procedure followed for data correction.

2.3.1 Solid Topography Data

Japan's topography features consist of deep trenches surrounding the Japanese island arc and mountain chain systems due to the interactions of the plates. The gradual subsidence of the Pacific plate and the bending of the arc lithosphere generated a smooth topography in NE Honshu (Von Huene and Lallemand, 1990). The submarine topography at the margin of the Japan Sea and NE Honshu arc consists of the range structure and basin formed by the inverted tectonics of the rifted arc (Okamura et al., 1995). The oblique Philippine Sea plate subduction affects the topography of the forearc sliver of the Nankai trough and trench wedge active accretion (Sugiyama, 1994). The Okinawa Trough's rifting caused crustal thinning that generated the submerged Ryukyu arc (Kimura, 1985; Sibuet et al., 1998). The topography map

of the area is derived from the global model of ETOPO1 (Amante and Eakins, 2009), which ranges from -9000 to 1500 m (Fig 2.2).
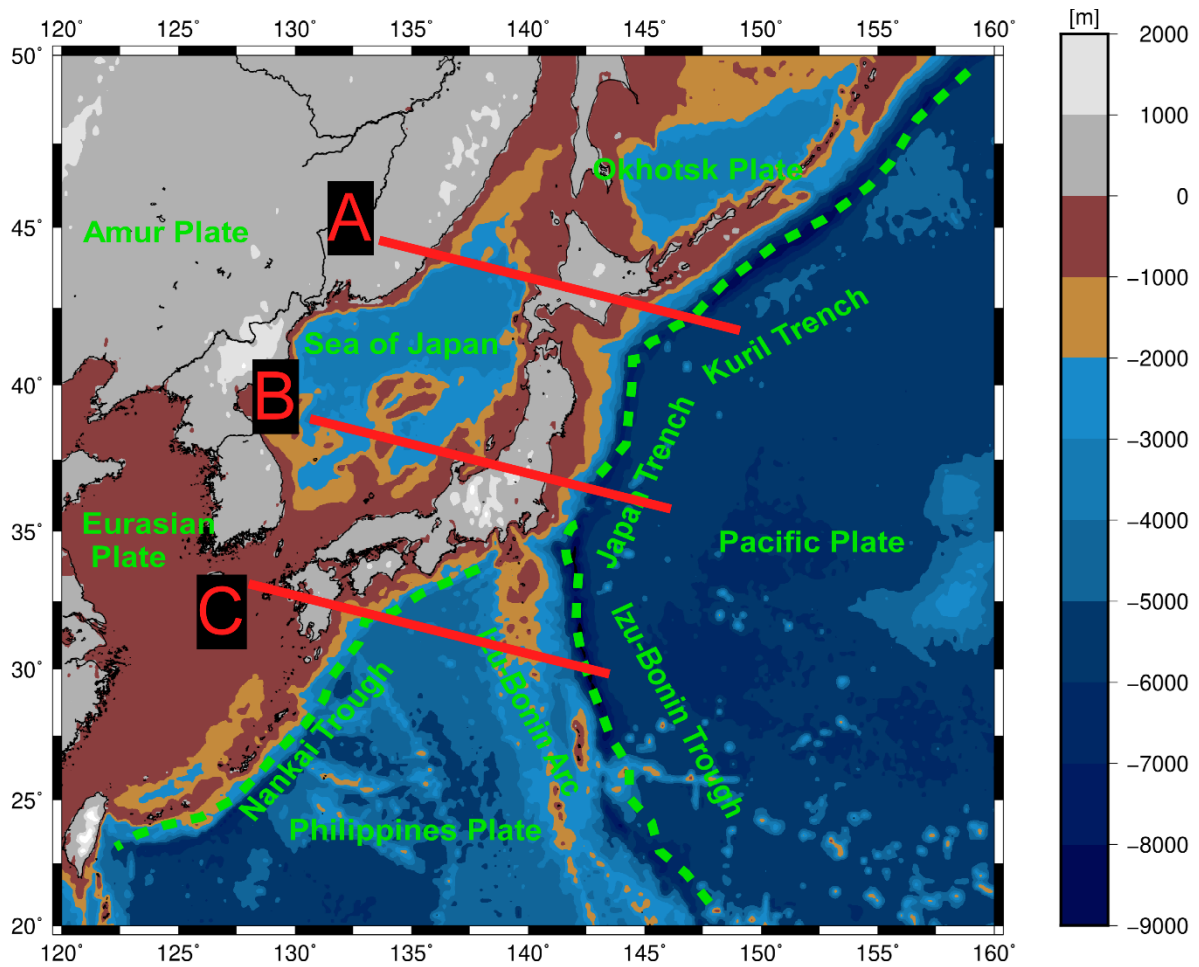
Figure 2.2: Topography map of the Japan island arc system based on ETOPO1 Global Relief data (Amante and Eakins, 2009). The area can be classified into three units according to geomorphology: 1) high-altitude in the continental areas and Japan islands, 2) central elevated areas in the Japan Sea and at the Okhotsk and Eurasian plates, and 3) least-elevated areas offshore at the Pacific and the Philippine Sea plates. A, B, and C are the location of three 2-D cross-sections of Kuril trench, Japan Trench, and Izu-Bonin and Nankai Trough.

2.3.2 Satellite gravity data

In this study, raw gravity data were generated from the satellite-only spherical harmonic model GOCO06S (Kvas et al., 2019), which is considered the latest release of the GOCO project initiated in the frame of the European Space Agency's (ESA) GOCE. The GOCE mission was launched in 2009 to determine the gravity field and geoid with high precision and a spatial resolution of approximately 80 km (Floberghagen et al., 2011). GOCO06s is a satellite-only global gravity field model up to degree and order 300, with constrained secular and annual variations up to degree and order 200 and a spatial resolution of 70 km. GOCO06s have been used to synthesize the Bouguer anomaly (BA) signal at a constant altitude of 50 km above the ellipsoid. For this study, the representation of the field at 50 km was chosen as it offers a higher level of detail in the signal than at the satellite altitude itself and maintains the noise amplification at an acceptable level (Sebera et al., 2014). The synthesized BA signal was then inverted to obtain initial estimates of the Moho depth. This new release was utilized in this study due to its various improvements within the processing chain compared to previous versions and its high accuracy and high resolution as a static global gravity field model. In addition, it can capture long-wavelength anomalies related to deep-seated crustal and upper mantle structures. The model is available via the International Center for Global Earth Models (ICGEM) Service (Ince et al., 2019).

Gravity data corrections

The anomalous density distribution must be isolated before inversion in gravity field modeling. In this study, the target is the Moho relief undulating around a reference Moho depth. Therefore, all other effects from gravity observations were removed. The scalar gravity of the ellipsoidal reference Earth (normal Earth) was removed from the raw gravity data to produce gravity disturbance, which was calculated using the closed-form solution presented by (Li and Götze, 2001). Signals anomalous to the normal Earth due to terrain, sediment, and elevation remained in the gravity disturbance (Fig 2.3). The obtained gravity disturbance was corrected for both topographic and bathymetric effects using the geometrical model from the ETOPO1 (Amante and Eakins, 2009) global topography model with 1 arc-min resolution, and the thickness of the crust layers was derived from the CRUST 1.0 model (Laske et al., 2013). These corrections were computed simultaneously by applying the open-source software

Tesseroids (Uieda and Barbosa, 2016), which discretizes the study area into tesseroids (spherical prisms). 5-degree padding was used in all directions, extending the study area's actual topography/bathymetry model to avoid edge effects, even for the far-field topography (Szwillus, Ebbing, and Holzrichter, 2016a). The topographic gravity correction was computed for a homogenous density distribution because of the lack of information about the topographic density distribution in most parts of the study area. In particular, I used a density value of 2670 kg/m^3, which is typically adopted to represent the upper continental crustal density and 1030 kg/m^3 for the ocean seawater.
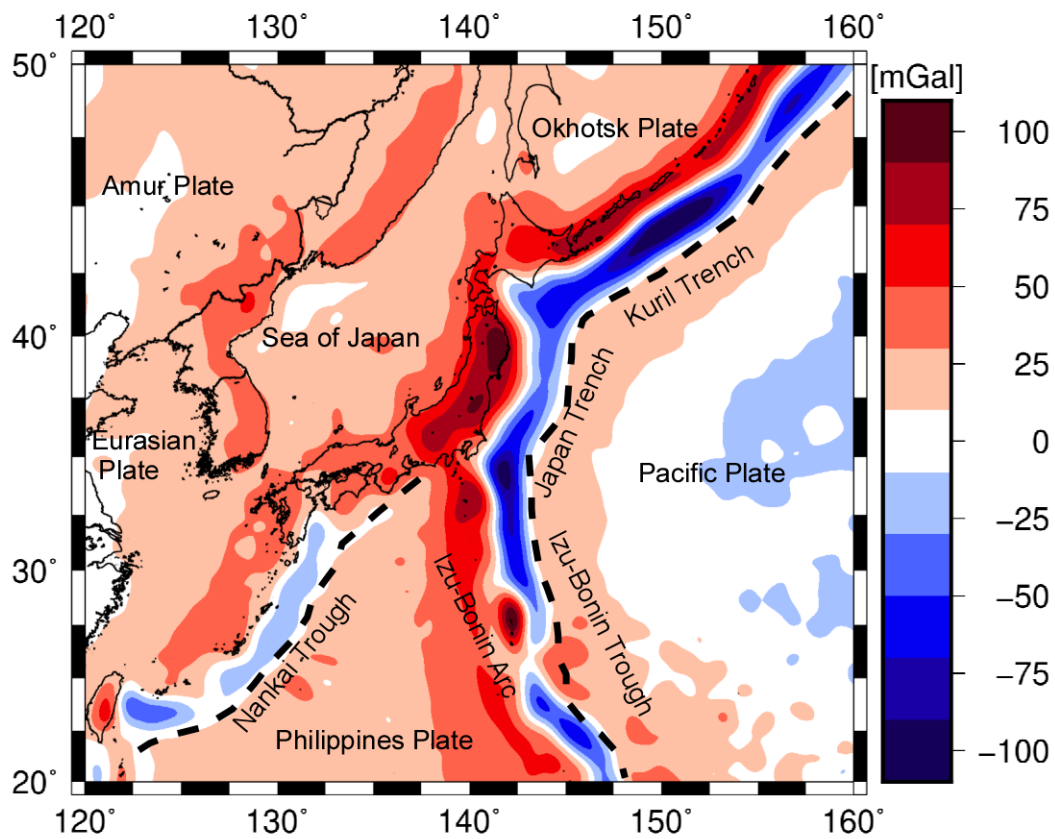
Figure 2.3: Free-air data derived from the GOCO06s model of
the area.

The gravity effect from sedimentary basins was also removed from the Bouguer gravity disturbance. The density of the sediments is smaller than the crustal density, which introduces an overcompensated anomaly to the data after Bouguer plate correction. The three sediment layers of CRUST1.0 (Laske et al., 2013), with different densities based on the depth of each layer, were used to calculate the gravity effect separately. The calculation is based on the

density contrast between each layer and the Earth's crust. The topography effect g^T (Fig 2.4) was removed from the disturbance to produce the Bouguer map (Fig 2.5).
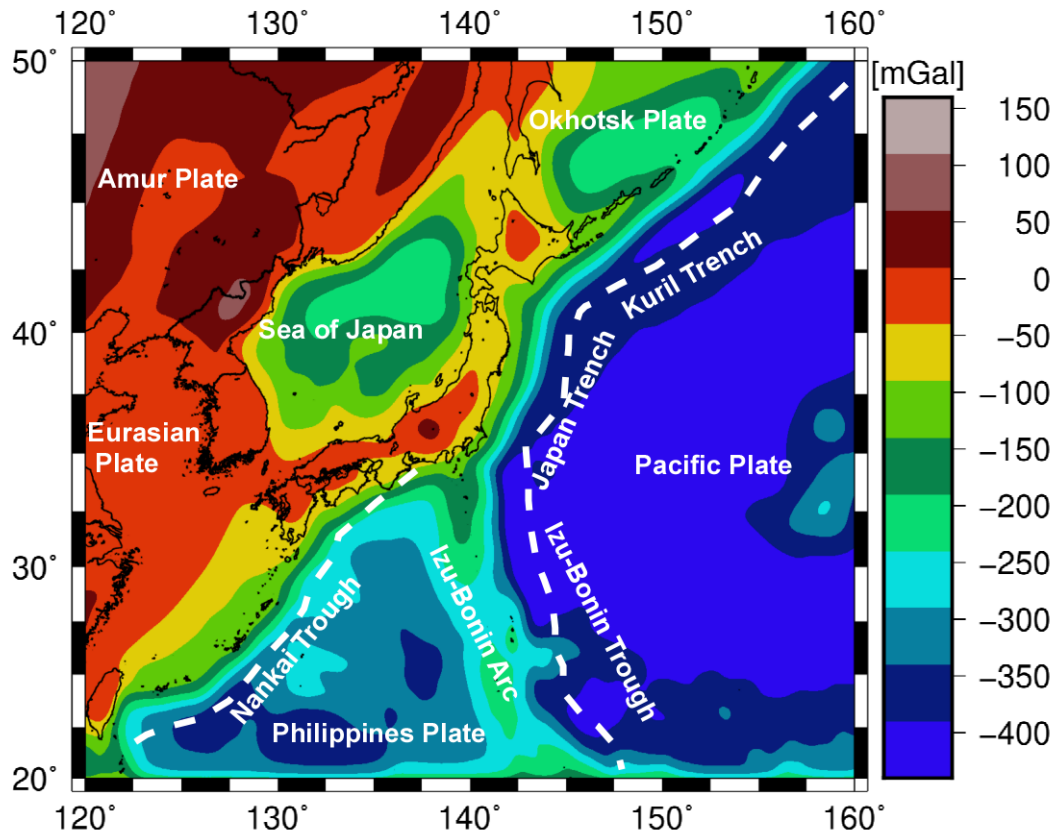
Figure 2.4: The calculated topography effects on gravity in the area

The next step was to remove the total gravity effect of the sediment layers (Fig 2.6) to produce the complete Bouguer gravity disturbance, as shown in Eq. 1. Finally, the gravity correction procedure assumes that the only remaining effect is that of the anomalous Moho relief (Tenzer et al., 2009; Tenzer et al., 2015; Uieda and Barbosa, 2016; Tenzer and Chen, 2019; Rathnayake et al., 2021) (Fig 2.7).

$$\delta g^B = \delta g^{dis} - g^T - g^{T,\delta\rho} - g^B - g^{Ms} - g^{Is} - g^C \tag{2.1}$$

where δg^B is the complete Bouguer gravity disturbance without any sediments effect, δg^{dis} is the gravity disturbance The gravity disturbance, g^T is the Topography gravity effect (for a uniform topographic density), $g^{T,\delta\rho}$ is the anomalous-topographic gravity correction (for an anomalous topographic density), and g^B, g^{MS}, g^{IS}, g^C are, the bathymetric, marine sediment, inland sediment, and consolidated crust gravity corrections, respectively.

15
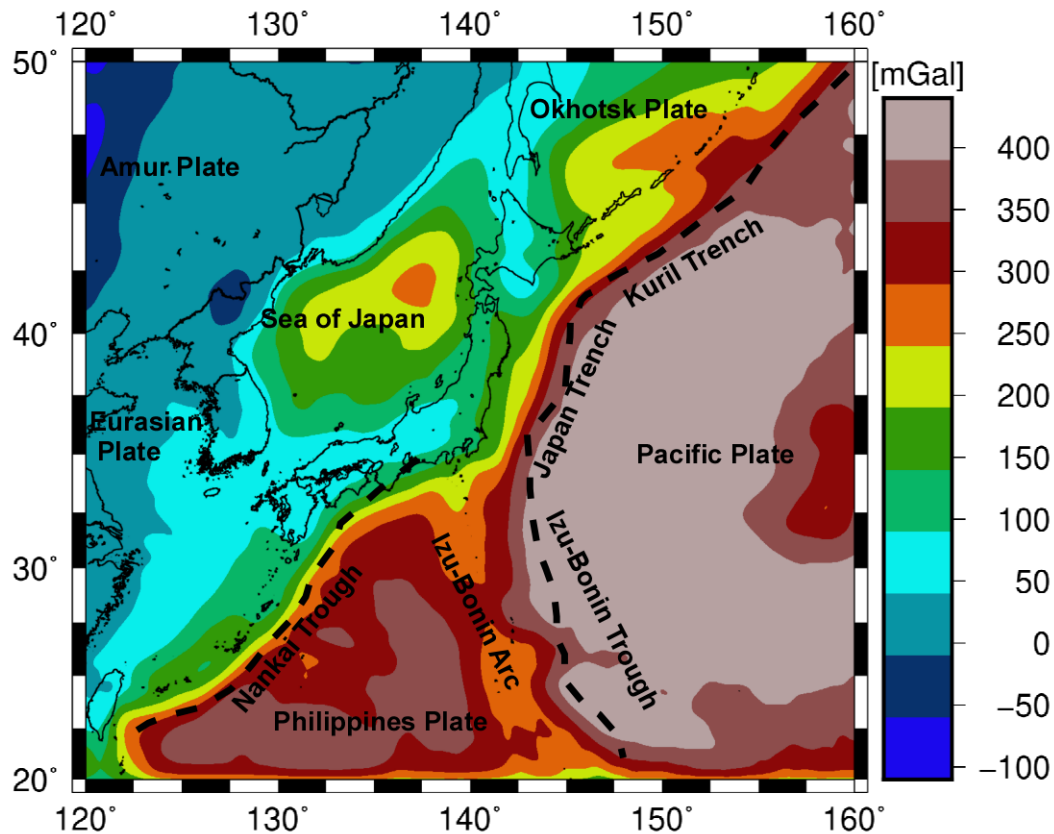
Figure 2.5: The calculated Bouguer anomaly in the area

2.3.3 Seismic data

Many studies have investigated the depth of Moho discontinuity in this region Table (2.1). Katsumata (2010) carried out a tomographic inversion of regional body wave arrival times to estimate the crustal structure and the depth of the Conrad and Moho discontinuities. He used the least-squares method to estimate the depth of discontinuities simultaneously. His results ranged from 40 km in central Honshu to 12 km in northern Kyushu, Kanto, SW Chubu, and Chugoku 2.8. The Moho depths are consistent with previous seismic refraction surveys and receiver function analyses.

2.4 Methods

I performed forward and inversion techniques to create a three-dimensional (3-D) density model that defines crustal deformation and the relief of the Moho boundary.
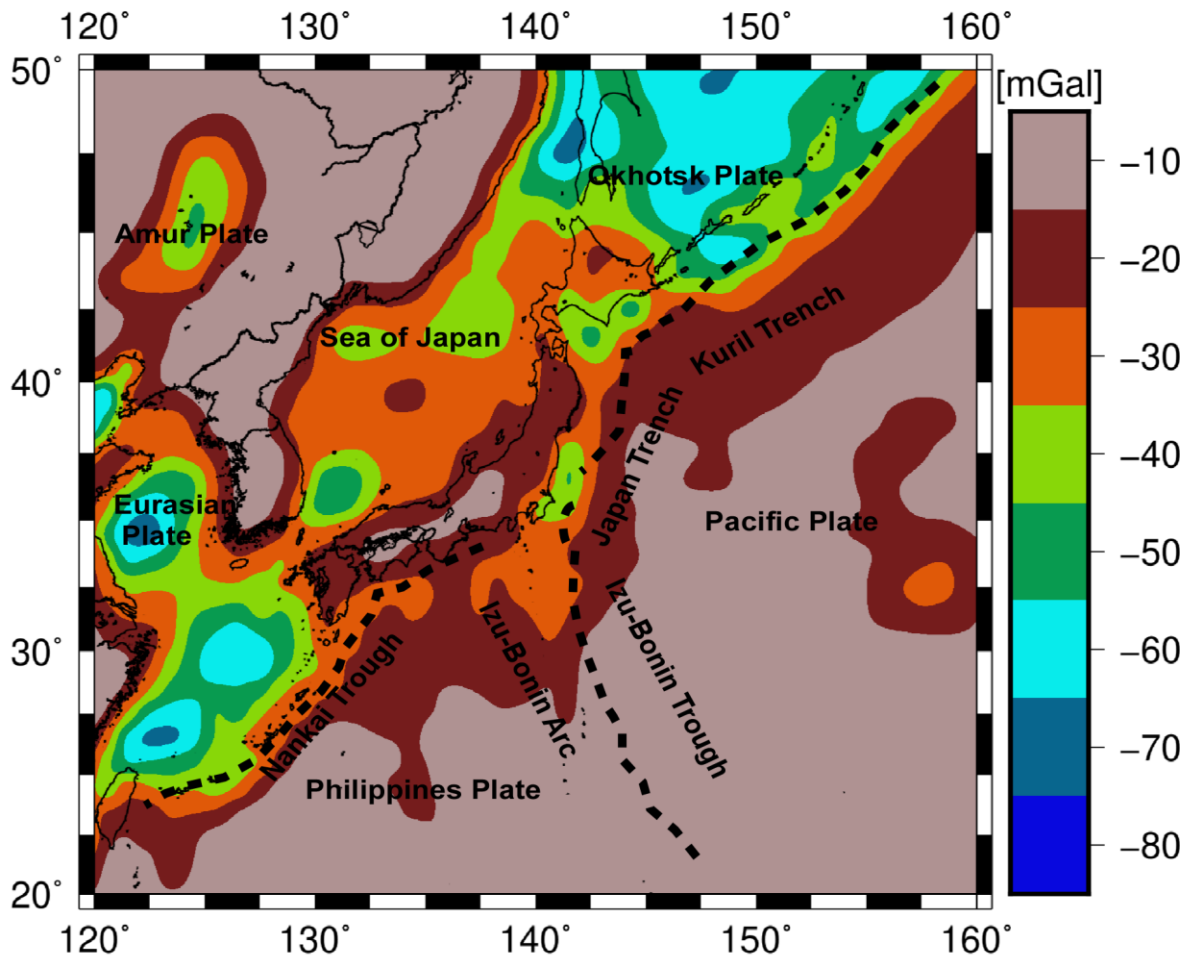
Figure 2.6: the calculated sedimentary layer effects on gravity in the area

2.4.1 Gravity inversion for Moho depth

I followed the methodology of (Uieda and Barbosa, 2016) and (Sobh et al., 2019; Sobh et al., 2020), who applied a non-linear inversion algorithm to gravity and seismic data using the Python code package Fatiando. The inversion algorithm is based on the Gauss-Newton formulation of Bott's equation (Silva et al., 2014). Uieda and Barbosa, 2016 revealed the ill-posed inverse problem within a well-posed matrix by applying tesseroids (spherical prisms) instead of a rectangular prism and introducing a Tikhonov regularization parameter into the inversion to stabilize the computed solutions and avoid the Bott method's instability. The resulting algorithm considers the Earth curvature using tesseroids for forward modeling. A tesseroid model is created to reproduce the preprocessed gravity signal, parameterized by (1) a regularization parameter that controls the smoothness of the model; (2) the reference depth (normal Earth Moho depth: Zref); and (3) the density contrast $\Delta\rho$ at the Moho boundary. The

regularization parameter was estimated by the inversion of multiple test sets derived from the original dataset. The parameter value resulted in the least mean square error. The two other parameters, Zref and Δρ, span a parameter space for the given intervals. Since the mean depth of the Moho and its density contrast is poorly known, I set a wide range for both parameters: The reference depth was set as 2.0 km steps from 20.0 to 50.0 km, and the density contrast as 50.0 kg/m^3 steps from 250.0 to 600.0 kg/m^3. Inversion was performed with the previously estimated regularization parameter for each reference depth and density contrast pair in this discretized parameter. Sediment-free Bouguer gravity data were used as inputs in the inversion process and the seismic constraints.
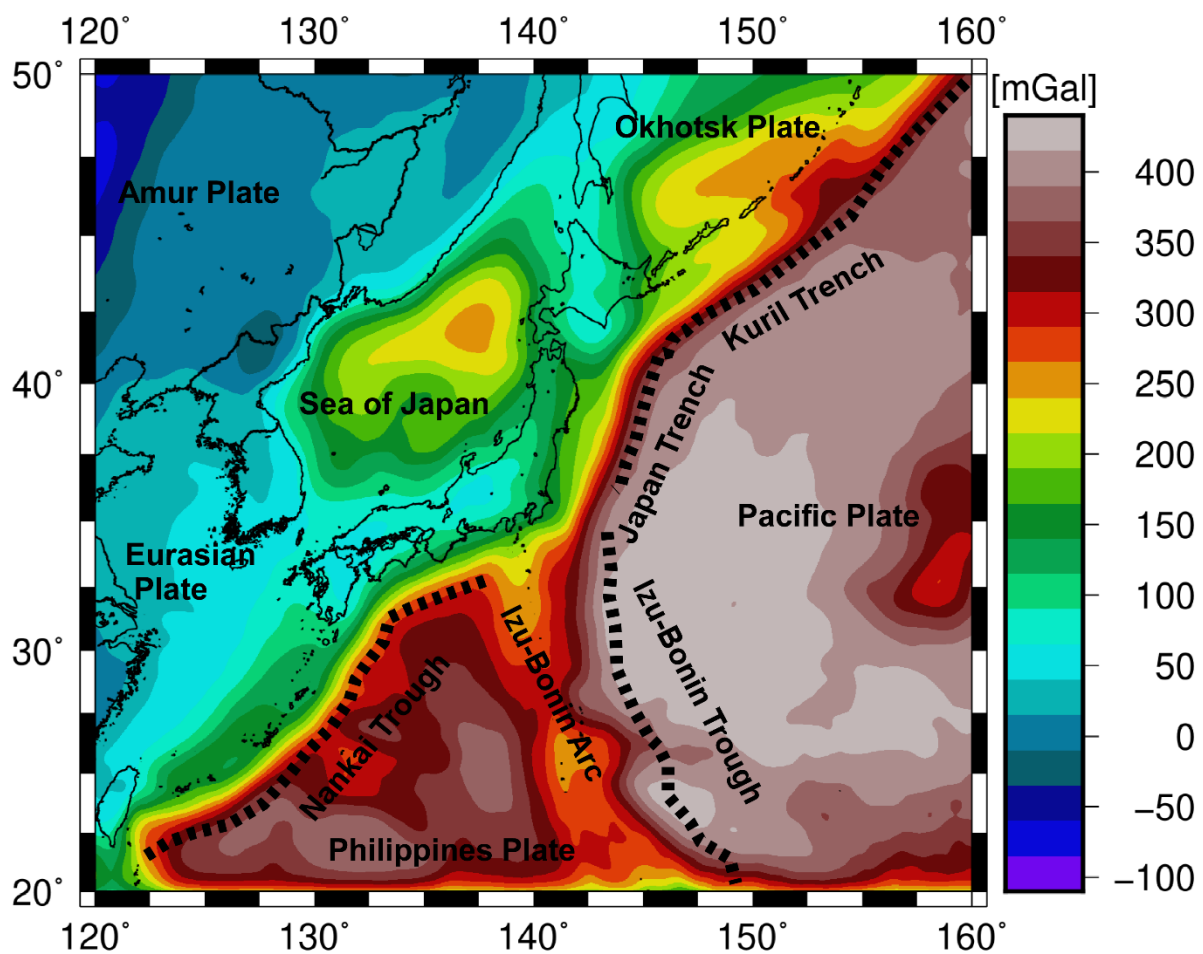
Figure 2.7: sediments-free Bouguer map. The area can be divided into three classes to follow up and distinguish the impact of each: The first group includes offshore, the Pacific Ocean, Philippine seashore, and trenches; the second group includes the failed rifted Japan Sea and the Okhotsk plate; the third group includes the Japan islands and continental regions.
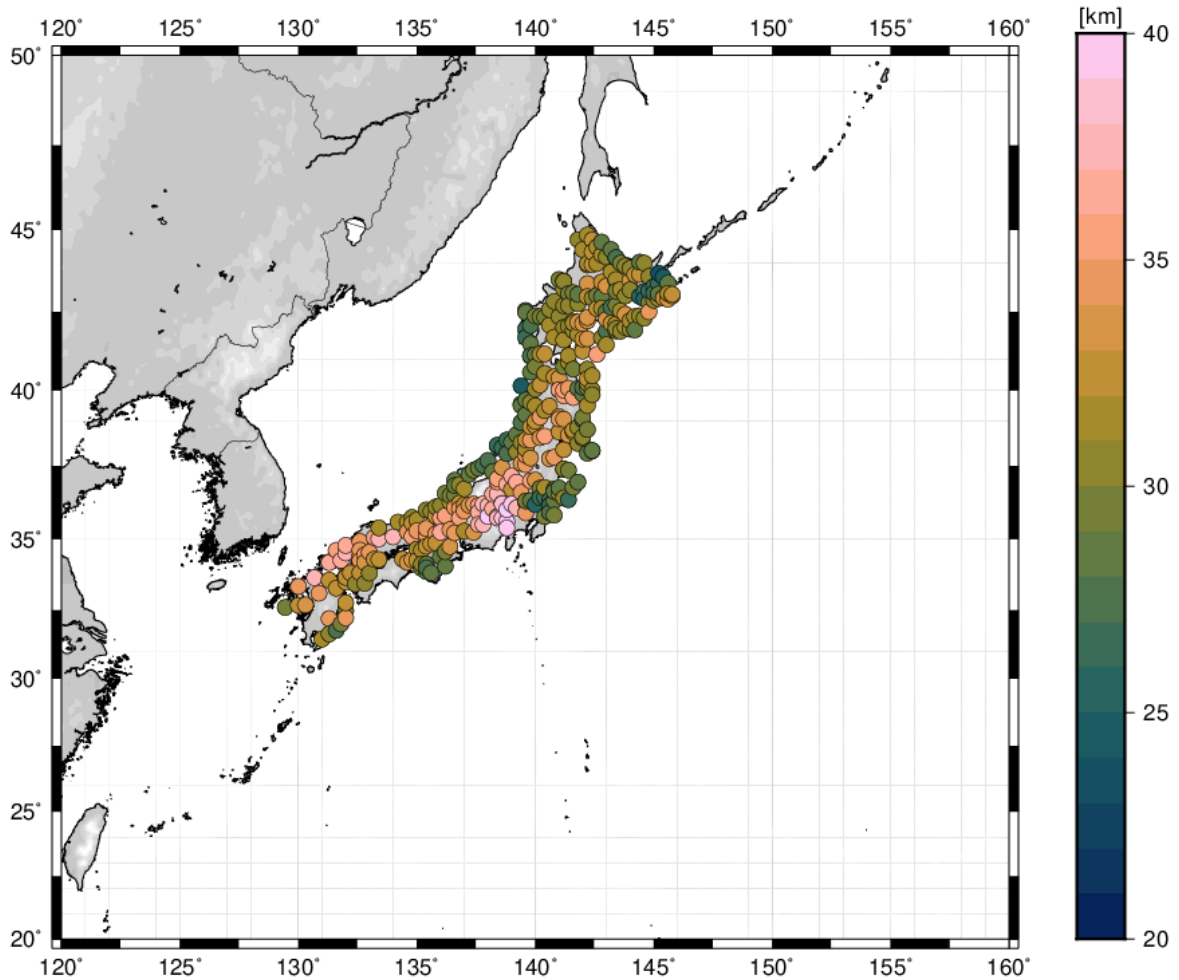
Figure 2.8: Locations of calculated Moho depths from a travel time analysis (Katsumata, 2010). Areas of low Moho-depth lie within the Pacific and Philippines Sea plates and the Japan Sea (i.e., the eastern and western edges of the Japan islands), while areas of high Moho-depth lie beneath the Japan islands.

Table 2.1: Previous Seismic Data.

Reference	Mantle P-wave	Avg. Moho depth
Iwasaki et al., (2002)	7.5–7.9 km/s	33 km
Nakajima et al., (2002)	7.6–7.7 km/s	32 km
Iidaka et al., (2004)	7.6–7.8 km/s	35 km
Shiomi et al., (2006)	7.6–7.8 km/s	34 km
Iwasaki and Sato, (2009)	7.5–7.9 km/s	32 km
Katsumata, (2010)	7.5–7.9 km/s	34 km
Igarashi et al., 2011)	7.8–8.0 km/s	36.2 km
Matsubara et al., (2017a)	7.8–8.0 km/s	34 km

The final reference Moho depth was 34.0 km in my study area, and the density contrast was 600.0 kg/m^3 Fig. (2.9).

2.4.2 The normalized Analytical Signal technique (NAS)

Cooper and Cowan (2006) used the first vertical derivative to normalize the total horizontal derivative to delineate and trace the sources and their edges in potential geophysical methods. From this, Yao et al., (2016) newly proposed the normalized analytical signal (NAS) method that used the absolute of the first vertical derivative ($\frac{\partial f}{\partial z}$) to normalize the analytical signal, AS, as shown in Eq. 2:

$$AS = \sqrt{\left(\frac{\partial f}{\partial x}\right)^2 + \left(\frac{\partial f}{\partial y}\right)^2 + \left(\frac{\partial f}{\partial z}\right)^2},$$

$$NAS = arctan^{-1}\left((AS)\,/\,\frac{\partial f}{\partial z} + p * max(AS)\right) \qquad (2.2)$$

where p is a positive value between 0 and 0.5, representing the importance of avoiding false edges when the data contain positive and negative values.

2.4.3 3-D forward modeling with GM-SYS

To compile a 3-D density model of the stagnant slabs around the Japan Islands, the Oasis montaj software with the GM-SYS extension has been used; a 3-D geomodeling package developed based on the simultaneous forward modeling of gravity, gravity gradients, and magnetic fields. The GM-SYS extension offers an interdisciplinary 3-D modeling approach integrating independent seismic, boreholes, and geological datasets, thus reducing the ambiguity of the potential field inversion. The model consists of several parallel cross-sections, in which the vertical sections run from east to west with a separation offset.

2.4.4 Constraining data for the 3-D modeling procedure

The initial model consists of four layers: sediments, two different crustal domains, and the upper mantle. Moreover, the initial model considered all significant geological and geophysical observations. Subsequently, the free parameters of the initial model can be modified until the forward computed gravity signal best fits the measured values.

Geometrical constraints

The 3-D model is initially constrained by deep seismic profiles (Wei et al., 2012; Fukao and Obayashi, 2013; Zhao, 2015; Liu et al., 2017; Matsubara et al., 2017b), receiver functions, seismic tomography cross-sections, and geological information. Moreover, the gravity inversion-based Moho and the isostatic Moho interface are used to constrain the Moho depths in regions where seismic observations are null. In addition, the sedimentary layer is constrained by the thickness data of the sediments retrieved from the global sediment thickness compilation of the Crust1 tectonic model of the world. I used the GAP P4 tomography model (Fukao and Obayashi, 2013) to create the subducted slabs' two-dimensional (2-D) cross-sections. I use the Slab 2.0 model (Hayes et al., 2018) to constrain the geometry of the subducted slabs. Figure (2.10) shows that stagnant subduction slabs appear clearly with a blue color (high P-wave velocity). Fukao and Obayashi, 2013 studied and classified stagnant slabs around the circum-Pacific.
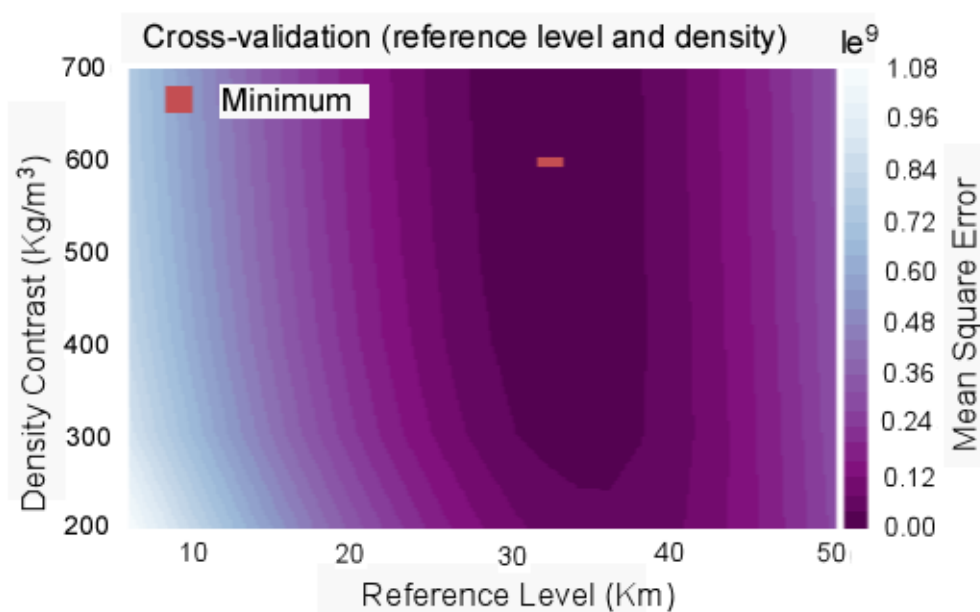
Figure 2.9: The gravity inversion parameters. The regularization parameter is 10^{-10}, the reference depth Z_{ref} is 34.0 km, and the density contrast $\Delta\rho$ is 600.0 kg/m^3.
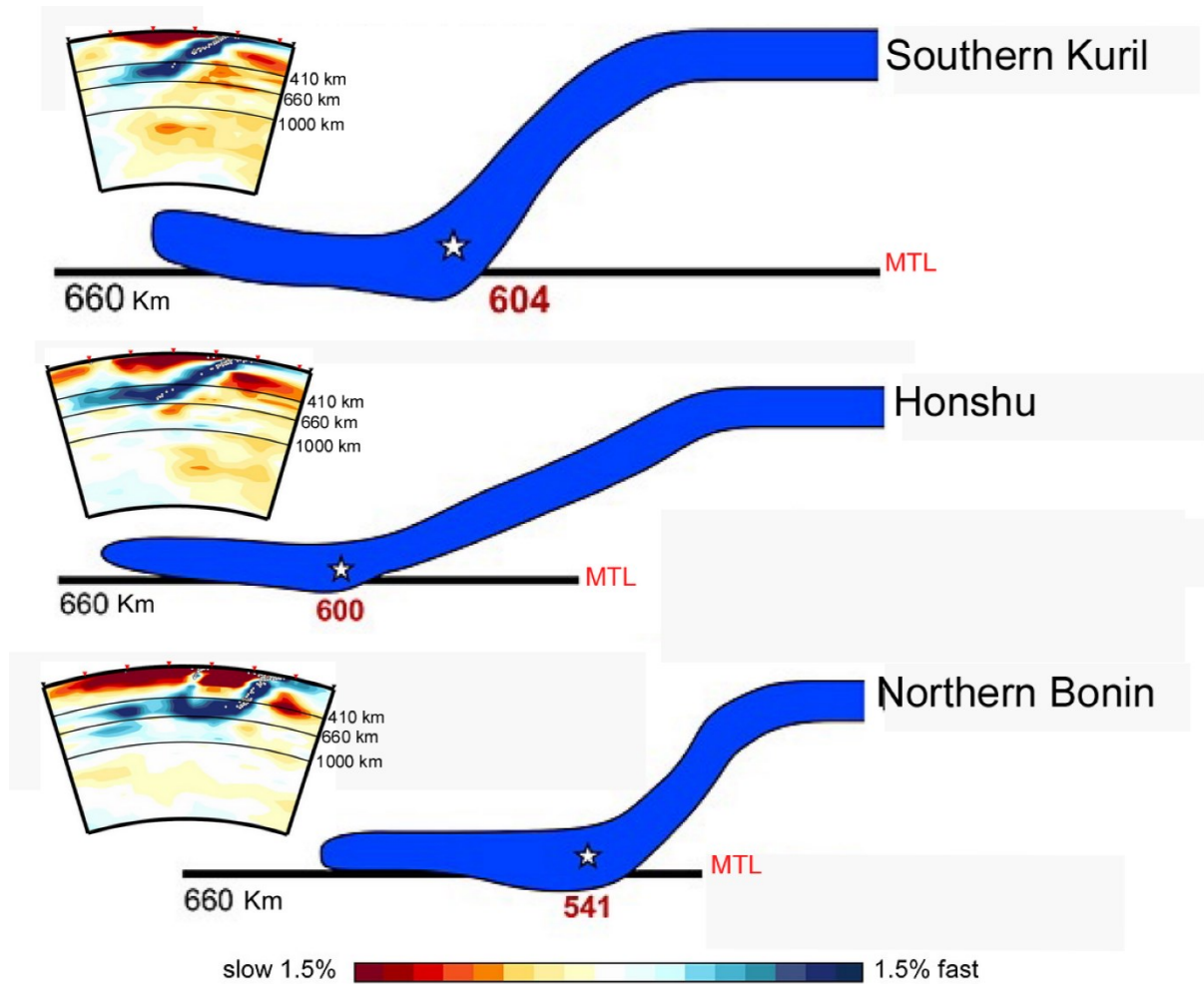
Figure 2.10: The GAP P4 tomography cross-sections and the stagnant slabs around the Japan islands, modified after (Fukao and Obayashi, 2013): (top) Kuril trench, (middle) Japan trench, and (bottom) Izu-Bonin and Nankai trenches.

Crustal density constraints

The densities of the crustal models of the Japan Islands were defined by exploiting the rock density values of the various studies. Density-related studies were carried out on all of the Japan Islands. The P-wave velocities of (Tsuru et al., 2000) were consequently transformed into densities by applying the non-linear relationships (Christensen and Mooney, 1995). Table (2.2) shows the prototype layers' density obtained from the CRUST1.0 model (Laske et al., 2013). Figure (2.11) shows the velocity depth 2-D model for the Pacific and Honshu arc subduction zones. I used the (Christensen and Mooney, 1995) non-linear relation to derive the density of each layer using the P-wave velocity of each layer. The Moho geometry was constrained by the gravity inversion based on Moho depth, while the thickness of the sedimentary layer was derived from global sediment thickness models (CRUST1.0 (Laske et al., 2013)), previous deep seismic studies (Wei et al., 2012; Fukao and Obayashi, 2013; Zhao, 2015; Liu et al., 2017; Matsubara et al., 2017b), receiver functions, and global tomography cross-sections.

Upper mantle density constraints

The initial density of the upper mantle was obtained based on the P-wave tomographic model by Fukao and Obayashi (2013), which is converted to densities. The model demonstrated very small density changes with the upper mantle density structure at 40 km depth.

Table 2.2: P-wave velocity (in km/s) and Densities (in kg/m^3) of the Initial Model's layers obtained from the CRUST1.0 model (Laske et al., 2013).

		Parameters					
		Mantle	Lower Crust	Middle Crust	Upper Crust	Sediments	Forearc Sediments
Pacific Plate	P-velocity	7.9	6.1	-	5.8	1.65	-
	Density	3350	3000	-	2850	2100	-
Continental Plate	P-velocity	7.8	6.8	6.2	4.2	1.6	3.1
	Density	3300	2920	2760	2550	2100	2500
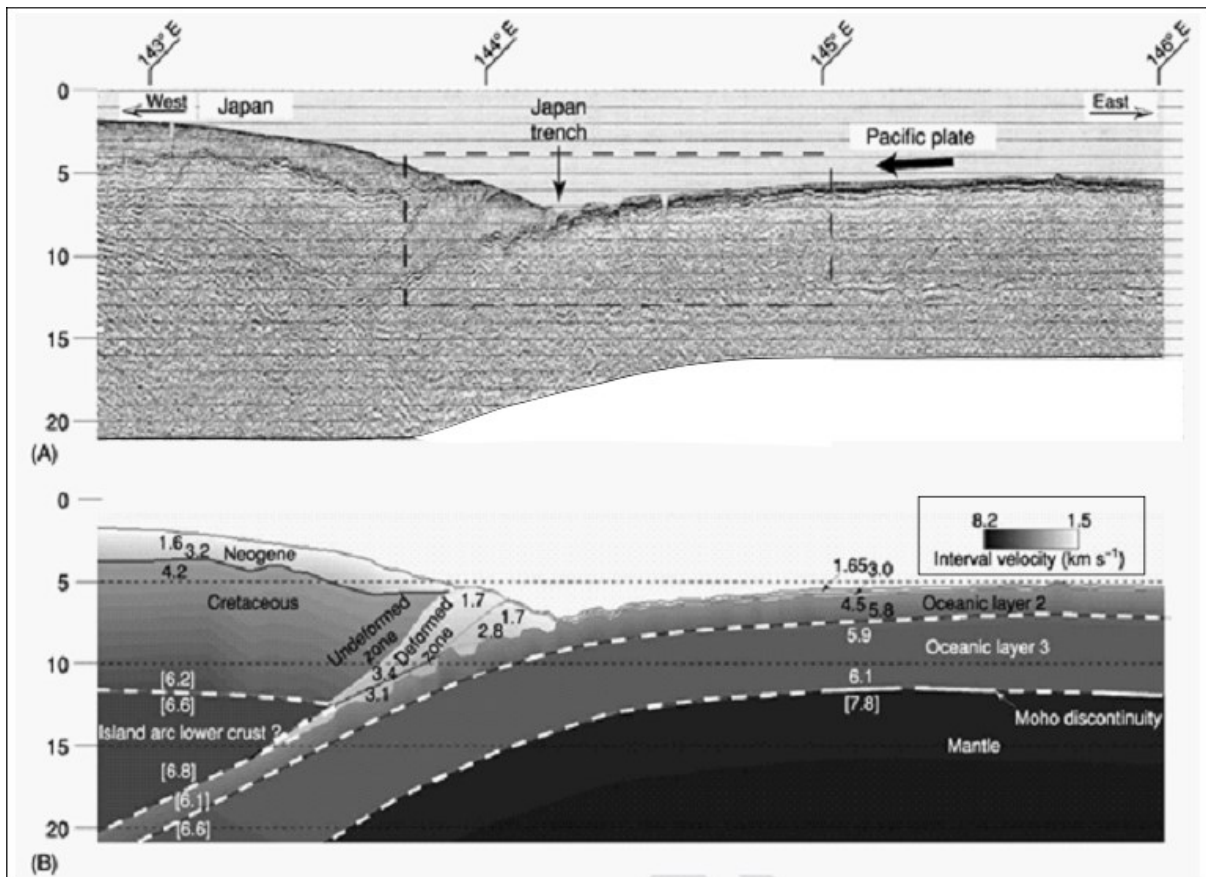
Figure 2.11: Japan trench cross-section (modified after Tsuru et al., (2000) clearly showing that the Pacific Oceanic crust is thinner than the continental crust of the Japan islands. The area with the lowest topography indicates the Japan trench.

2.5 Results

Moho Depths

The Bouguer gravity data were inverted to calculate the depth to Moho and the crustal thickness, helping to model stagnant subduction slabs around the Japan Islands. Figure (2.12a) shows that the Moho depths is between 14 and 43 km beneath the ground surface. The depths were divided into three levels. The first level is the shallowest and is located in the eastern part of the Pacific Ocean, appearing in the middle of the figure in the Sea of Japan. The second level is medium in depth and reflects the continental part of the region (i.e., the islands of Japan and the continent of Asia). The third level represents the highest level of the Moho depth in the central, western, and northwestern parts of the study area and reflects the mountainous

regions and volcanoes in the continental part of the study area. Finally, the model that gives the smallest MSE in this evaluation is considered the best fitting (Fig.2.12b).

NAS

Source edge detection is typically used in potential field methods to distinguish between different sources with different parameters of physical properties, depth, and degrees of inclination. Figure (2.13) shows the application of the NAS method for this study, with p = 0. The Pacific Ocean floor, the Japan Sea region, the Philippine Sea plate, and other scattered areas east of the Eurasian plate show high anomalies reflecting high density and high Bouguer values. Lower values indicate lower density areas. I used the NAS map to sharply delineate the boundaries of each plate, which made stagnant slabs more accurate.

2.5.1 Vertical Cross-sections of the 3-D density model

Figure (2.2) shows the locations of cross-sections concerning the Japan Islands and the subduction plate strike direction. The initial model consists of the following seven layers: 1) the lower Mantle layer extends from 600 km to 1000 km; 2) the MTZ layer (mantle transition zone), which is the deepest layer and extends from 410 to 600 km below the topography; 3) the mantle divided into two layers (mantle below the Pacific plate and mantle below the Japan Islands) with different densities and depths; 4) the stagnant Pacific crust (upper and lower); 5) the crust layers of the Philippine Sea plate (upper and lower); 6) the upper, middle, and lower crust under the Japan Islands; 7) a sedimentary layer; 8) the forearc sediment layer at the subduction zones. First, I adjusted the initial parameters of the prototype to reduce the misfit between the observed and calculated gravity.

Then, I shifted the Moho and sedimentary layer surfaces up and down to reduce the gravity signal misfit. That was done because variations in the density contrast between the MTZ, Moho, crust, and sedimentary layers could cause rising misfits and adjust the Pacific slab geometry. The common characteristic of all profiles is that the depth to the east was less than that to the west. This difference in depths was due to the layer density and depth differences.

25
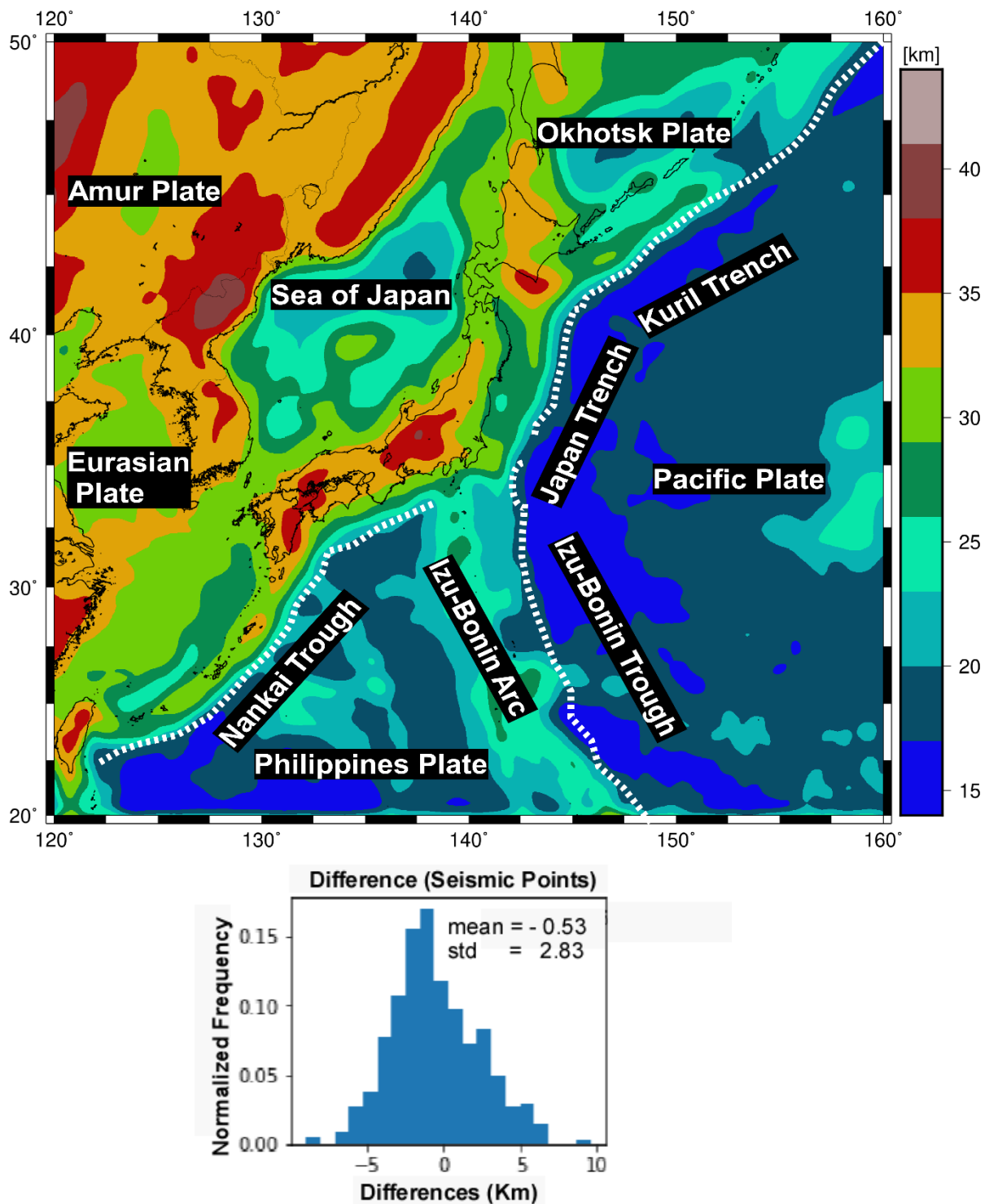
Figure 2.12: (a) Moho depths from the gravity inversion in the area, ranging from 14 to 43 km. The areas of shallowest Moho-depth are the Pacific and Philippines Sea plates, while the areas of medium Moho-depth are the areas of the Japan Sea, Okhotsk Plate, and Izu-Bonin arc highest Moho-depth are the continental regions of the Japan islands and the Asian plate. (b) The misfit between the estimated Moho depths from gravity inversion and Moho depths from the (Katsumata, 2010) seismic study.
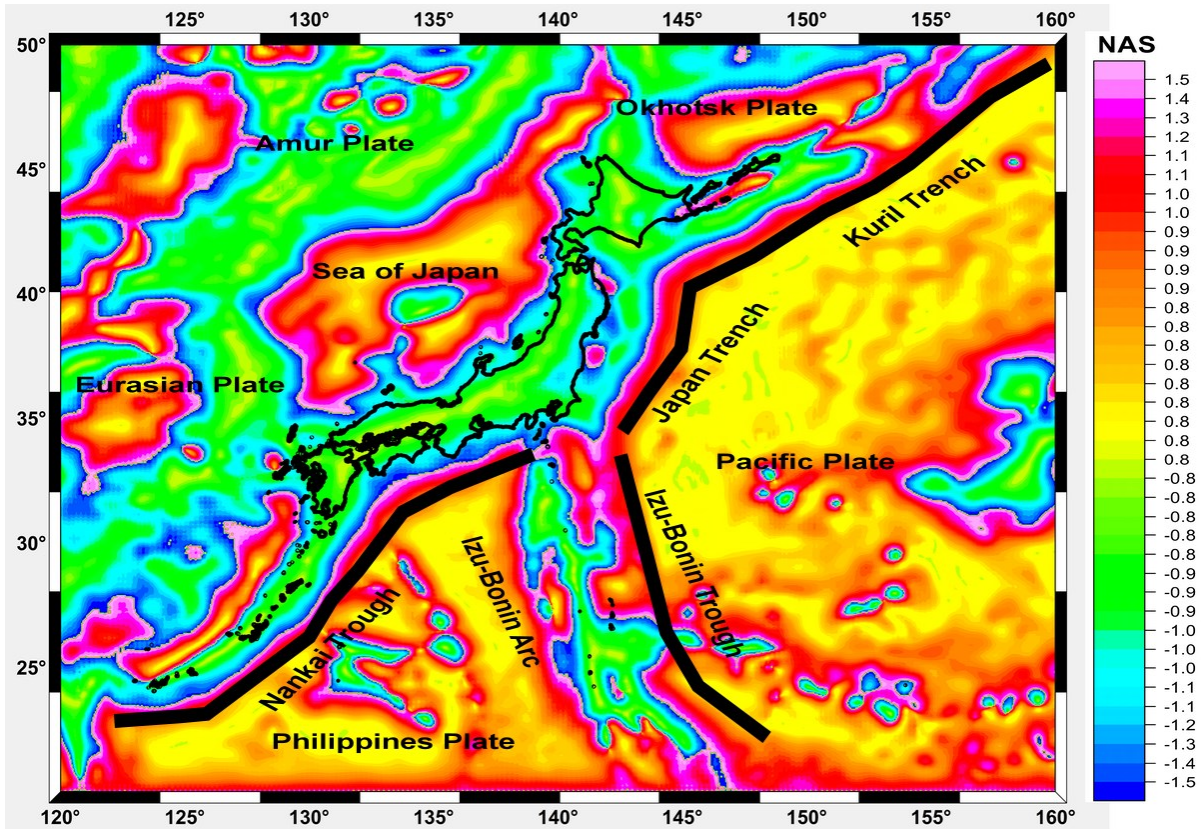
Figure 2.13: NAS map showing the edges of the Pacific, Eurasian, and subduction plates using p=0. The highest-anomaly regions on the map reflect the areas of highest densities and lowest depths. The NAS map helps detect all plates' boundaries to aid in the modeling.

For example, the geometry of the effects of the sedimentary layers appeared at shorter wavelengths, while in contrast, the Moho effect appeared at longer wavelengths. Finally, the cross-sections could be summarized into three categories: 1) profiles columnar to the Kuril Trench (Fig 2.14a); 2) profiles columnar to the Japan trench (Fig 2.14b and 3) profiles columnar to the Izu-Bonin and Nankai troughs (Fig 2.14c). The stagnant slabs tend to be denser with depth, according to (Duesterhoeft et al., 2014). The shape of stagnant slabs is derived from (Zhao, 2021; Fukao and Obayashi, 2013; Huang and Zhao, 2006). The subducted slabs geometry was obtained from the Slab2 model (Hayes et al., 2018).
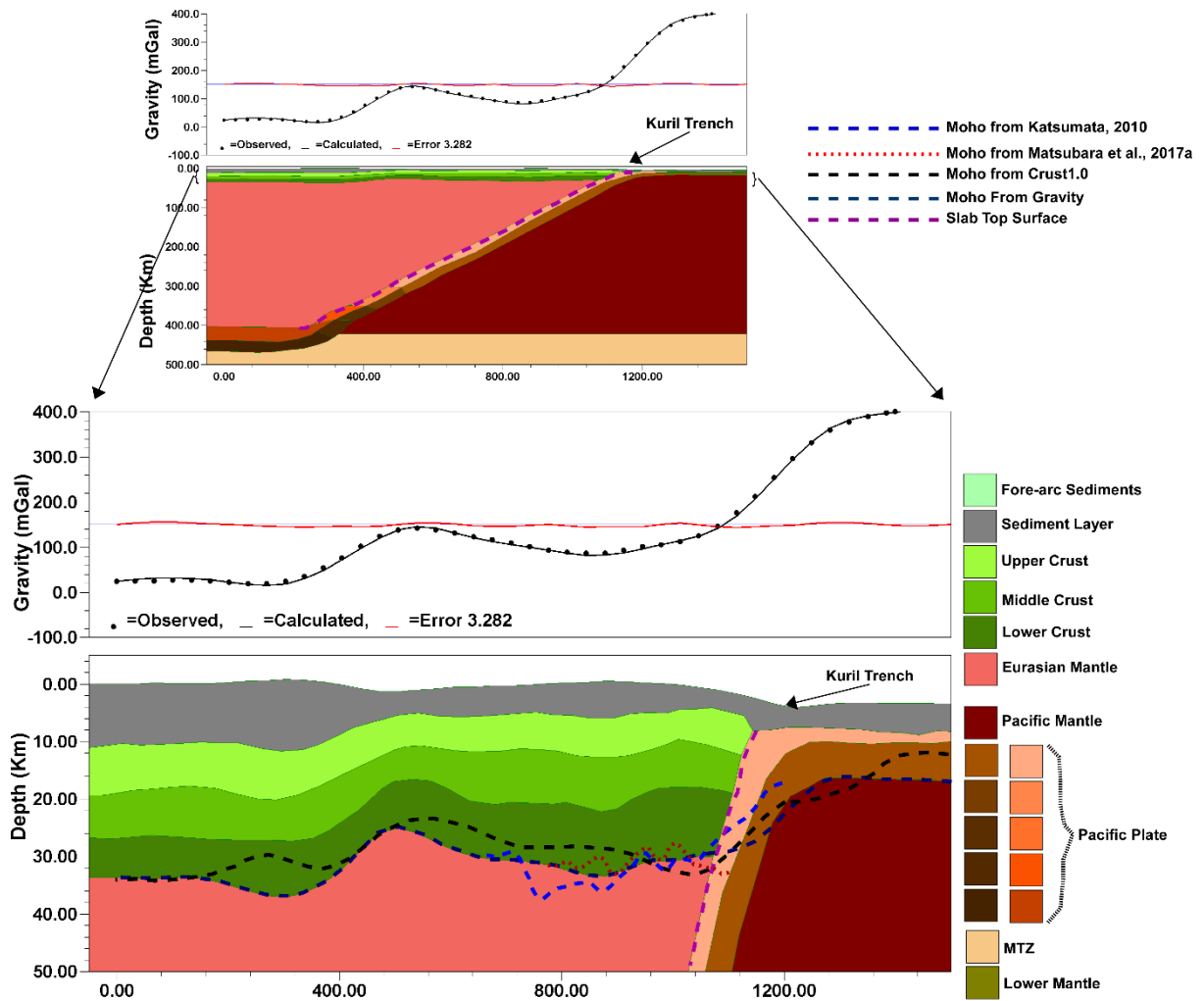
Figure 2.14: a) 2-D cross-section for the Kuril Trench (continued)
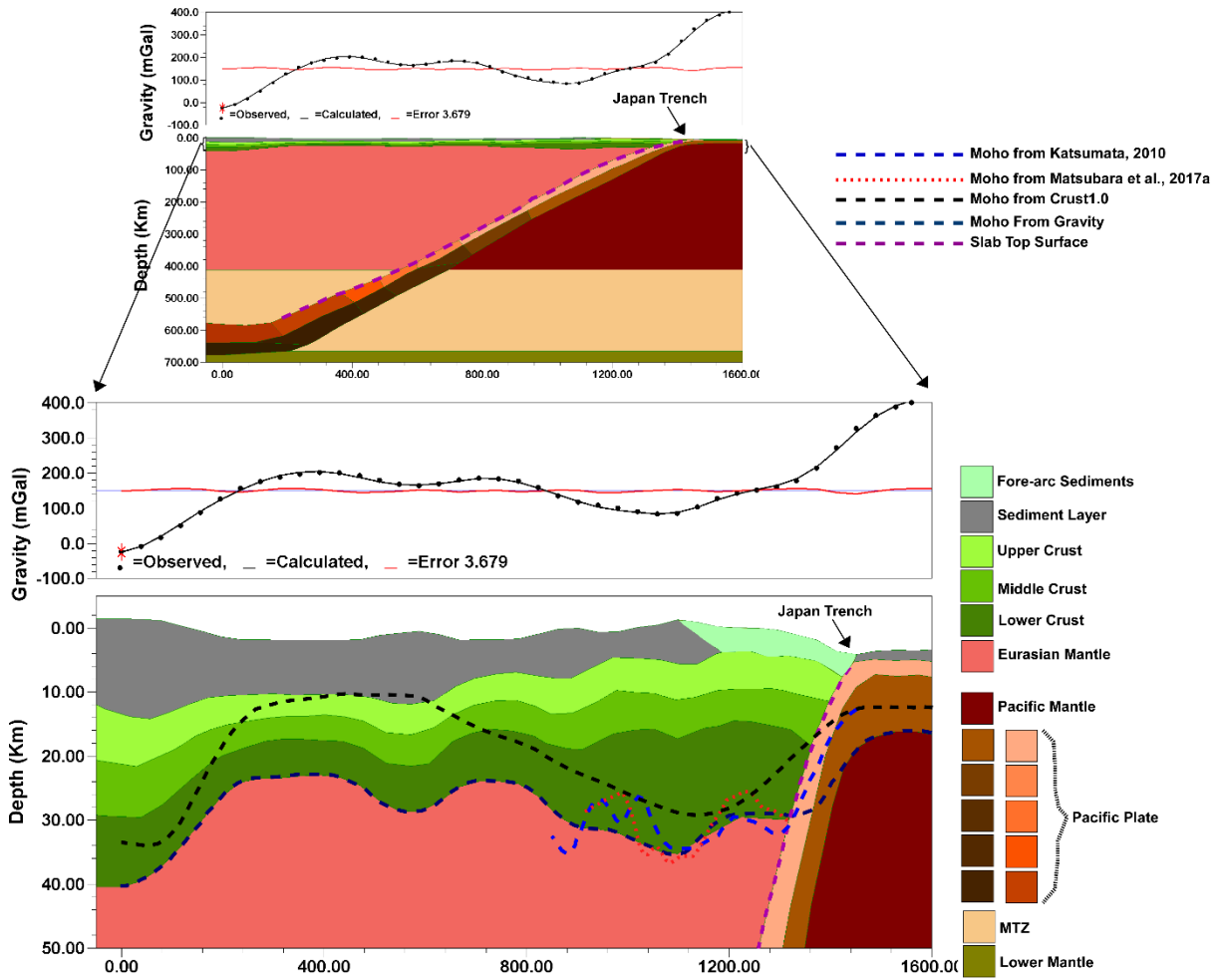
Figure 2.14: b) 2-D cross-section for the Japan Trench (continued)
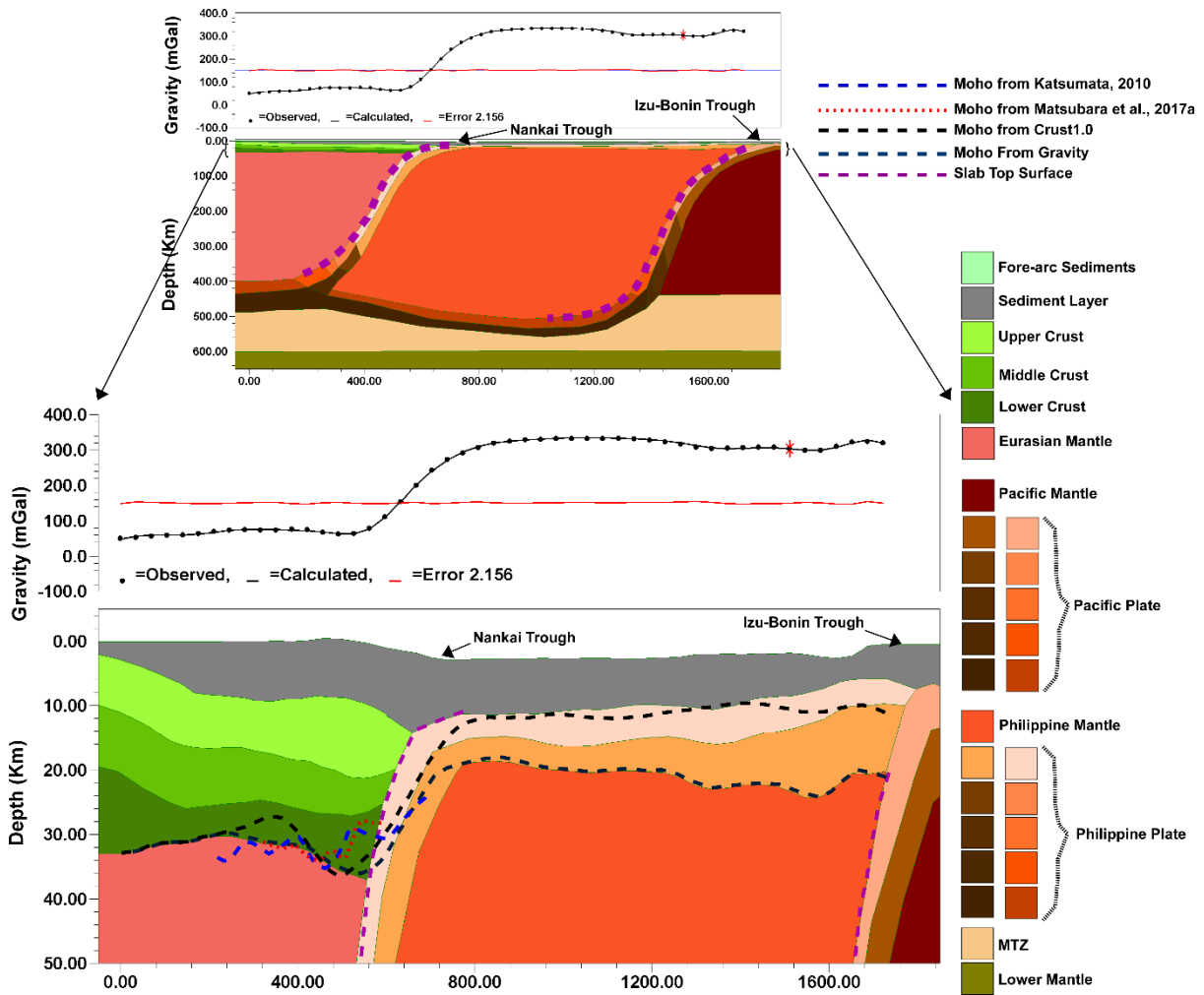
Figure 2.14: c) 2-D cross-section for the Izu-Bonin and Nankai trough. The misfit of all three cross-sections among the calculated and observed Bouguer data is around 3.0 mGal, with the majority of the misfit occurring in the areas of stagnant slabs and trenches. The oceanic crust has high density and low thickness, unlike the continental crust with high thickness and low density.

2.6 Discussion

2.6.1 Tectonic implications of Gravity inverted Moho

I used gravitational data because of their wide coverage to compensate for the lack of data and studies in offshore areas. Based on Bott's method and Tikhonov regularization, the anomalous Moho was discretized using tesseroids to develop the first-order Moho depth map. The 3-D Moho depth model was then constrained using the available deep seismic profiles, receiver functions, and geological information to produce a regional crustal thickness model for the subduction plates around the Japan Islands. The depth of the Moho map covers the area around the Japan Islands and subduction zones northwest of the Pacific plate. The developed Moho depth model was compared with the compilations of seismic estimates showing good agreement and high levels of consistency. The variation of Moho depths from one region to another along and around the Japan Islands refers to the different ages and origins.

Moreover, the geological and tectonic events that created and affected the formation of the crust layers can be identified as follows: 1) arc–arc collision (i.e., the buoyant subduction of the Philippine Sea plate in SW Japan and the Hidaka and Izu collision zone); and 2) back-arc extension (Okinawa Trough) and the Japan Sea (Matsubara et al., 2017a). Generally, tensile tectonic stress causes the crust to become thinner, owing to such extension. While the Japan Sea formed in the Miocene and Pliocene, the Japan Islands separated from the continental crust and bent southeastward. During the late stages of the back-arc opening of the Japan Sea, the failed rift basins then developed in the middle of the Miocene. The thin crust of the Japan Sea (i.e., shallow Moho) formed consistently during rifting. Beneath the rift basins, a slightly convex mafic core with high Vp is evidence of the continental rift zones (Matsubara and Obara, 2011; Matsubara et al., 2017a).

Furthermore, low gravity reflects high post-rift sediments reaching about 6000 m (Tsuchiya, 1990; Sato, 1994). In NE Japan, the sedimentary basins have at least 2000 m Upper Cretaceous to Lower Miocene sedimentary thickness and trends NNE. Likewise, the accretionary wedge in the Shimanto belt reflects immature middle and lower crust development beneath the trench sediments. In contrast, in the collision zone of Izu and Hidaka, the arc–arc collision synchronizes with the thickening of the crust. In Hokkaido's central region, a thick crust was formed by the collision of the Kuril arc with the northeastern arc of Japan in the Miocene. South of the Japan Islands (Kyushu and Shikoku), the Moho depth is relatively deep because

of the thick crust around the mantle wedge. The Moho depth map shows deep depths consistent with the collision axis, reflecting negative BAs. In the northern region, the upper crust of the Izu collision zone accretion to the overriding Eurasian plate as the accretion of the middle and lower crust of the Philippine plate deepens the Moho in this area. The deep Moho north of Japan reflects the original crustal character of the stable arc block.

Crustal thickening refers to under-plating and shortening deformation since the Pliocene. Magma under-plating plays a role in the crustal thickening process. The stable craton is a crustal character of the Korean Peninsula, where SW Japan was attached and has since separated. The high thickness of crust in the SW region of the study area resulted from the intrusion of Cretaceous granites and intense magmatism along the margin of the Asian continent. Liu et al., (2017) estimated that the age of the eastern edge of the Pacific slab is approximately 90 Ma, while the part near the Japan trench is approximately 135 Ma. The slab was deformed and stagnant in the MTZ and uppermost lower mantle. The sinking rate of the Pacific slab is 3.1–6.9 cm/yr, and the slab advancing rate is known to have changed from 6.1 to 7.7 cm/yr. The subduction of the Paleo-Pacific (Izanagi) plate destroyed the North China craton during the Early Cretaceous. In contrast, the extensive volcanic intraplate spread of the East Asia back-arc Cenozoic lithosphere destruction occurred due to the movement of the present Pacific slab.

2.6.2 Gravity inverted Moho compared with isostatic Moho

I estimate the depth of the isostatic Moho surface using Airy's theory (Steffen et al., 2011a; Fu et al., 2014; Fu and She, 2017). The isostatic Moho associated with the geoid anomaly can refer to the crustal compensation depth (Haxby and Turcotte, 1978; Hees, 2000; Fullea Urchulutegui et al., 2006), whereas the gravity Moho reveals the undulation of the true Moho (Hao et al., 2006; Shin et al., 2007; Steffen, Steffen, and Jentzsch, 2011b; Guy, Holzrichter, and Ebbing, 2017; Xuan, Jin, and Chen, 2020). The gravity Moho is identical to the isostatic Moho by only a few kilometers (Fig 2.15). The earth's crust's isostatic stage is usually determined by directly comparing isostatic Moho and gravity Moho (Guy, Holzrichter, and Ebbing, 2017). A significant discrepancy is visible in the Kuril and Japan trench area and the high mountain areas, which appear compared with the region's topography (Fig 2.2),

suggesting a state of non-isostatic compensation of the crust. Figure (2.16) shows a discrepancy between -4 and 4 km in most areas.
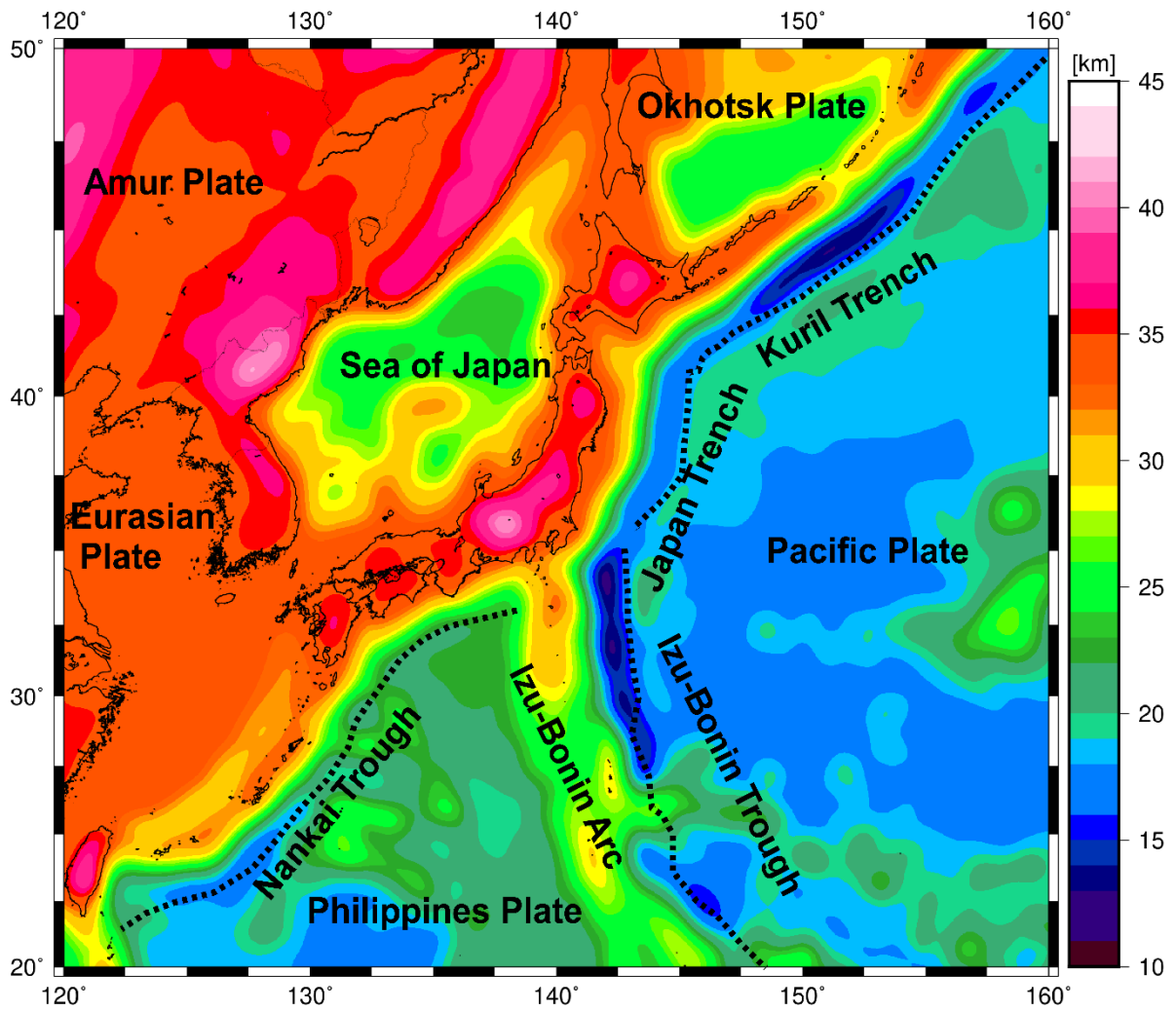
Figure 2.15: Isostatic Moho depth.
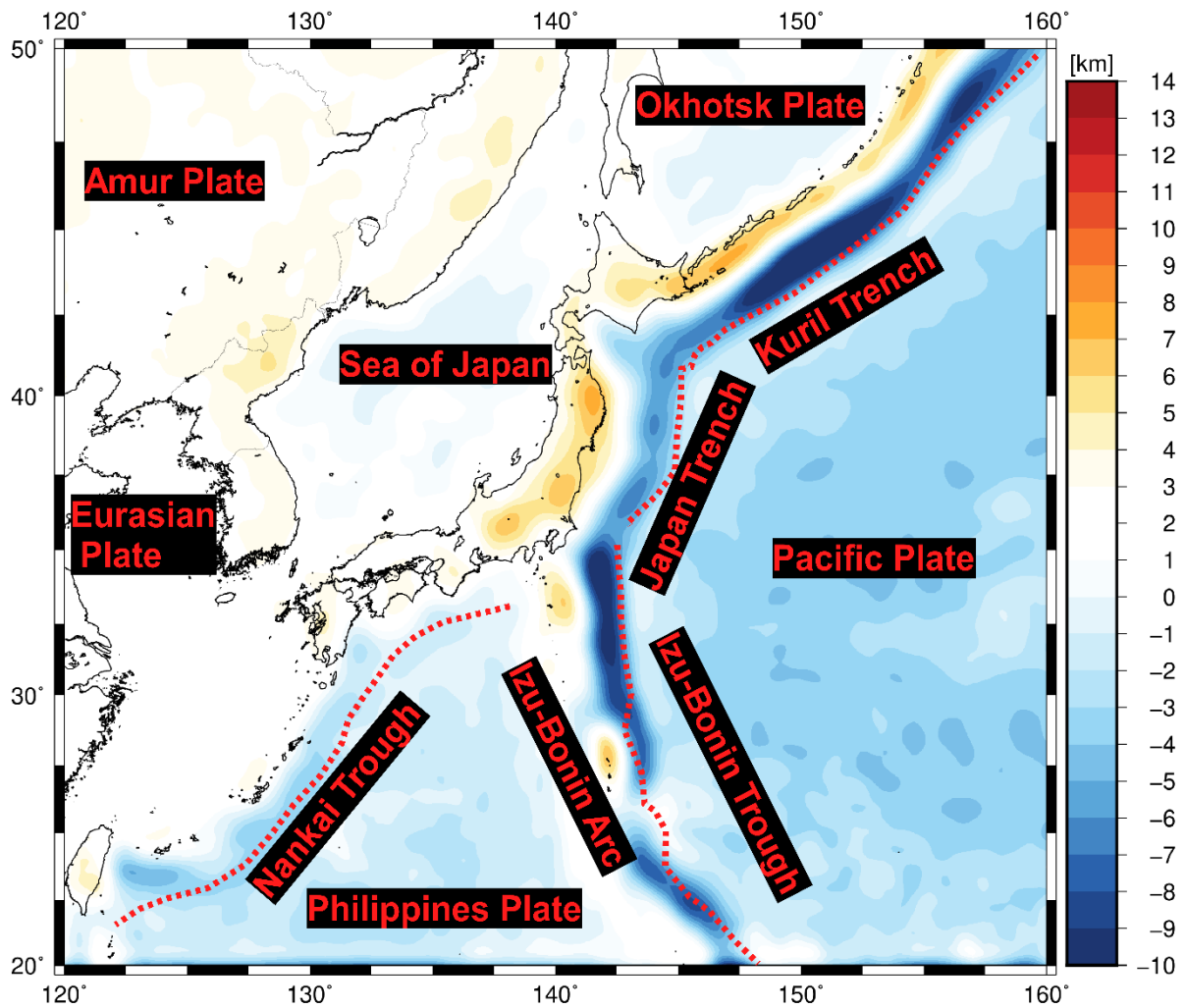
Figure 2.16: Discrepancy between the Moho depths from isostasy and gravity inversion, clearly showing the non-isostatic compensation at the Kuril and Japan trench and high topographic areas.

2.6.3 Uncertainties

Crustal layers Thickness

I used layer thickness data from the CRUST 1.0 model (Laske et al., 2013). To measure the accuracy of the thickness of the layers in the area and the subsequent calculation of its effect in Bouguer anomaly, I calculated the Moho depths by inversion of Bouguer anomaly without removing the sediment layer effect Fig 2.17. The divergence between the Moho depths with sediment layers and Moho depths without sediment layers is shown in Fig 2.18

Misfitting between gravity and seismic Moho depths

The Moho depths also show clear agreement with the tectonic features of the area. When there is unlikeness, the misfit lies within the margin of the differences between the two different physical properties. The differences between the mean and standard deviation of the Moho depths were estimated by comparing seismic depths (Katsumata, 2010) and Moho depths estimated from gravity inversion Fig 2.12b. The differences ranged between 0.7 and 7.0 km, with a mean of -0.78 km and a standard deviation of 2.69 km.

2.1.1 Discussion Summary

The modeled Moho depths exposed crustal thinning trends toward the Pacific and Philippine Sea plates. The eastern part of the region (the western Pacific Ocean) is characterized by a shallow Moho depth and low thickness of the crust and sedimentary layers. In addition, the oceanic crust density values were higher than those of the western part of the region (i.e., the eastern part of the Eurasian plate). Trenches (i.e., subduction zones) are characterized by the lowest layer thickness, lowest depth, and lowest topography. The Japan Sea has a relatively high crust and sedimentary layer thicknesses and a high Moho depth. Significant variations in the Moho geometry appear to be sensitive to the large-scale tectonic framework along the trenches. Finally, my model demonstrates the advantage of gravity data inversion in studying the 3-D density structure of geologically unique formations, where the bouguer anomaly data are combined with a priori information retrieved from petrophysical (e.g., density values) and seismic datasets. I found that Moho depths can be estimated accurately using gravity inversion

in areas with limited seismic data. Most of the inaccuracy in the 3-D density model occurs within the trenches.
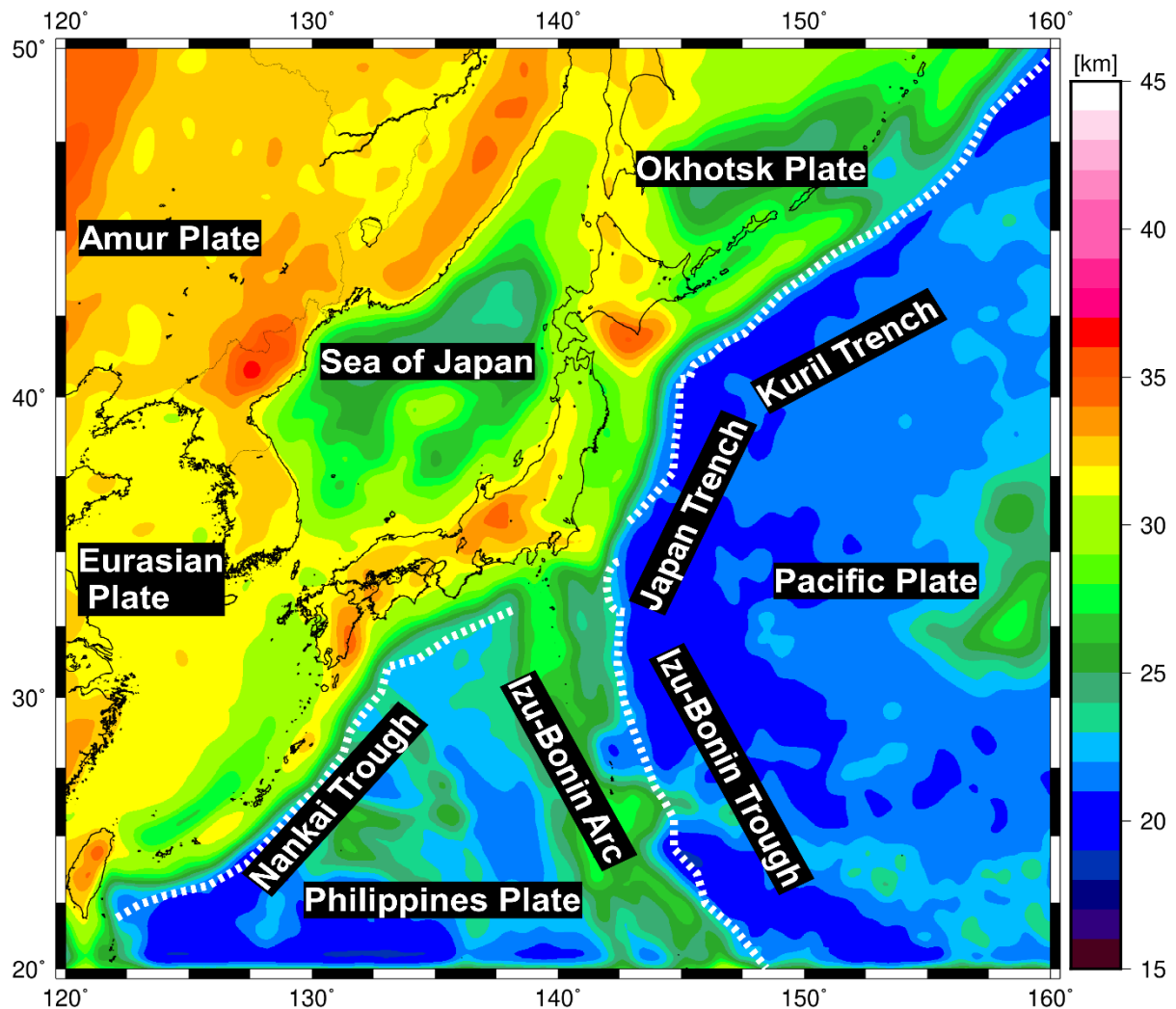
Figure 2.17: Moho depths from the gravity inversion without removing the sediment layer effect, ranging from 18 to 40 km. The areas of shallowest Moho-depth are the Pacific and Philippines Sea plates, while the areas of medium Moho-depth are the Japan Sea, Okhotsk Plate, Izu-Bonin arc, and the areas of highest Moho-depth arethe continental regions of the Japan islands and the Asian plate.
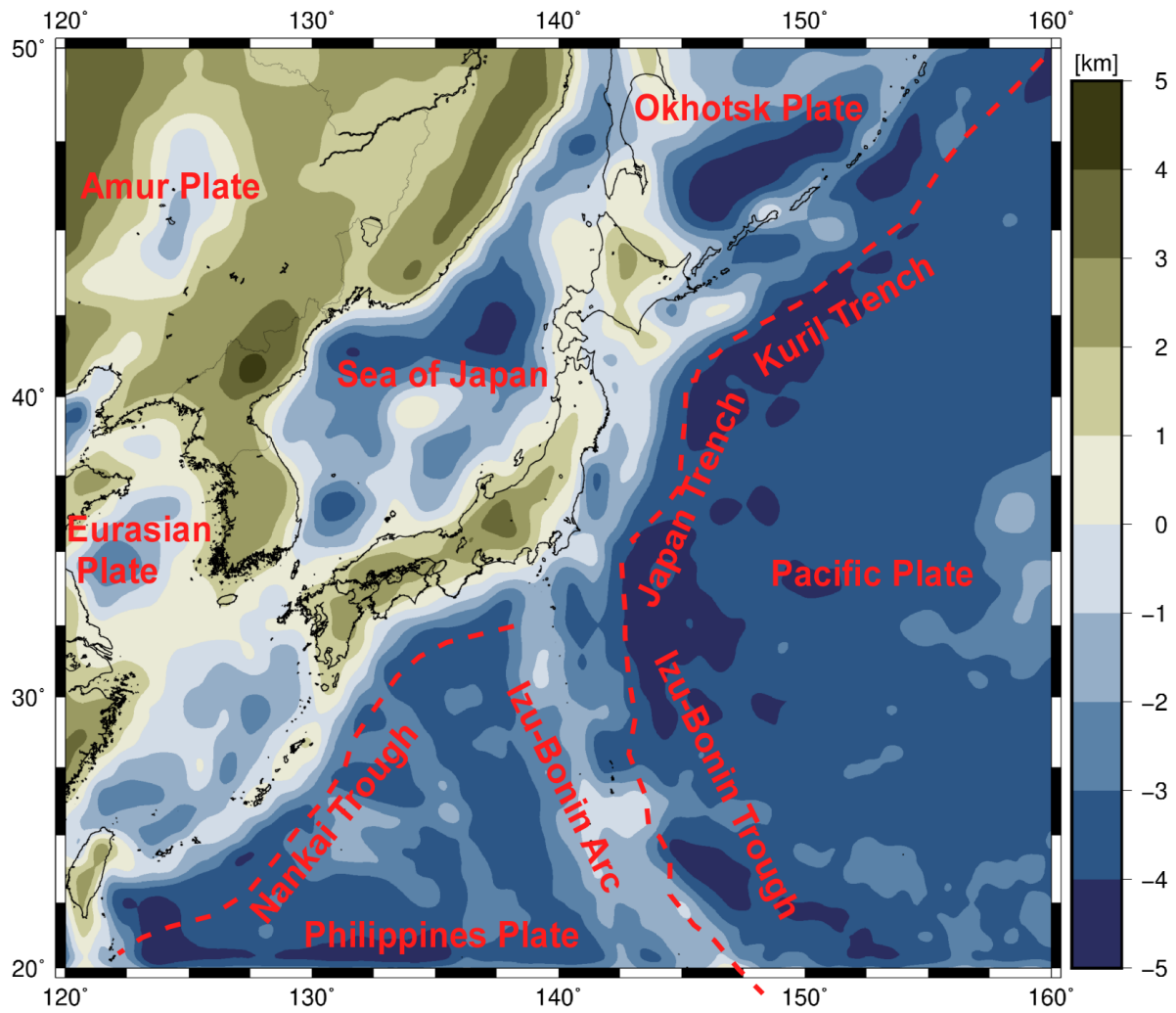
Figure 2.18: The misfit between the Moho depths with and without removing the sediment layer effect from the Bouguer data. The range of misfit is between -5.0 to 5.0 km, which is acceptable in potential field methods.

2.7 Conclusion

The subduction plates that surround and have formed the Japan Islands represent a result of the collision between the Pacific and Eurasian plates. The Pacific Ocean crust has a high density and low thickness compared to the Eurasian crust, which caused the subduction of the Pacific slab under the Eurasian plate. That is the same as the Philippine Sea plate with different directions and speeds. The extensive coverage of satellite gravity data allowed us to create a 3-D model of the earth layer density distribution. From this, I performed the first 3-D gravity data inversion of the area around the Japan Islands and subduction plates west of the Pacific plate. The inversion aimed to model subduction plates around the Japan Islands and estimate the Moho depths and crustal thickness. The inversion and modeling processes were constrained to the available receiver function, tomography, crustal thickness models, and geological information. The Bouguer data for the western Pacific subduction zone area were calculated using the free-air data derived from the latest GOCE model (GOCO06s), topography data from the ETOPO1 model, and crustal thickness of the CRUST1 model. Comparing the estimated Moho depths and the model appears compatible and consistent with previous seismic tectonic features. Slab2 model constrains the geometry of the stagnant Slabs in the cross-sections, whereas the CRUST 1.0 model constrains the thickness and density of each layer.

Chapter 3

Integrated Geophysical and Petrological Modeling of Lithosphere beneath the Japanese Islands

3.1 Introduction

The northwestern Pacific Ocean offers an outstanding opportunity to study the Lithosphere and asthenosphere boundary at the Subduction zones. My aim is to analyze the thermochemical structure of the mantle in the Northwest of the Pacific Ocean. Factors like seismically active zones, ore deposits, seismic velocity anomalies, sedimentary basins, and tectonic boundaries are the basis of the evolutionary model of the Lithosphere and sub lithospheric upper mantle. The layer between the rheologically strong mantle (Lithosphere) and the rheologically weak upper mantle (asthenosphere) is called Lithosphere Asthenosphere Boundary (LAB). I have used integrated geophysical-petrological Lithospheric Modeling (LitMod3D) software (Fullea et al., 2009) to model the Lithospheric thermochemical structure. LitMod3D integrates the fitting of the available geophysical and petrological/geochemical observations simultaneously to reduce the uncertainties associated with fitting each observable separately. The study aims to (1) the origin and evolution of the Lithosphere beneath the Japanese Islands, (2) the nature of the lithospheric/sub lithospheric mantle coupling, (3) the relationship between surface features and deep-seated processes, and (4) the emplacement of significant ore deposits, among others. By combining geological, geophysical, and petrological parameters in a thermodynamic framework, I present a new crust and upper mantle cross-section of the Japanese Islands and Northwest Pacific Ocean. Integration Interpretation of various geophysical and geological data would constrain and minimize the interpretation uncertainty. The variations in the lithospheric mantle composition retrieved from global petrological data are compatible with the Lateral variations of the seismic anomalies. To study the configuration factors of the lithosphere beneath the Japanese Islands and at the Northwest Pacific plate, I need a well-constrained model of the crust and upper mantle's structural, thermal, geochemical and petrophysical architecture. I implemented integrated geophysical-petrological modeling of the lithosphere structures. The output model is the most fitted to gravity observations, geoid undulations, surface heat flow, elevation and the mantle seismic velocities, and the chemical composition, pressure and temperature of stagnant slabs. Seismology assesses the Earth's internal very well. The Logistic and Technical processes are responsible for the lack of seismic studies in Oceanic regions. The fundamental parameters for modeling lithosphere structures are seismic velocities, rock densities, temperature, and composition.

The Lithosphere structure of the area around the Japanese Islands is poorly explored due to the seismic network coverage covering only the continent areas and the complex tectonic situation.

Since the density milestone of the Moho, which is the interface between the crust and the mantle, and the base of the Lithosphere, which is the rigid tectonic plate, robust knowledge of the area xenoliths petrology in addition to the seismic tomography can combine with gravity gradients from the Gravity Field and Steady-State Ocean Circulation Explorer satellite to preserve the thermal and compositional structure of the Lithosphere. This study can use a self-consistent 3-D lithospheric density and temperature model depending on the satellite gravity gradients, Isostasy, and the thermodynamic petrology model of the xenoliths from the mantle beneath the Japanese Islands and the area around. The resulting crustal and Lithospheric thickness models can be compared with the global models and modified until the misfit is accepted. This study is the first of its kind to study the nature of the crust and mantle in the Northwest region of the Pacific Ocean and the area around the islands of Japan. This area is considered a challenge for any researcher due to the subduction zones and stagnant slabs.

3.2 Tectonic Setting of Japanese Islands

The Japanese Islands were formed by interacting with four plates, two oceanic plates (Pacific and Philippine), and subducted beneath two continental plates (North America and Eurasian). This interaction made the area active with volcanoes and earthquakes, which affected the geometry of subducted slabs. The released fluids of subducted slabs played essential roles in the geodynamic and geochemical phenomena along the arc (Nakamura et al., 2019) Fig.(3.1).

The Pacific plate subducts beneath the North American and Philippine Sea plates at the deepest Kuril–Japan–Izu-Bonin trench, which is 1,500 km wide from north to south (Goudie, 2004), while the Philippine Sea plate subducts beneath the Eurasian plate at the Nankai Trough parallel to the Median Tectonic Line, which is one of the most significant fault systems in Japan arcs. The subducted Pacific plate occupies a widespread area beneath the Japanese islands and forms a stagnant slab that partly overlaps with the subducted Philippine Sea plate beneath Central to SW Japan. The complex geometry of these plates, their interactions, and the unstable torque balance near the triple junction are mainly responsible for the evolution of Japan arcs (Takahashi, 2006a). Western Pacific had been impacted by plumes or hot regions (Miyashiro, 1986).

The complexity of Mantle peridotite's petrography and geochemistry reflects the active tectonic environment. The petrology of the sub-arc Mantle is less known because of the
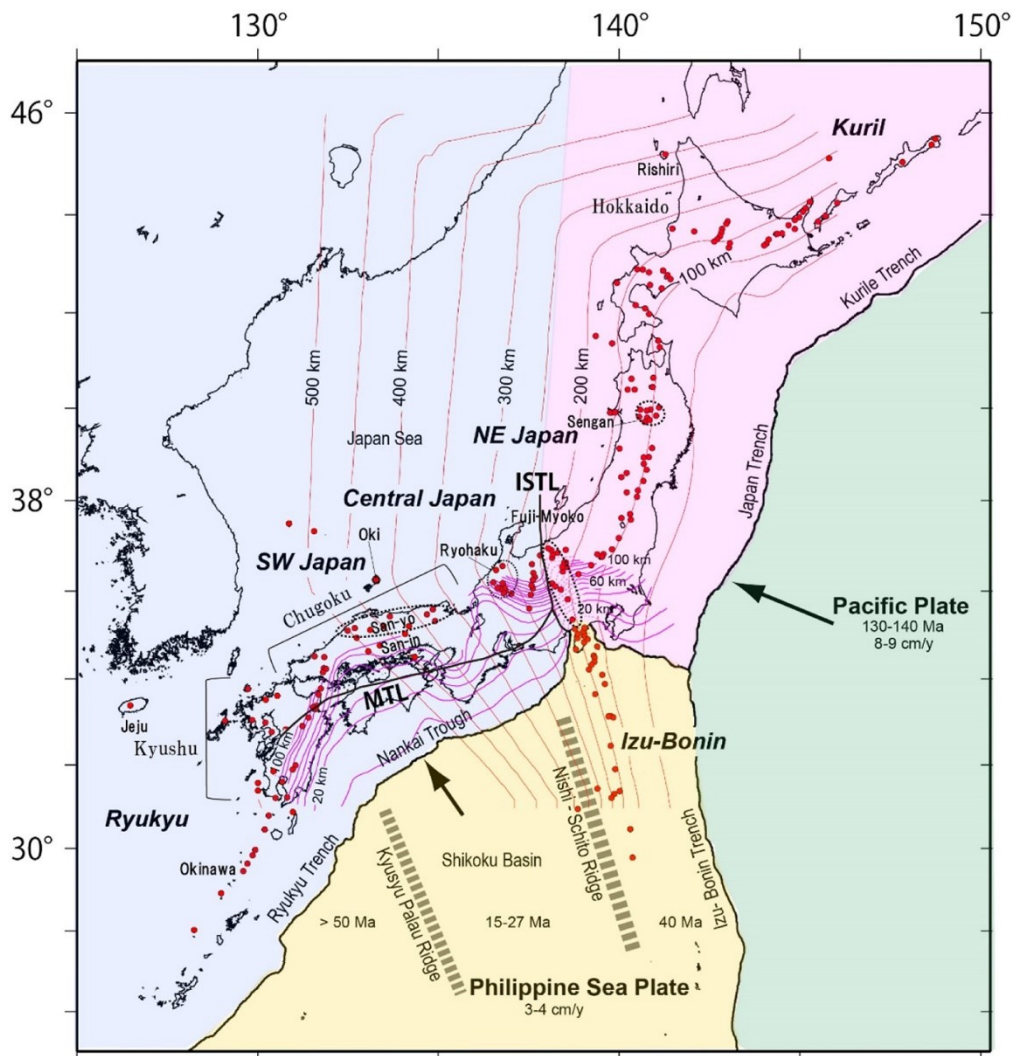
Figure 3.1: The Japanese Islands' tectonic setting. The depth contours of the Pacific and the Philippine Sea slabs are shown by thin red and pink lines, respectively (Nakajima and Hasegawa, 2007a; Hirose et al., 2008). Four transparent pink, blue, green, and yellow patches depict continental (North American and Eurasian) and oceanic (the Pacific ocean and the Philippine Sea) plates associated with Japan arcs. Small red circles depict Quaternary volcanoes in SW Japan, including several Neogene volcanoes dating 10 Ma. The six Japan arcs are displayed in strong italics (Kuril, NE Japan, Central Japan, Izu-Bonin, SW Japan, and Ryukyu) after (Nakamura et al., 2019)

deficiency of xenoliths (Nixon, 1987). Mafic and Ultramafic xenoliths from volcanos can refer to the materials and structures of the Lower Crust and Upper Mantle (Arai et al., 2000). Takahashi (1978) petrologically studied 85 mafic inclusions from 15 volcanoes west of Northeast of Honshu Arc and North of Southwest Honshu Arc Table (3.1). I intend to clarify the petrological properties of the upper mantle beneath the Southwest and Northeast of Japan. The importance of the xenoliths is to study the genesis of magma, the evolution of the island arc, and the structures of the crust and mantle. The basaltic magmas and their derivatives vary in composition from the volcanic front towards the inner arc, i.e., tholeiitic basalt, high alumina basalt, and alkali basalt, accompanied by calc-alkali rocks (andesite and dacite) (Kuno, 1960; Kuno, 1966). Sakuyama (1977) and Sakuyama (1979) suggested that the temperature varies from the high temperature at the volcanic front to the low temperature away from the volcanic front, and there are variations in chemistry and mineral assemblage of the rocks. The lower Crust of the Japanese Islands is composed of gabbro, amphibolite, and granulite. The lower Crust in Northeast Honshu is more hydrous than the lower Crust in Southwest Honshu. The peridotite at the volcanic front of active arcs Avacha of Kamchatka arc and Iraya of Luzon-Taiwan arc are highly depleted and low-pressure spinel harzburgite.

In contrast, the high-pressure origin fertile spinel lherzolite has been found through intermediate lherzolite–harzburgite of the backarc side of Japan island arcs at the Eurasian continental margin (from the Sikhote-Alin through Korea to eastern China) (Arai et al., 2007). The depleted sub-cratonic peridotite has been replaced with the fertile spinel lherzolite beneath the continental region by Asthenospheric upwelling. The xenoliths from the frontal part of the arc have differed from The xenoliths from the continent in lithology and geochemistry.

3.2.1 Southwest Japan

Takahashi (1975) studied mafic and ultramafic xenoliths, including spinel lherzolite from alkali-olivine basalt at the Oki-Dogo islands. The lower Crust and Upper Mantle were stratified with mafic and ultramafic rocks within basaltic magma. The xenoliths are categorized into five groups. The upper mantle is mainly composed of layers of spinel lherzolite, banded spinel peridotite, and banded plagioclase peridotite from lower to upper. The spinel lherzolite group is highly magnesian than the other groups. Because of the structures and chemical

compositions, the banded spinel peridotite and plagioclase peridotite were cumulated from anhydrous basaltic magmas. Some of their samples contain metamorphic textures. The upper mantle comprises several cumulated layers of peridotite and pyroxenite (Takahashi, 1978). The lower Crust is mainly composed of cumulates of gabbro and a highly recrystallized metamorphic granulite group. The equilibration temperatures from the geothermometer by Wood and Banno (1973) show that spinel lherzolite is about 1100° to 1200° C, banded spinel peridotite is from 1050° to 1150° C, banded plagioclase peridotite is from 1000° to 1100° C, gabbro is from 950° to 1050° C, and granulite is about 800° to 1000° C. Upper Mantle and lower Crust in this area are characterized with anhydrous conditions. The asthenosphere upwelling is the main reason for raising the temperature of peridotite xenoliths from Noyamadake, Kawashimo and Fukuejima, the Southwest Japan arc, to around (1250 – 1300° C). The absence of hydrous xenoliths in alkali basalts is due to melting and dissolution within the ascending basaltic magmas. The P-wave velocity of the lower Crust is about 7.0 km/s. The P-wave velocity increases gradually with the depth up to 8.0 km/s at the Moho discontinuity. The gradual increase of seismic velocity refers to the increase of peridotite and pyroxenite layers.

Table 3.1: Average compositions of the mafic inclusions (Takahashi, 1978).

Mineral	Northeast Honshu Arc	Southwest Honshu Arc	Izu-Mariana Arc
SiO_2	44.29	47.34	48.64
TiO_2	1.21	1.56	0.75
Al_2O_3	18.21	16.25	19.02
Fe_2O_3	5.08	5.06	4.47
FeO	5.99	5.93	6.19
MnO	0.15	0.16	0.16
MgO	8.51	8.51	5.83
CaO	12.45	11.31	12.37
Na_2O	1.62	2.28	1.49
K_2O	0.46	0.34	0.18
H_2O^+	1.28	0.82	0.68
H_2O^-	0.59	0.34	0.28
P_2O_5	0.15	0.08	0.05
Total	99.99	99.99	100.11
	26 analysis	38 analysis	21 analysis

3.2.2 Northeast of Japan

The ultramafic xenoliths were found in Northeast of Honshu arc, defined as granet lherzolite, spinel lherzolite, plagioclase lherzolite, olivine websterite, and hornbledite. The mafic xenoliths were defined as hornblende gabbro, pyroxene gabbro, and amphibolite. Shallow origin xenoliths like granite, metavolcanic, and metasediments (Takahashi, 1978). Kuno (1967) considered the ultramafic and mafic host magma slightly alkalic basalt. Katsui et al. (1979) reanalyzed the basalt lapilli and indicated that the basalt is magnesian high-alumina basalt. The lower Crust beneath the Northeast Honshu comprises hornblende gabbro and amphibolite. The upper mantle is composed of lherzolitic layers (garnet lherzolite, spinel lherzolite, plagioclase lherzolite) from lower to upper with a minor amount of olivine websterite (Takahashi, 1978). Garnet lherzolite has high Ca and Na, and lower Cr and Ti. Its bulk composition is represented by magnesian olivine and calcic plagioclase, which is why it is interpreted as metamorphosed plagioclase lherzolite. Pyroxene geothermometers estimated the equilibration temperature of spinel lherzolite from 800° to 1000° C, olivine websterite and websterite from 800° to 1000° C, hornblende gabbro and amphibolite from 600° to 700° C. Olivine, clinopyroxene, spinel, plagioclase, oxide, and glass were observed in half of the lherzolite xenoliths suggested that ultramafic xenoliths had hydrous mineral assemblages. The xenoliths of lherzolite were exposed to several partial melting and crystallization within hydrous mantle conditions and relatively geotherm slope (Takahashi, 1978) Table (3.2). The P-wave velocity is 6.6 km/s at the lower Crust, while in the upper mantle, the attenuation is high with an abnormal low velocity of 7.5 km/s.

Table 3.2: The petrological models of the mantle-crust stratification (Takahashi, 1978).

	Northeast Honshu Arc	Southwest Honshu Arc
Lower Crust	hornblende, gabbro, amphibolite	pyroxene, gabbro, granulite
Uppermost Mantle	plagioclase lherzolite with hornblende	dunite, wehrlite, pyroxenite without hydrous minerals
Upper Mantle	spinel lherzolite with hornblende	spinel lherzolite without hydrous minerals
Geothermal Gradient	800°C/30km	1000°C/30km

3.3　Methodology

The main aim of my study is to model the thermo-chemical structure of the lithosphere at and around the Japanese Islands.

3.3.1　Moho depth from Gravity Inversion

Uieda and Barbosa (2016) developed a nonlinear inversion of gravity data constrained with seismic results. One of the algorithm pros is using the tesseroids for forward modeling to overcome the Earth's curvature. I conducted the gravity inversion to overcome the ambiguity of the gravity method. High-precision satellite gravity data provide coverage of the earth's planet, which overcomes the lack of data over oceanic areas. The GOCE satellite gravity data used have the fortunate advantage that they are limited to wavelengths larger than 50 km, which makes them ideal for studying the regional crustal or lithospheric setting (Braitenberg et al., 2011; Braitenberg, 2015), for example, the Moho determination (Reguzzoni and Sampietro, 2012; Sampietro et al., 2014; van der Meijde et al., 2015), and lithospheric modeling (Hosse et al., 2014; Bouman et al., 2015; Sobh et al., 2019). This improved resolution and accuracy are of great interest for studies of the Earth, mainly in places where limited or inhomogeneous data is available and provides a unique opportunity for improving our knowledge of basic crustal structure in areas with inadequate data coverage like the Japanese Islands. The inversion algorithm is based on the modified Bott's method (Silva et al., 2014) with a Tikhonov regularization to stabilize the computed solutions in a two-step procedure. I used the Moho reference depth and the density contrast lower crust and uppermost lithosphere in the conducted gravity inversion. The reference depth was set as 2.0 km steps from 20.0 to 50.0 km, and the density contrast as 50.0 kg/m^3 steps from 250.0 to 600.0 kg/m^3. I used the combination of reference Moho depth and density contrast to produce the lowest misfit between the Moho depth from gravity inversion and previous seismic studies.

3.3.2　Integrated Modeling by LitMod3D and Model Assumptions

LitMod3D (Lithospheric Modeling in a 3-D geometry) (Fullea et al., 2009) performs combined geophysical-petrological modeling of the Lithosphere and sub-lithospheric upper mantle

within a thermodynamic geophysical framework. Parameters like temperature, pressure, and composition are prominent factors in this model. The output model figures the temperature, pressure, surface heat flow, density, seismic wave velocities, geoid and gravity anomalies, elevation, and lithospheric strength for every point fitting all geophysical and petrological observations. The approach of LitMod is based on the joint 2-D modeling of several geophysical observables (gravity anomalies, geoid height, surface elevation and surface heat flow) and seismic proxies (seismic velocities from wide-angle modeling and tomography results) that are interrelated through their dependence on the thermo-physical properties of the crust and mantle. LitMod3D (LIThospheric MODelling in a 3-D geometry; Fullea et al., 2009) is a forward modeling framework that uses the finite differences method to recalculate the temperature and heat flow gravitational and Isostasy for Lithosphere and sub-Lithospheric upper mantle. LitMod3D defines the LAB using Petrological, rheological, and thermal (1250-1350° C) definitions. In seismic, LAB is the layer between the Lithosphere (where high S-wave velocity) and the Asthenosphere (where low S-wave velocity). The LitMod3D software discretizes the model layers into regular cells in Cartesian coordinates. The first model consists of crust, Lithosphere, and the sub-lithospheric mantle. For every layer in the model parameters like bulk density, compressibility, thermal expansion coefficient, thermal conductivity, and radiogenic heat production. The algorithm depends on the temperature- and pressure-dependent model (Hofmeister, 1999) to calculate the thermal conductivity of the mantle considering the crust's thermal conductivity is constant. Constant surface temperature and constant LAB temperature define the conduction-dominated regions' thermal boundary conditions. The high-pressure and high-temperature experiments show that the bottom temperature is 1500∘ C (Fullea et al., 2009).

The density in crustal layers follows the thermal expansion and compression:

$$\rho(T, P) = \rho_0 - \rho_0\alpha(T - T_0) + \rho_0\beta(P - P_0), \tag{3.1}$$

where ρ_0 is the bulk density, α is the thermal expansion coefficient, and β is the compressibility. I used the Perple_X software (Connolly, 2005) to calculate the densities for the sub-crustal layers depending on the geochemical mantle composition (CaO, FeO, MgO, Al_2O_3, and SiO_2) scheme under the mantle conditions of temperature and pressure. Afonso et al. (2008) considered that these oxides are a reasonable basis for modeling the equilibria phase of the mantle. Each layer's heat production and thermal conductivity are established. A "transition"

47

zone (a buffer layer) with variable thickness and a continuous linear super-adiabatic gradient is assumed between the lithosphere and sub-lithospheric mantle (i.e., heat transfer is regulated by both conduction and convection, see (Fullea et al., 2009) for additional information). The geothermal gradient is supplied by an adiabatic temperature gradient below the buffer layer, which is forced to be in the range of 0.35 to 0.6°C/k. I used the scheme of the oxides from the previous xenoliths analysis (Takahashi, 1978).

3.4   Data Sets for Model Building

Data sets were used to build the model of the Japanese Islands can be categorized into three groups and summarized: (1) regional surface geophysical observables (elevation, surface heat flow, and potential field data) collected from global databases; (2) results on the crustal and lithospheric mantle structure from previous studies; and (3) lithospheric mantle compositions consistent with the lithospheric age and with the geochemistry of mantle xenolith suites.

3.4.1 Geophysical Fields Observables

Elevation

ETOPO1 is a 1 arc-min global elevation model produced by (Amante and Eakins, 2009). Fig 3.2 shows the variation of topography in the Northwest of the Pacific Ocean plate in the Japanese Islands area. Elevation ranges from -9000 at the Trench areas to 1500 m in the mountainous areas in the Japanese Islands and Eurasian Plate. Data of topography represent two domains. The first is the oceanic domain (the Pacific Ocean, the Philippines Sea, and the Sea of Japan), while the second is the continental domain (Eurasian plate and Japanese Islands).

Potential Field Data

The static gravity field of the earth is pivotal for geophysical and geodetic applications. One of these models is solely derived from satellite observations. The satellite data is sensitive to the long wavelength of the gravity field (Montenbruck and Gill, 2000; Rummel et al., 2002). The GOCE mission (2009-2013) was launched to increase the spatial resolution by 70 km for the requirements of geodetic,
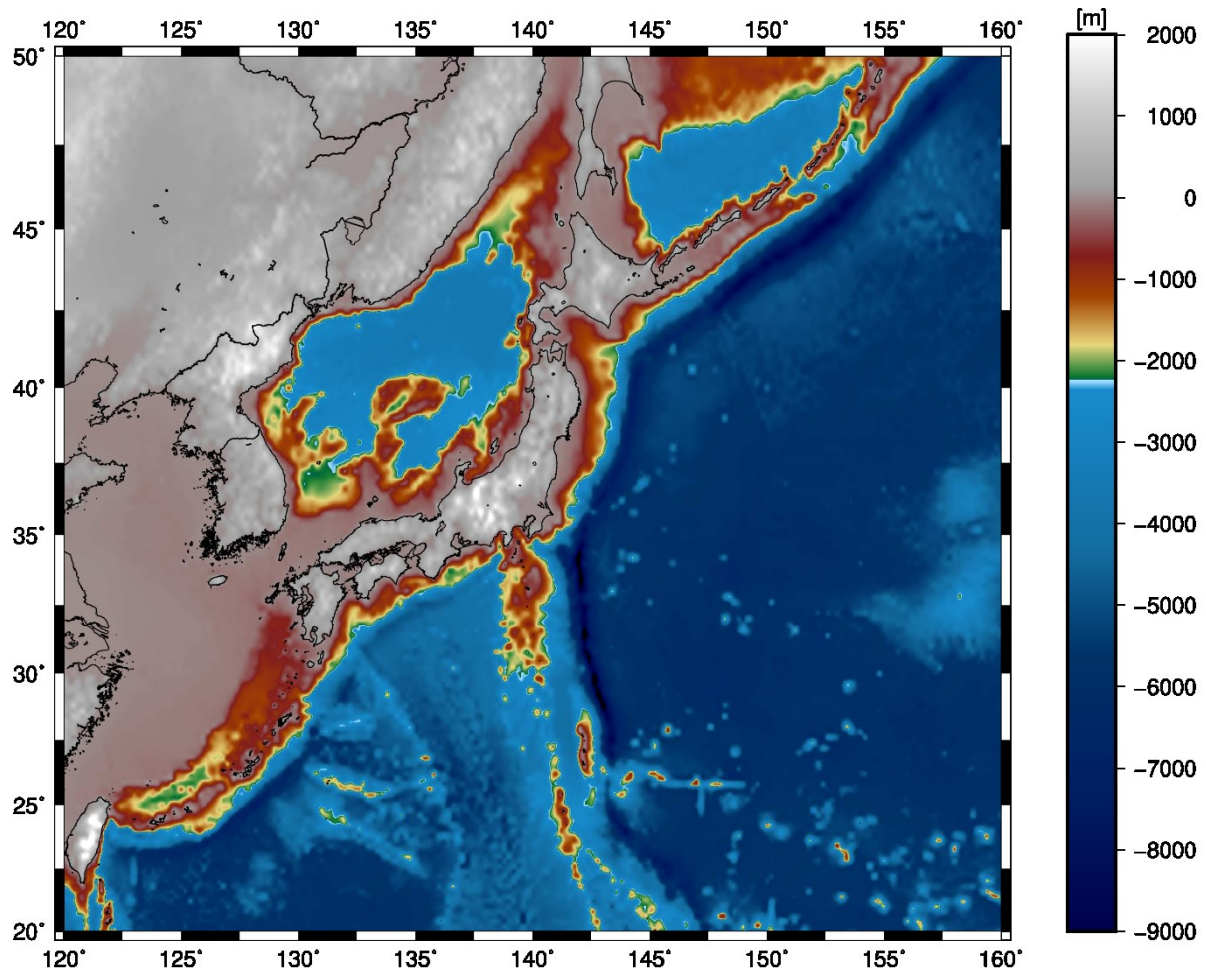
Figure 3.2: Topography map of the Japan island arc system based on the global model of ETOPO1 Global Relief data (Amante and Eakins, 2009). The area canbe classified into four units according to geomorphology: 1) high-altitude in the continental areas and Japan islands, 2) mid-elevated areas in the Japan Sea and at the Okhotsk and Eurasian plates, and 3) least-elevated areas offshore at the Pacificocean and the Philippine Sea plates.

geophysical and oceanographic applications. The focus of GOCE is on the static gravity field solution up to degree and order 300. The latest release of combined models is GOCO06s (Kvas et al., 2021). The satellite-only gravity field model combines gravity observations from multiple satellite missions and measuring techniques. In Lithospheric modeling, the different components of the full gravity gradient tensor are sensitive to potentially different depths. Theoretically, near-surface mass anomalies are detectable by gravity gradients (Martinec, 2014), while in reality, the contribution of every depth interval depends on the locations of the sources in the study area. In GOCO06s, the GRACE mission determined the long to medium spatial wavelengths, while the medium to short wavelengths was covered by the GOCE mission (Kvas et al., 2021). The gravity gradients are sensitive to the density structure of the crust and uppermost mantle (Bouman et al., 2016; Guy et al., 2017; Szwillus et al., 2016b). I used the gravity gradients at level 225 km ellipsoid elevation to evaluate my modeling results Fig.(2.14). Figure (3.3) depicts the gravity gradients in the Japanese Islands region. The trenches and troughs are obvious in every gradient by low anomaly combined with high anomalies, whereas the distinct tectonic plates are visible in the Vzz component, indicating significant changes in the lithosphere geometry.

The disturbance gravity map was derived from the GOCO06s model at 50 km ellipsoidal height Fig (3.4). The disturbance map shows low anomalies associated with high anomalies, which refers to Trench areas, compared with the topographic map, which refers to low and high topographic areas. The Topography effect on gravity was subtracted from Disturbance data to calculate the Bouguer anomalies map Fig (3.5). I used 2670 kg/m^3 onshore and 1030 kg/m^3 for the ocean seawater. The algorithm of Uieda and Barbosa (2016) was used the tesseroids and ETOPO1 model with 1 arc-min spatial resolution (Amante and Eakins, 2009) to calculate the topographic correction. The high Bouguer anomalies refer to the Oceanic Crust of the Pacific Ocean and the Sea of Japan, while the lower Bouguer anomalies refer to the Eurasian Plate's continental crust and the Japanese Islands. Lithospheric distribution of the density and the masses geometry were obtained by Geoid anomaly (Bowin, 2000). Figure (3.6) shows the correlation of high geoid anomaly with the topography map of the area. Low geoid anomalies refer to trench areas, while high anomalies refer to continental areas.
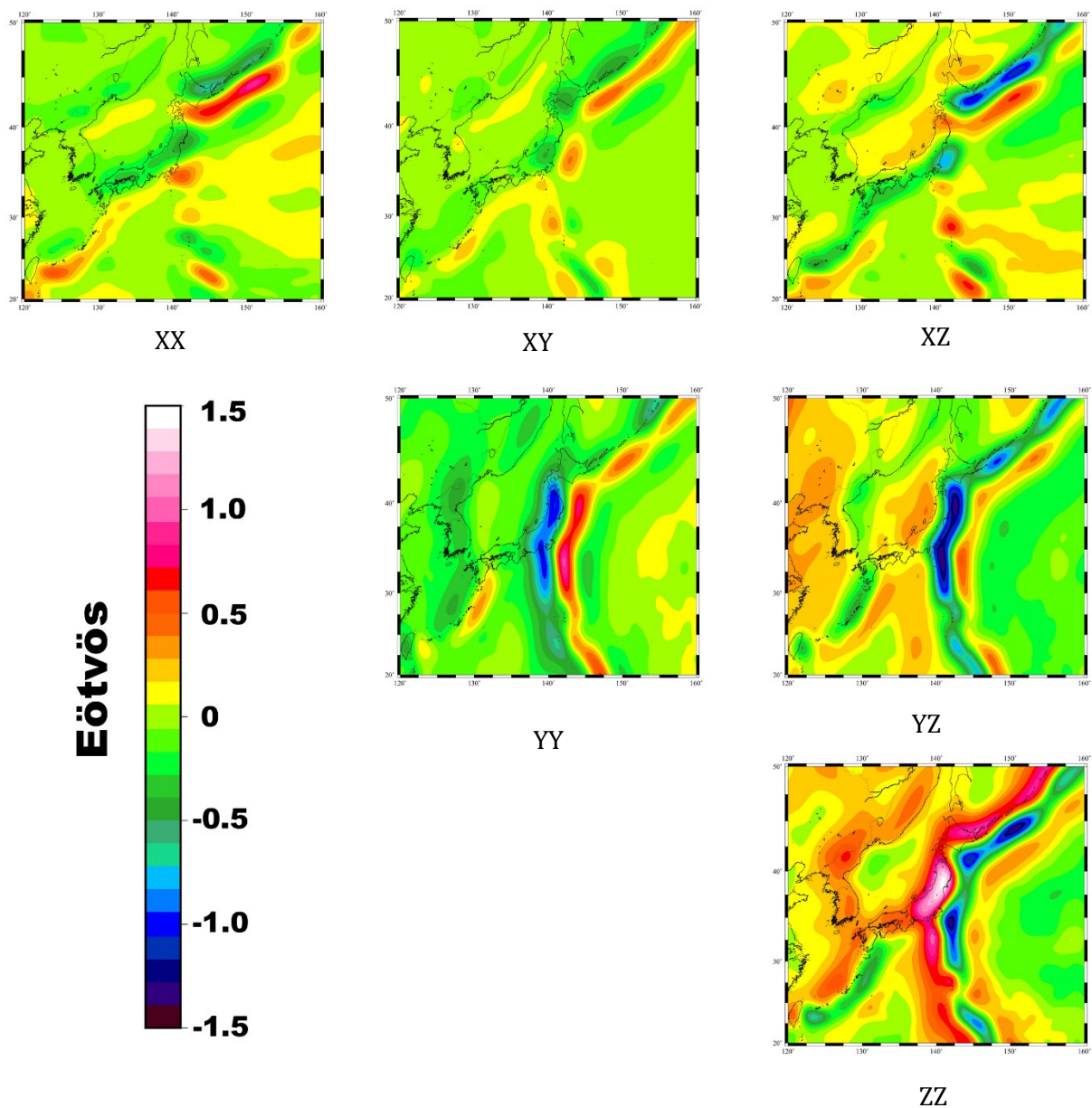
Figure 3.3: Maps of gravity gradient components derived from the GOCE satellite mission (Bouman et al., 2016) at 225 km above the ellipsoid. In the single maps, sub-indices of the gravity potential *V* denote its second derivatives of the Earth's potential (i.e., the gravity gradients). All gradient components were rotated into an Earth-related coordinate system suitable for forward modeling: *X* refers to the East, *Y* to the North, and *Z* points radially to the Earth-related center of the coordinate system in the Earth's center.
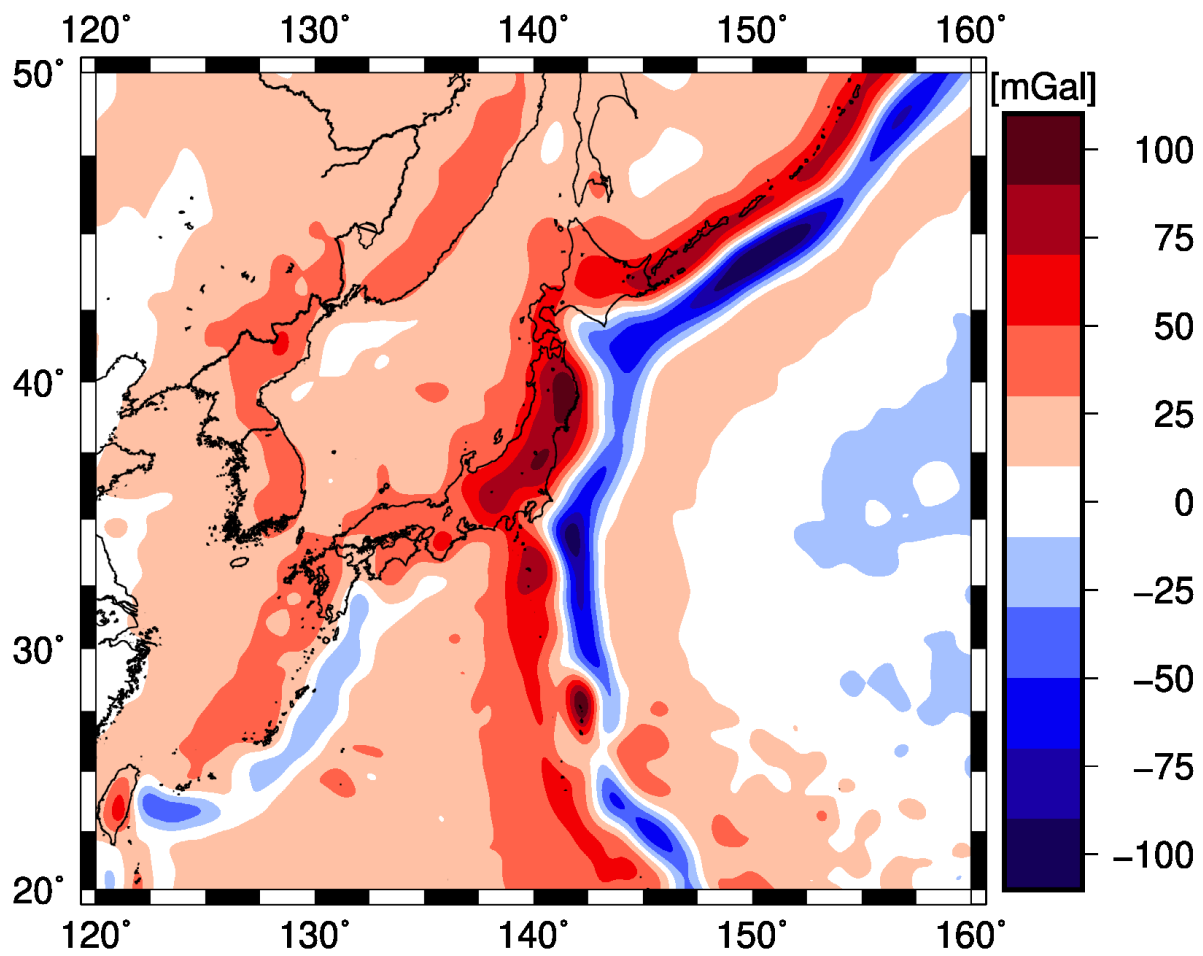
Figure 3.4: Disturbance map calculated from GOCO06s.

3.4.2 Basic Information for Model Building

Despite the spread of seismic monitoring station networks on and around Japan's islands, the marine areas were not well covered. There are differences among the regional models of Lithosphere based on the differences in spatial resolution, modeling technique (Laske et al., 2013; Reguzzoni et al., 2013; Tugume et al., 2013; Globig et al., 2016), spatial constraints, and the evolution of the models. The combination of available geological, seismic, and petrological data with the satellite gravity missions helped study and examine isolated geographical areas.
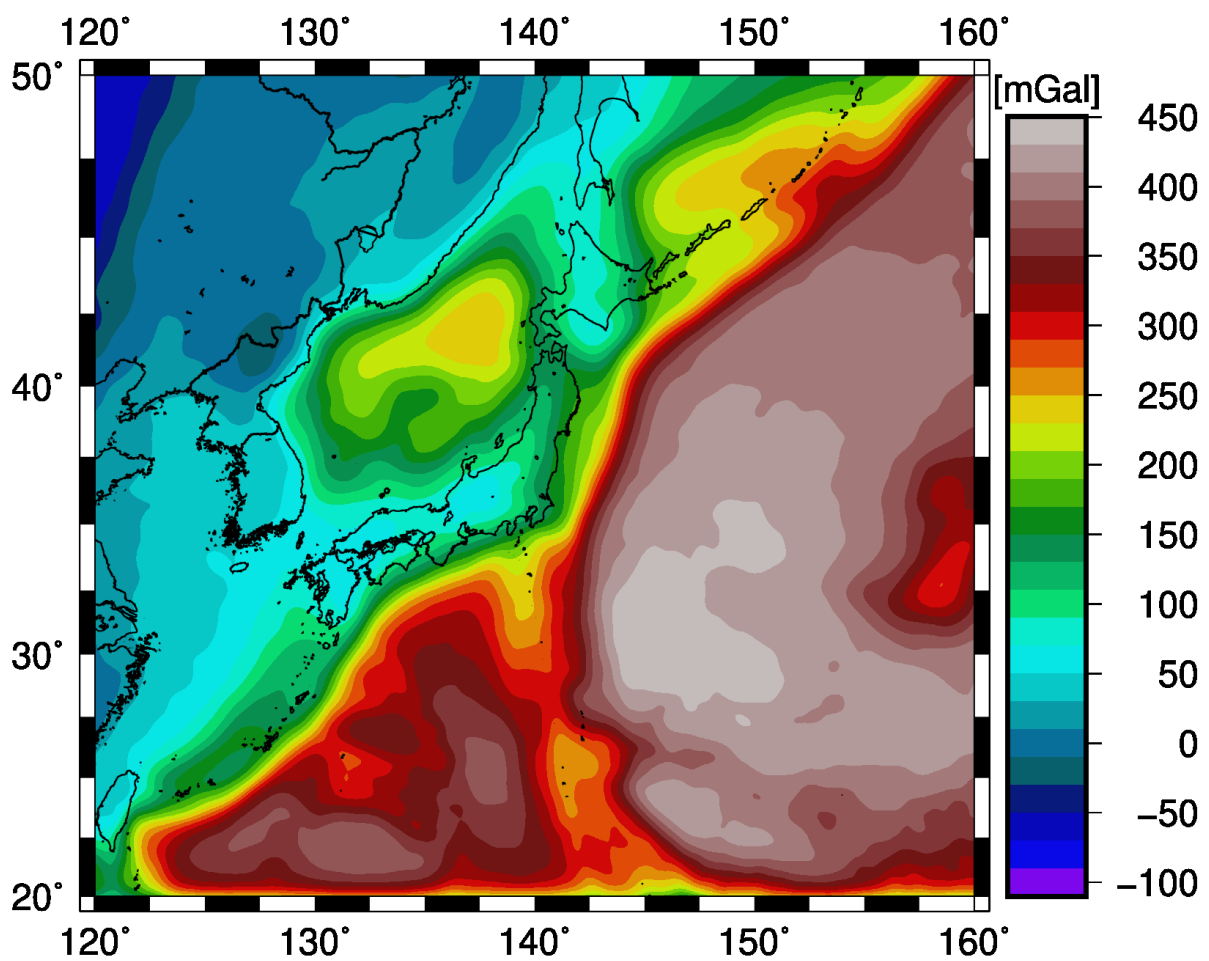
Figure 3.5: Bouguer gravity anomaly map from GOCO06s.
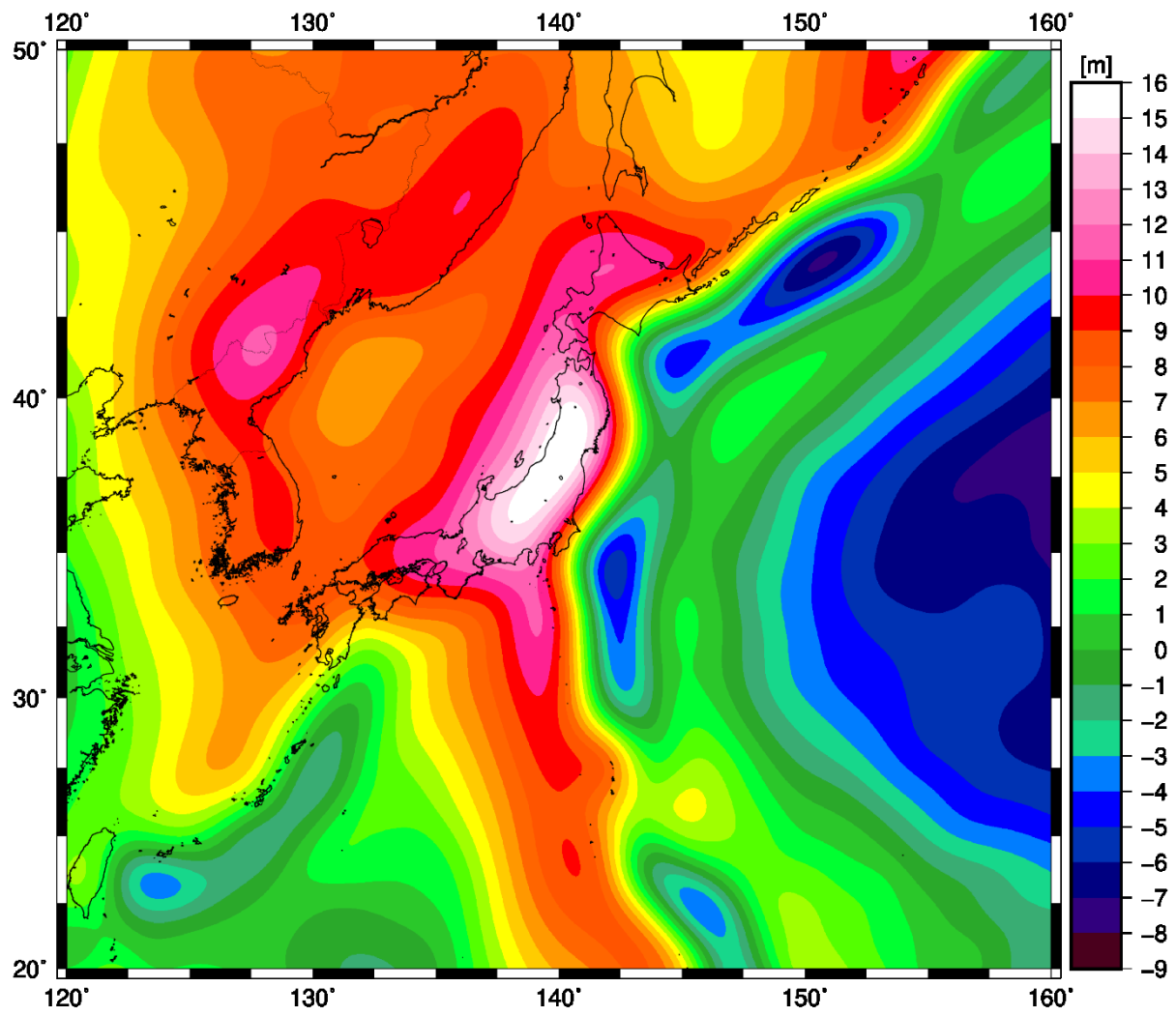
Figure 3.6: Geoid Height of the Japanese Islands area.

Gravity Inverted Moho

I used the disturbance map calculated from the GOCO06s satellite combined gravity model (Kvas et al., 2021) to calculate the sediments free Bouguer anomaly map by subtracting Topographic and total sediments effects from the disturbance map based on the algorithm of (Uieda and Barbosa, 2016). Figure (3.7) shows the previous Seismic results of Katsumata, 2010, used to constrain 3-D gravity inversion. A tesseroid model is created to reproduce the preprocessed gravity signal, parameterized by (1) a regularization parameter that controls the smoothness of the model Fig (3.8); (2) the reference depth (normal Earth Moho depth: Zre f); and (3) the density contrast $\Delta\rho$ at the Moho boundary. The final reference Moho depth was 34.0 km in my study, and the density contrast was 600.0 kg/m^3. Moho depths from the gravity inversion in the area range from 14 to 43 km. Figure (3.9) shows the mismatch between the depths of Moho estimated by gravity inversion and the depths calculated from seismic studies.

Sedimentary Thickness and Moho Interface

The Sediment layer thickness was retrieved from the CRUST1.0 model Laske et al. (2013). The thickness of sediment layers ranges from 0 to 11 km. The continental regions of the area (the Japanese islands and the Eurasian plate) contain a thick sediment layer, whereas the oceanic regions have a thin sediment layer Fig(3.10). The Moho depths from gravity inversion in the study region range from 13 km in trench areas to 43 km in mountainous areas Fig(3.11).

Lithospheric Thickness

The Lithosphere Asthenosphere Boundary (LAB) is the layer between the lithosphere (strong mantle) and the asthenosphere (weak upper mantle) (Artemieva, 2009). I utilized the LithoRef18 model by Afonso et al. (2019) to estimate the LAB thickness. The LAB depths in the region are depicted in Fig (3.12). LAB depths range from 27 to 218 km. Low LAB depths are observed in the Eurasian plate, the Sea of Japan, and the Izu-Bonin arc. The LAB layer is moderately deep in the Pacific Ocean and the Philippine Sea plates. The trenches and Japanese Islands have the area's deepest LAB layer. The first model can be built with Moho and LAB depths. The geometry of the layers can be modified to achieve low misfitting.
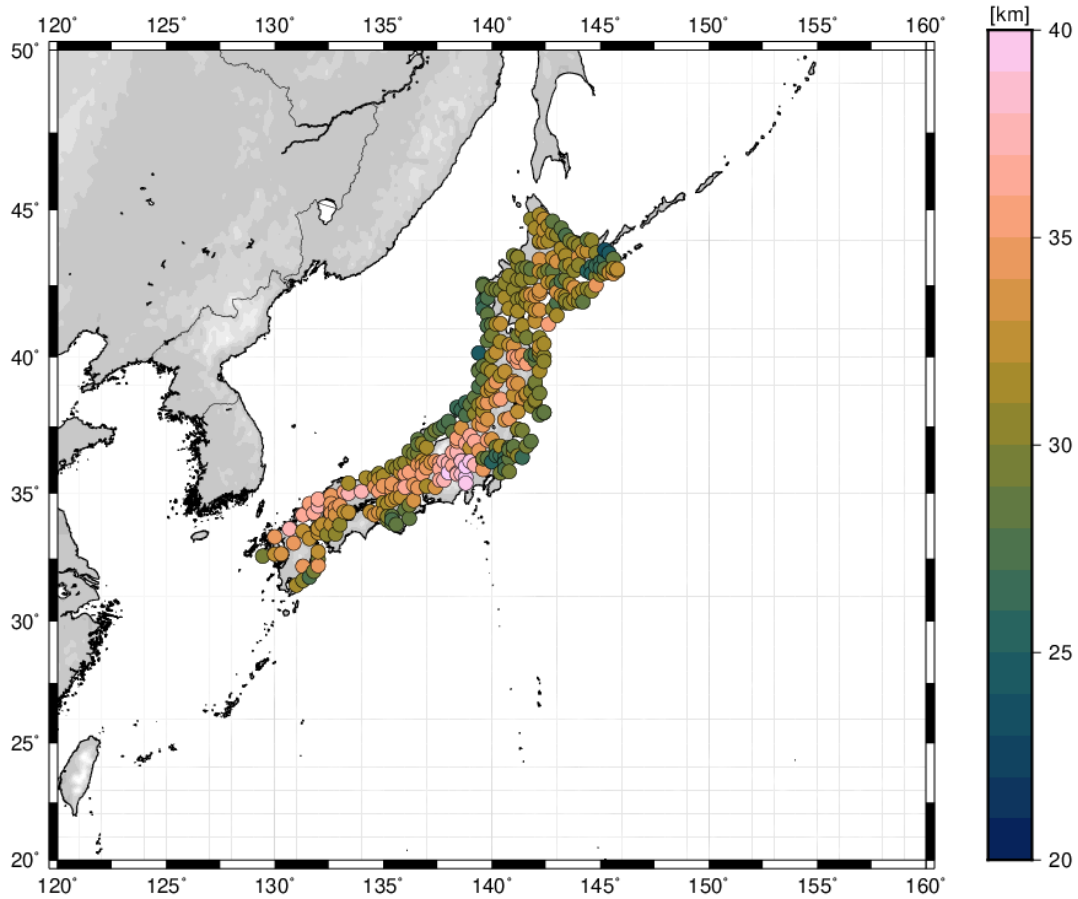
Figure 3.7: (Katsumata, 2010) Moho depth from travel time analysis.
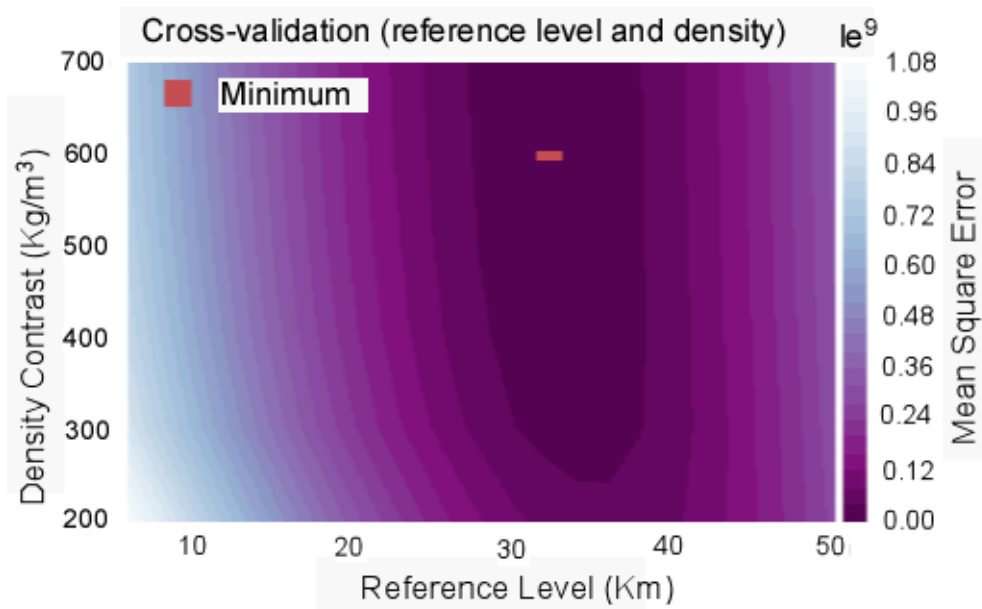
Figure 3.8: The gravity inversion parameters. The regularization parameter is $1e^{-10}$, the reference depth Z_{ref} is 34.0 km, and the density contrast $\Delta\rho$ is 600.0 kg/m^3.
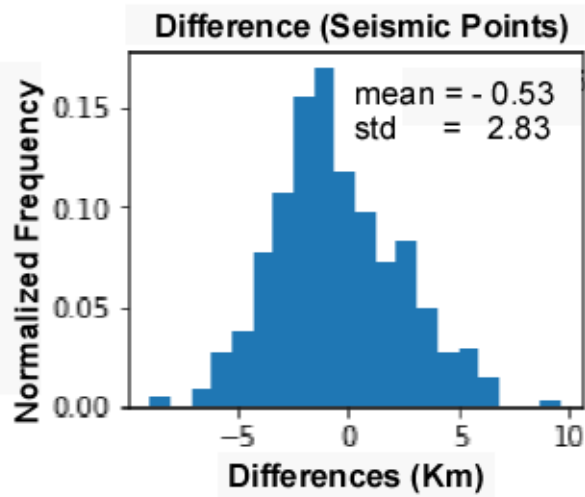
Figure 3.9: The misfit between the estimated Moho depths from gravity inversion and Moho depths from the (Katsumata, 2010) seismic study.
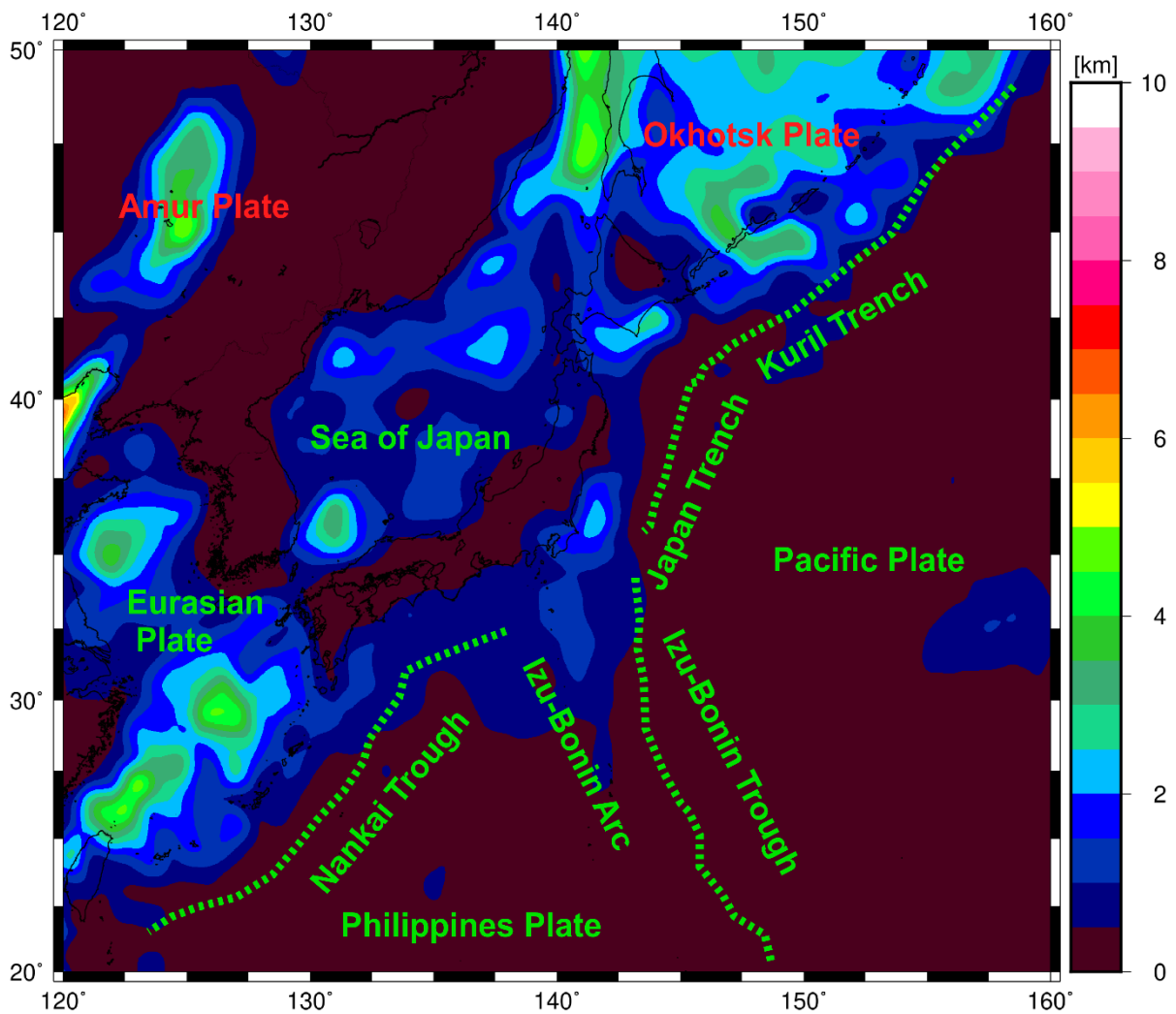
Figure 3.10: Thickness of sediments layer from CRUST1.0 model Laske et al. (2013).
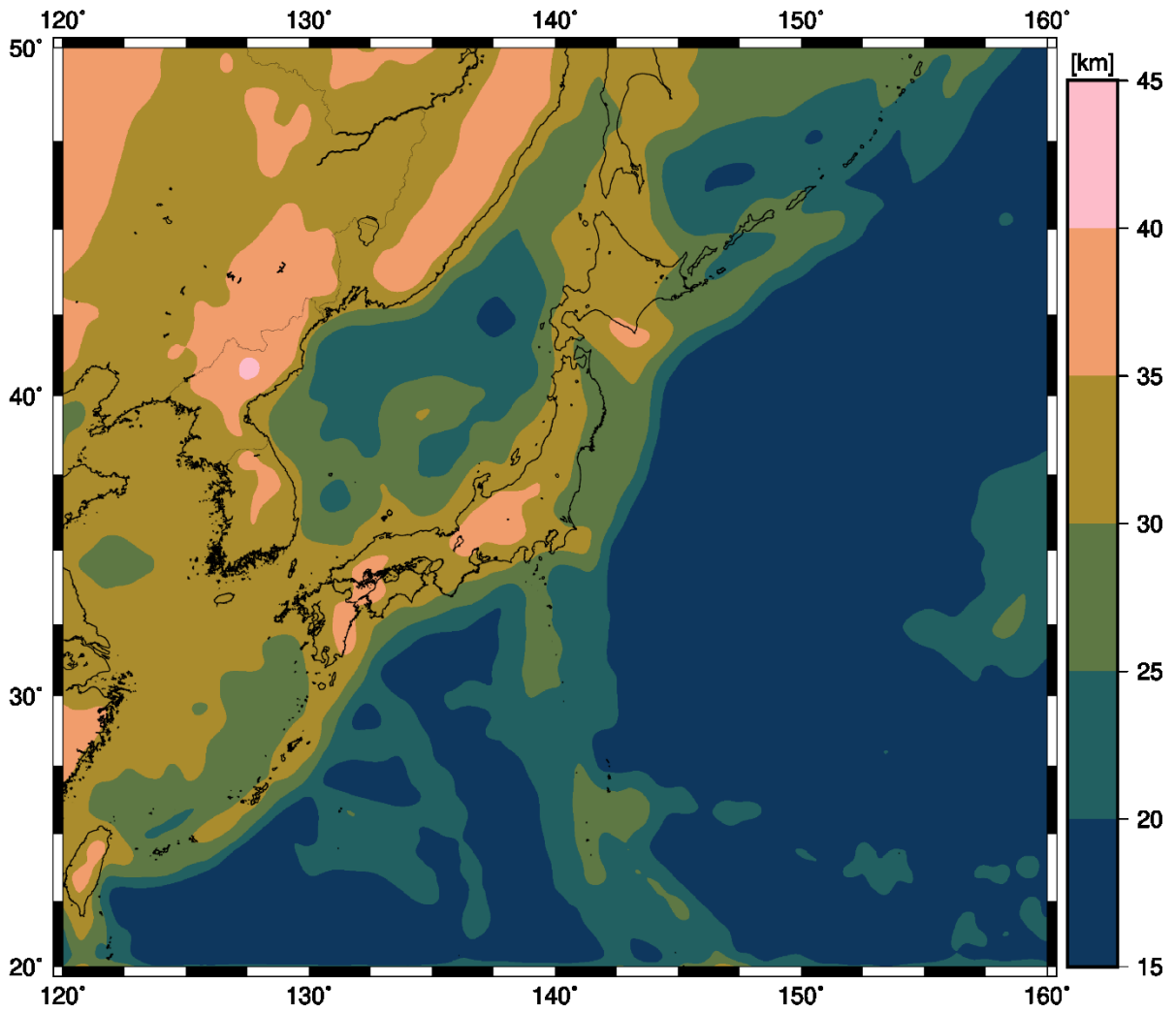
Figure 3.11: Moho depths from gravity inversion.
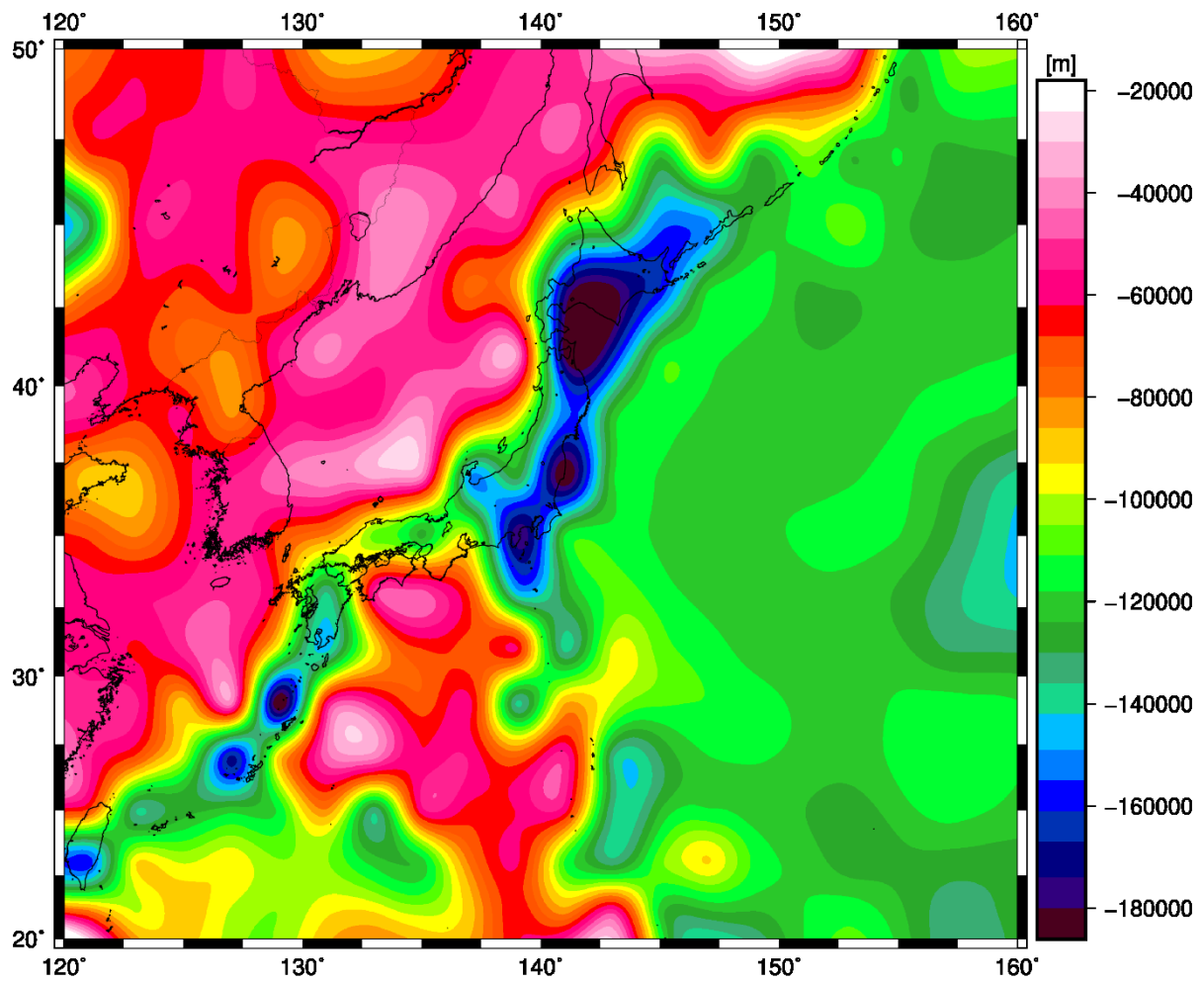
Figure 3.12: Lithosphere-Asthenosphere boundary from LithoRef18 model Afonso et al. ([2019](#)).

3.4.3 Composition of Japanese Islands

The tectono-thermal age of the overlying crust controls the Subcontinental Lithospheric Mantle (SCLM) composition (Griffin et al., 2003; Griffin et al., 2009; O'Reilly and Griffin, 2006). SCLM has a diverse density and composition (dunites, peridotite) controlled by pressure and temperature. The Mantle xenolith samples indicate that the SCLM in the area is Phanerozoic in age. Tectonic activities heated or re-fertilized the lithospheric mantle. My modeling approach used the lithospheric mantle composition from a published petrology analysis of mantle xenoliths.   The major oxide system (CaO, FeO, MgO, Al2O$_3$, and SiO$_2$)   was used. The complex of mantle peridotite petrology and geochemistry reflects the active tectonic environment. Mantle xenoliths can be employed to determine the lithosphere's transition properties from arc to continental edges.

The analysis of peridotite xenoliths found in volcanic rocks on arcs and continental margins provides information regarding Mantle petrology. The complex geological structure of the Sea of Japan reflects its origin as a back-arc basin (Tamaki et al., 1992) on the Eurasian continent's eastern margin (Otofuji and Matsuda, 1984; Otofuji et al., 1985). Japan's seafloor is composed of oceanic crust, stretched continental crust, and rifted continental crust (Tamaki et al., 1992). Mantle xenoliths can help in modeling the Lithosphere beneath the Sea of Japan. In the metasomatism of the Megata peridotites from the Northeast of Japan, some of the hydrous minerals replaced the primary anhydrous minerals (Arai, 1986; ABE et al., 1992). One of the information derived from the xenoliths is thermal condition. Lherzolite in southwest Japan is a high-temperature type because of the asthenosphere upwelling (Arai et al., 2007) Fig. (3.13). Xenolith samples from the Southwest of Japan show that the Lithosphere-Asthenosphere boundary is at the temperature level ($\sim 1250 - 1300^{\circ}$C).

3.4.4 Setup of Model Geometry and Rock Parameters

The area of my model is about $\sim 2,300 \times 2,750$ km with steep steps 2 km down to the depth of 410 km with a lateral resolution of 50 km. The initial model has two layers (Moho and LAB) for the whole area. The thermophysical properties of materials used in 3-D modeling are presented in Table (3.3).
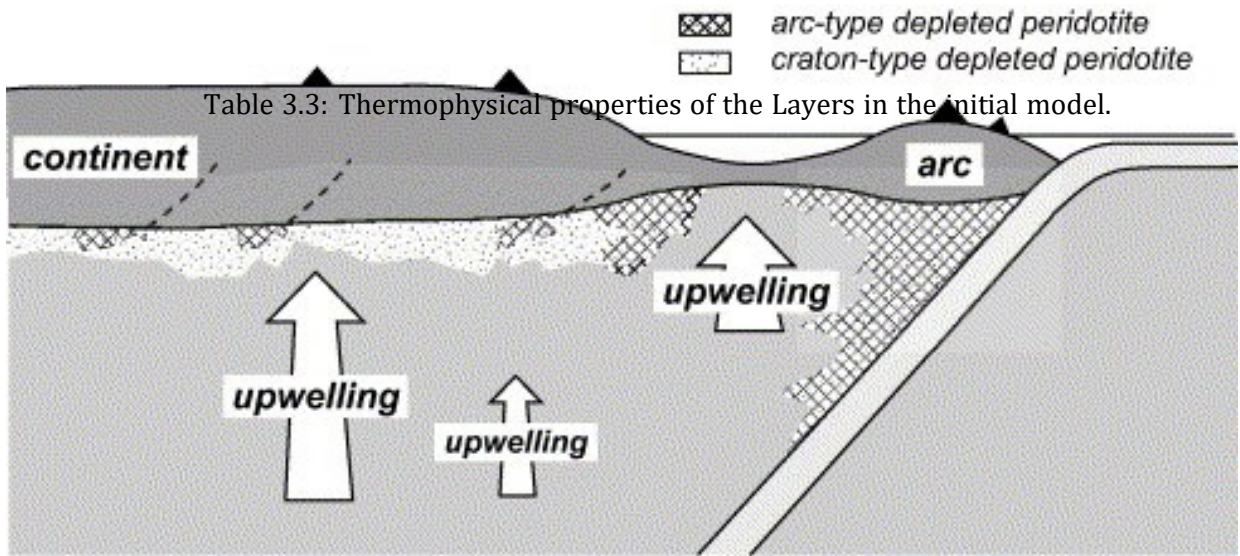
Figure 3.13: A cartoon to show the petrological constitution and evolution of the upper mantle of the Western Pacific after (Arai et al., 2007).

Table 3.3: Thermophysical properties of the Layers in the initial model.

	Density (kg/m^3)	Thermal conductivity$(W.m/K)$	Heat production rate$(\mu W.m^{-3})$
Lower crust	2,800 - 2900	2.0	0.4
Lithosphere	—	4.5	0.001
Mantle	—	—	—

3.5 Results and Interpretations

The results of the final model are discussed in detail.

61

3.5.1 Modeling Results

I utilized the starting values and geometries of the input layers in the first model (M0). The calculated gravity field data is highly inconsistent with the observed data, and the model appears to lack isostatic compensation. Calculations of gradients have a high misfit. High variation in LAB geometry, particularly in trench regions, implies that the original model could not accurately represent the lithosphere in the area Fig (3.14) and gravity gradients residuals in Fig. (3.15). Using trial and error forward modeling, I repeatedly changed the lithospheric geometry (depth to the Moho and LAB boundaries) based on the topographic misfit (residual elevation) to match the long-wavelength gravity field and isostatic elevation. The study area's isostatic balance's initial assumption was discarded to fit the gravity gradients data Fig (3.16). The Moho border and the LAB are modified for the final model (M1).

Consequently, the major step was done in the adjusted model, as the gravity gradient signal is simulated, resulting in extremely minimal residuals. On the other hand, the resulting elevation residuals are not minimum. One may explain the motivations for better fitting gravity gradients by stating that they are very sensitive, particularly to the density structure of the crust and uppermost mantle.

3.5.2 Crustal and Lithospheric Thickness

The output thickness map of the area's crust goes from $\sim$ 16 km in oceanic regions (thin portions) to $\sim$ 40 km in continental parts (thickest regions). The new Moho depths map indicates acceptable misfitting with the Moho depths from seismic research. The Moho depths map depicts the differences in crust thickness in the area, which is appropriate for the geology and tectonic history of the area. The LAB depths under the Japanese Islands approach $\sim$ 218 km (high Lithosphere thickness). High LAB thickness coincides with low seismic S-wave velocity, proportional to the S-wave global models. To minimize the residuals (misfit) of the output models, LAB depths have changed within $\pm$50 km, which is the uncertainty of LAB depths. The Moho depths also changed within $\sim$ 5 km to adjust the short-wavelength subsurface structures.
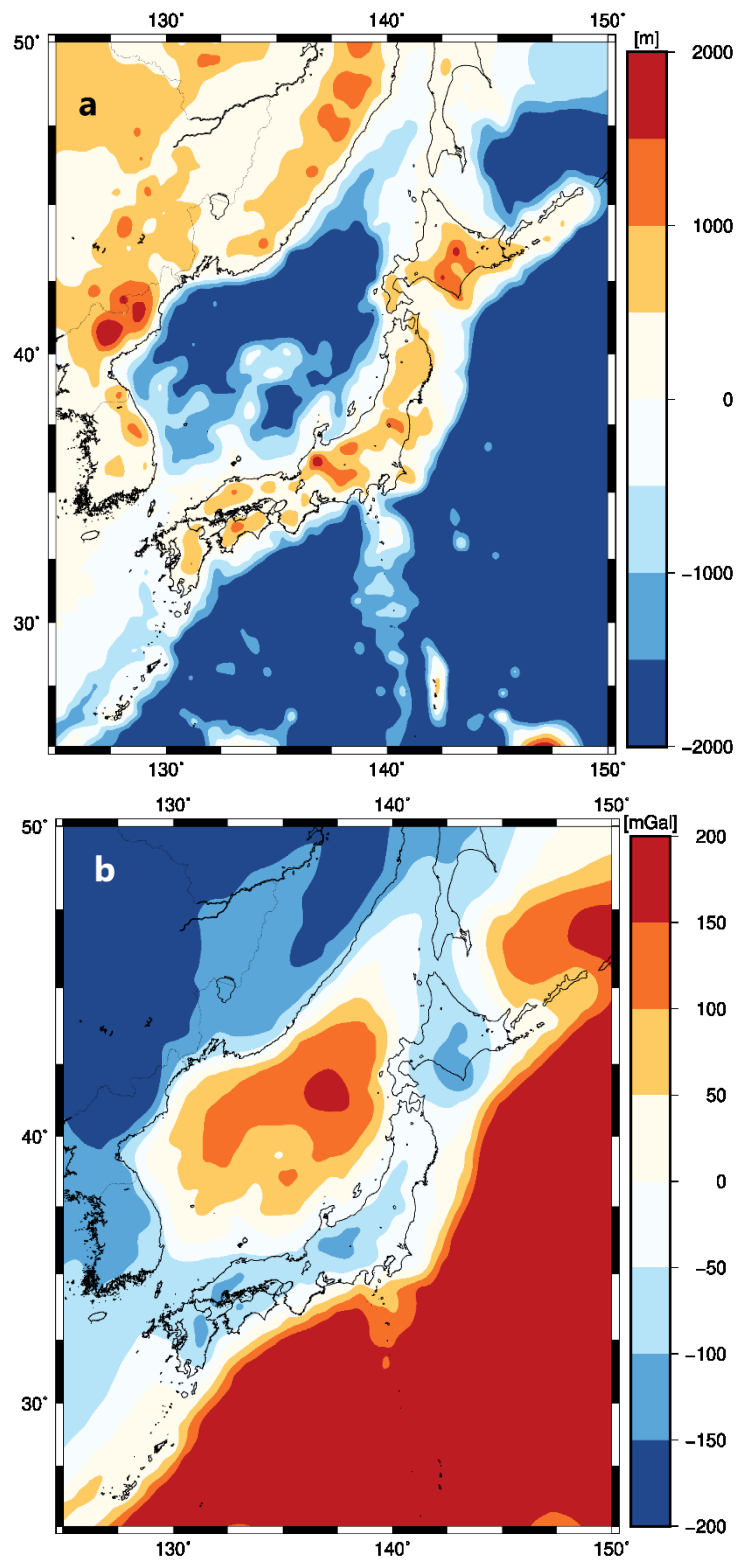
Figure 3.14: The residual fields of M0 in terms of a) Elevation and b) Bouguer Anomaly.
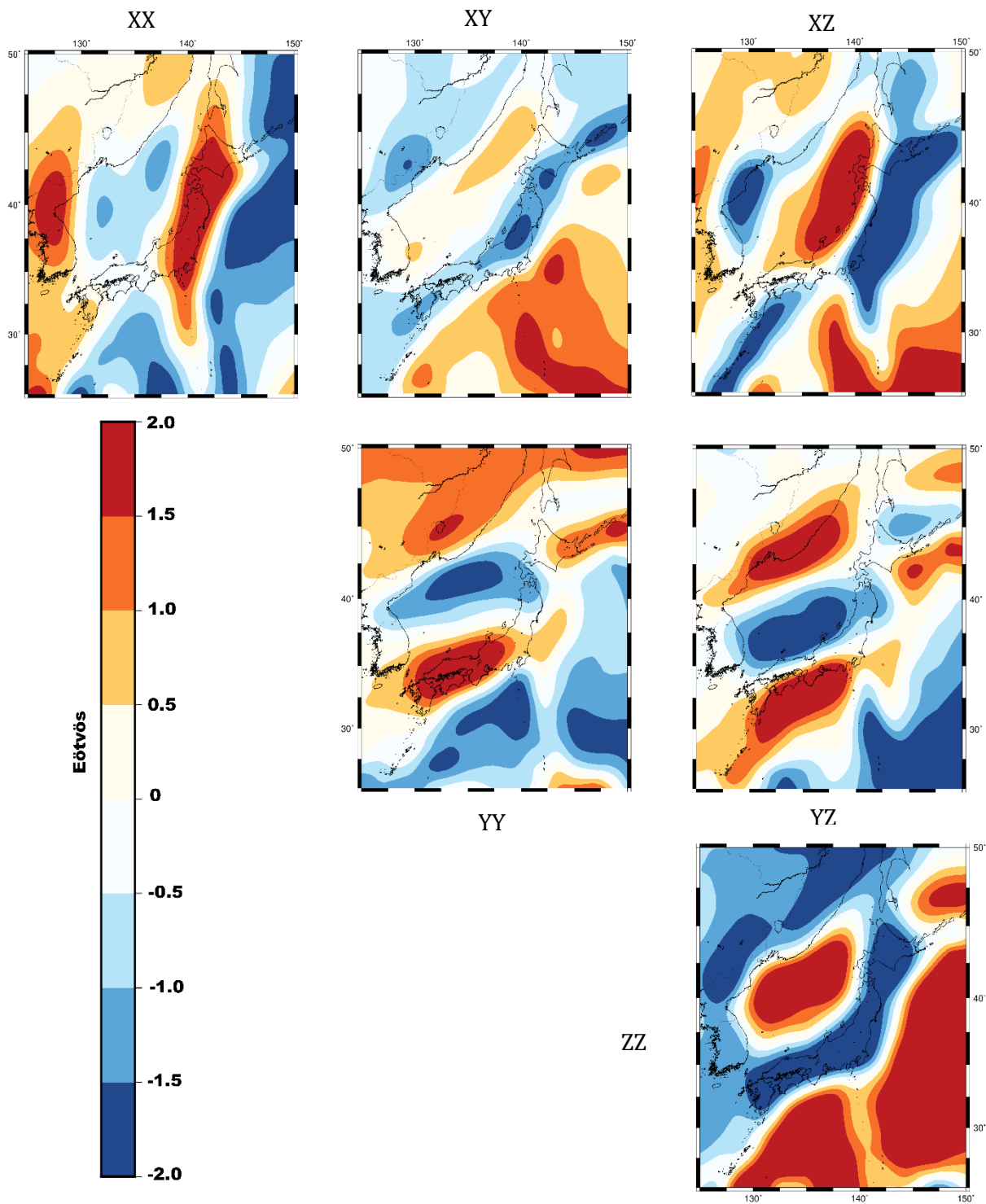
Figure 3.15: The residual fields of M0 in terms of gravity gradients components.
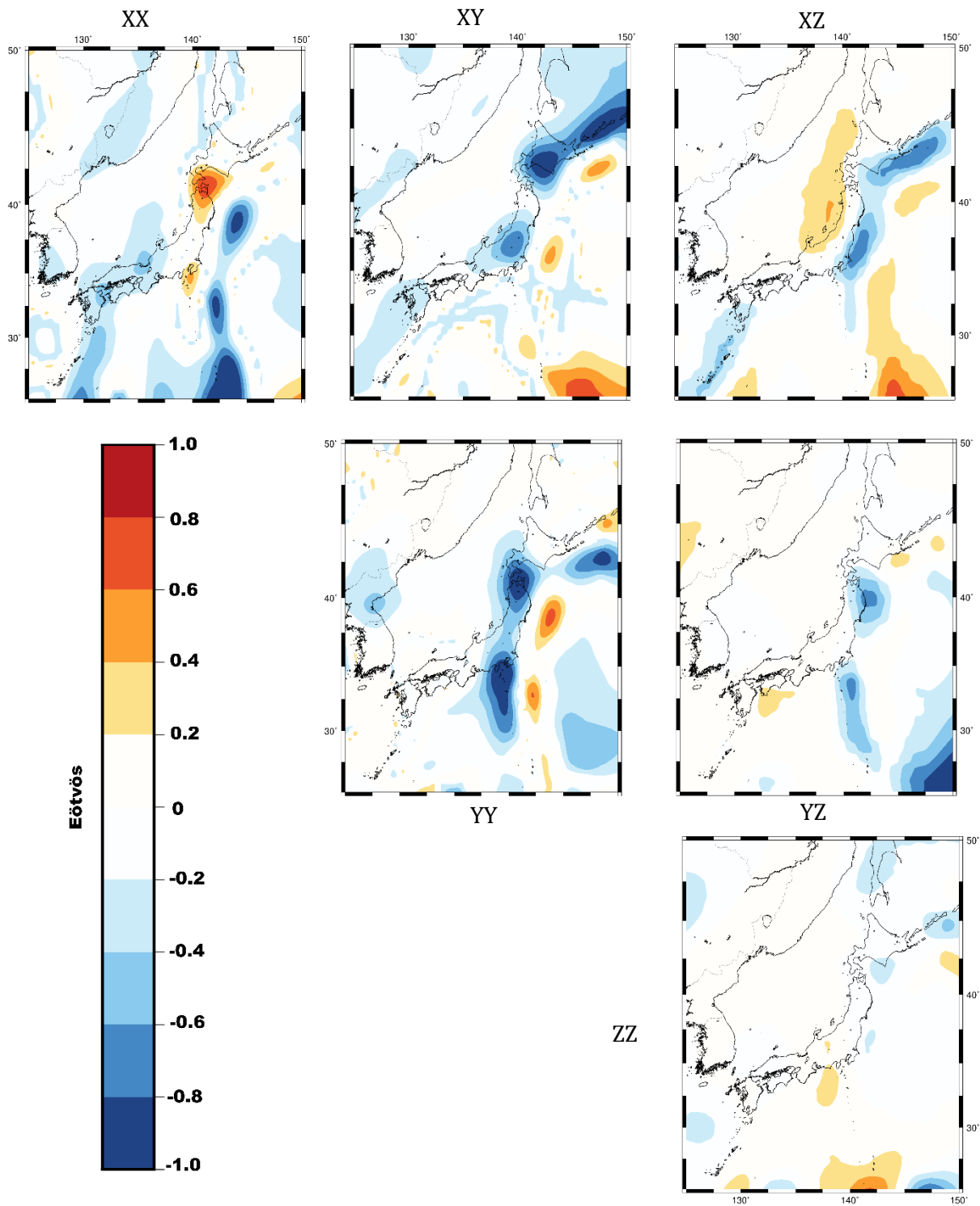
Figure 3.16: The residual fields of M1 in terms of gravity gradients components.
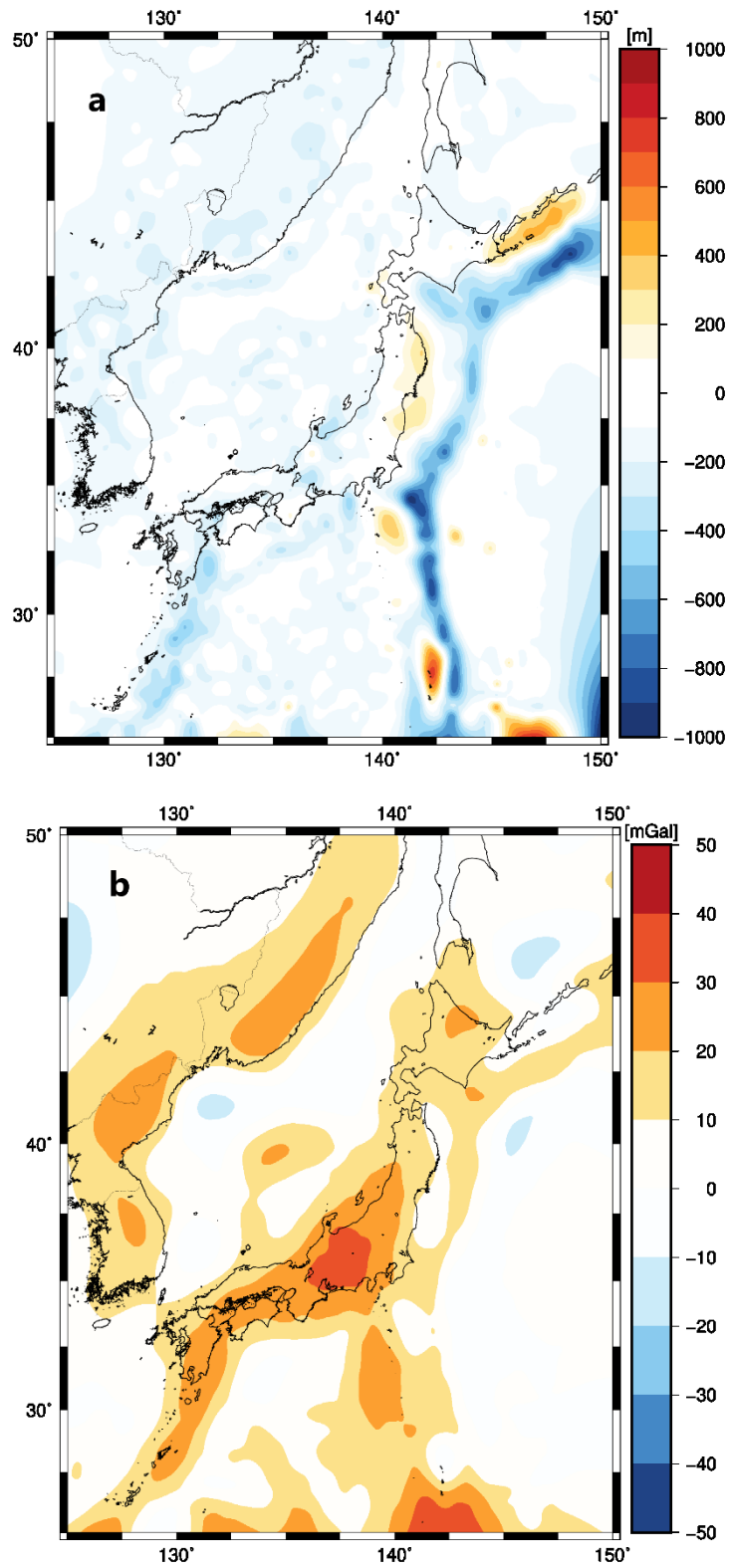
Figure 3.17: The residual fields of M1 in terms of a) Elevation and b) Bouguer Anomaly.

3.6   Discussion

Mantle xenoliths of volcanic rocks appear for the compositional and thermal structure of the Lithospheric Mantle. Chemical and Petrological analysis shows the differences between the Northeast and Southwest of Japan. The published xenolith analysis results represent only localized areas, which may not constrain the composition and evolution of the Japanese Islands. In this study, I applied the integrated inversion of geophysical observations and fields (elevation, crustal thickness, geoid height, gravity, and gravity gradients) with the Petrological analysis of Mantle xenoliths. The output model is the variations in temperature, density, composition, and the crustal and lithospheric thickness of the Lithosphere beneath the Japanese Islands and the area around. The methodology of (Afonso et al., 2019; Fullea et al., 2009) depends on the chemical composition through self-consistent thermodynamic calculations to compute the seismic velocities and density down to 410 km depth. To minimize the misfit between the forward and observed geophysical and field data, the geometry of the crust and the Lithosphere and the mantle composition were modified within the range of uncertainty. The mantle density and seismic velocity were calculated based on thermodynamic calculations and constrained by the temperature, pressure, and chemical composition.

3.6.1 Density Structure

Based on the specified chemical composition and pressure-temperature circumstances, the density of the Mantle was estimated. The density distribution at certain depths of 40, 100, and 200 km indicates the diverse tectonic provinces of the Lithosphere in the Japanese Islands and surrounding area Fig.(3.18). The density distribution horizontally and vertically, as we can see, reflects the various tectonic formations. The Pacific Ocean Plate and the Philippine Sea Plate are associated with high density (3350 - 3370 kg/m^3). The low density reflects the continental areas (eastern margin of Eurasian plate and middle of Japanese Islands) (3300 - 3330 kg/m^3). The rest of the area, including the Sea of Japan, has a moderate density (3330 - 3350 kg/m^3). At a depth of 100 km, we can see that the density distribution in the Northeast of the Japanese Islands differs from that in the Southwest, consistent with the tectonic history and mantle xenoliths. The density fluctuations are shown in two cross-sections, vertically and laterally Fig. (3.21).
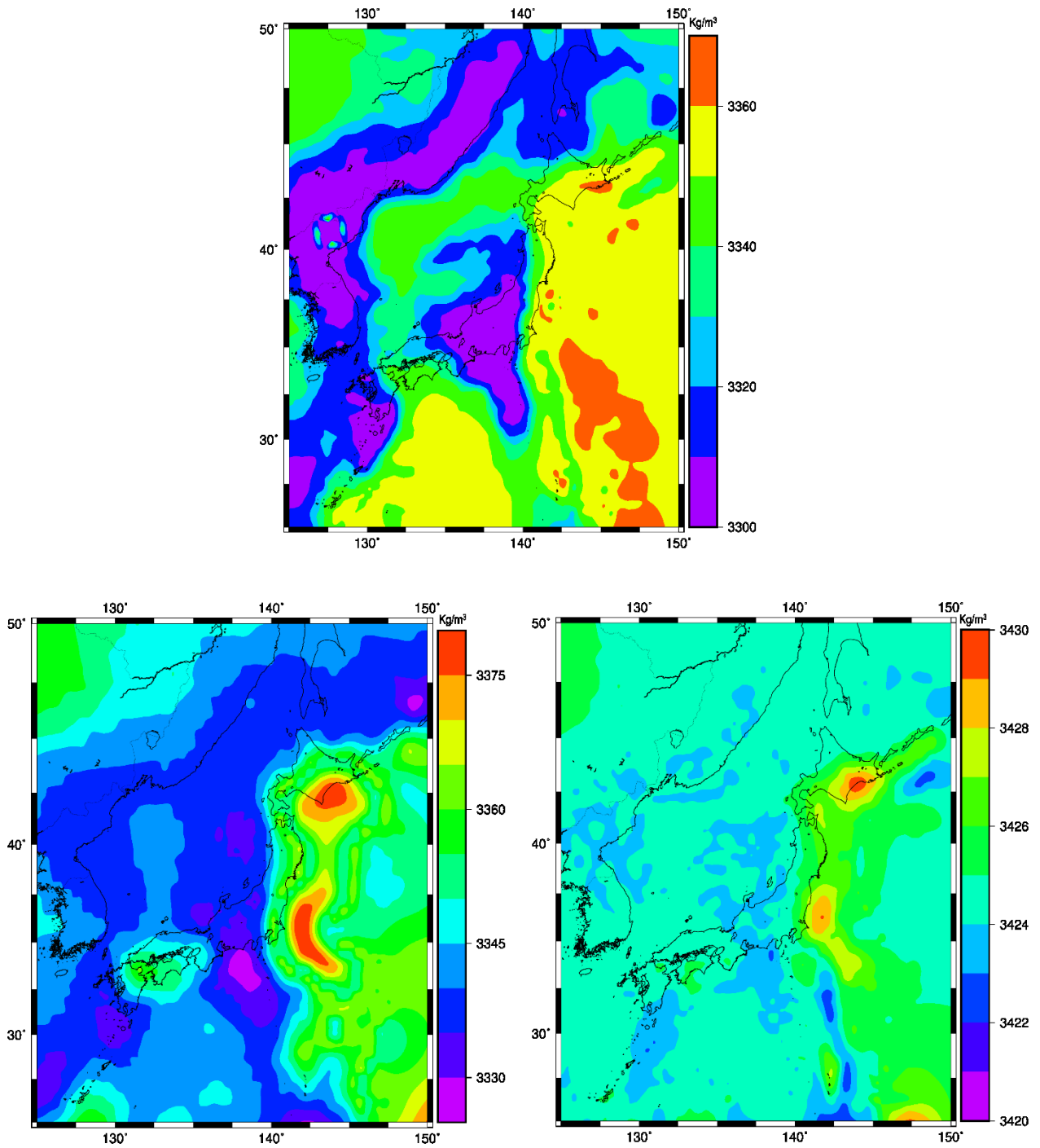
Figure 3.18: Horizontal slices of the 3-D Density model at a depth of (upper) 40, (lower left) 100, and (lower right) 200 km.

3.6.2 Temperature Structure

Fig. (3.19) depicts differences in subsurface temperature at depths of 40, 100, and 200 kilometers beneath the Japanese Islands and surrounding region. Fig. (3.21) depicts two cross-sections' lateral and vertical temperature distributions. Temperature variations are linked to differences in the chemical composition of various tectonic regions. Due to mantle upwelling, high temperatures expose the thin Lithosphere. The temperature distribution in the final model is comparable with the LAB depths map, with slight changes in anomaly amplitudes and locations. The Pacific Ocean and Philippines Sea plate has the lowest temperature. In contrast, the highest temperature in the area reflects the Continental regions (The eastern margin of the Eurasian plate and the middle of the Japanese Islands). The anomalies in the temperature model are connected to the anomalies in the density model.

3.6.3 Seismic Velocity Structure

Seismic S-wave velocities are one of the output models. When comparing my S-wave model with the area's tectonic map and previous seismic tomography models, low-velocity structures highlight the shallow upper mantle (thin Lithosphere) and high-temperature areas. Figure (3.20) shows the Vs at a depth of 100 km in the area. The Pacific Ocean plate and Northeast of the Japanese Islands have S-wave velocities from 4.55 to 4.65 km/s. The continental regions and the Sea of Japan have share wave velocities from 4.45 to 4.5 km/s.

3.6.4 Surface Heat Flow

The Mantle contribution (controlled by LAB depths) with radiogenic heat production and thermal conductivity of the crustal layers was used to estimate the area's Surface Heat Flow model. The area's SHF variety is related to the different tectonic provinces. The resulting SHF model is not well validated because of the weakly constrained thermal structure and the lack of heat flow data for the subsurface structures in the study area. Figure (3.22) shows the distribution of surface heat flow in the study area. The same different tectonic provinces are
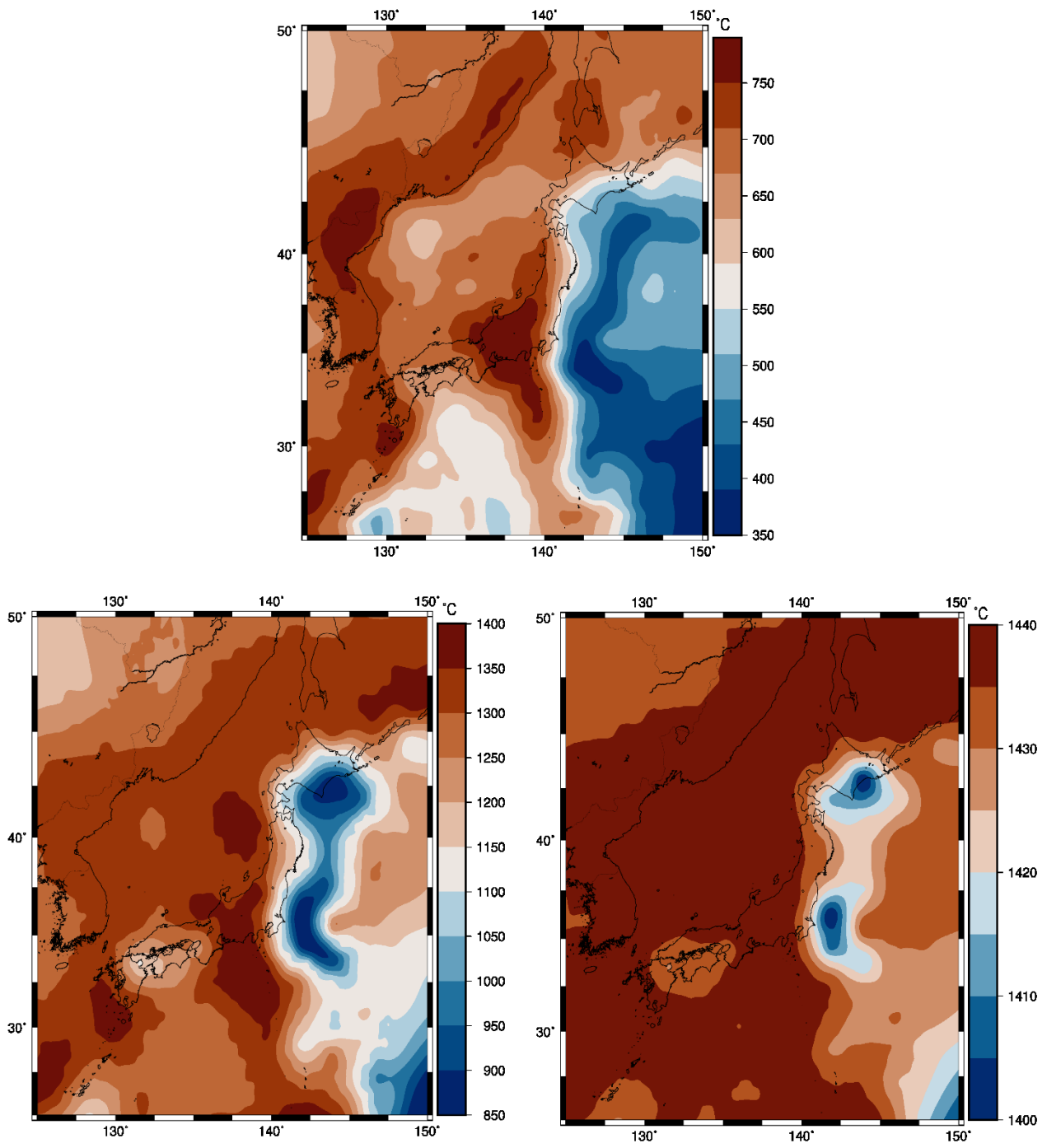
Figure 3.19: Horizontal slices of the 3-D Temperature model at depths of (upper) 40, (lower left) 100, and (lower right) 200 km.

well represented. The sea of Japan and the Izu-Bonin arc has the highest SHF, while the Pacific Ocean plate and Northeast Japan have the lowest area. The upwelling of the mantle can be shown as scattered anomalies.
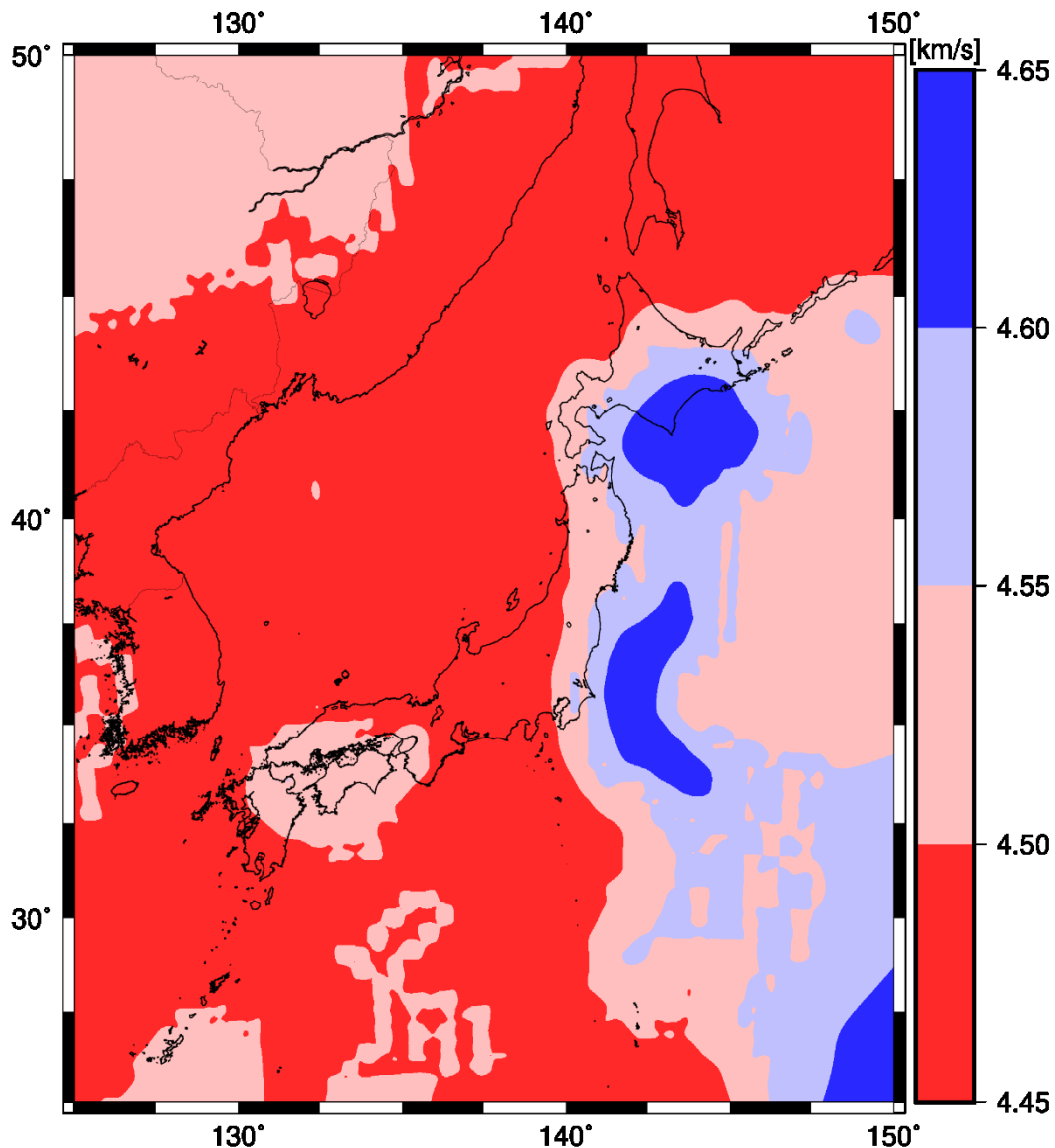
Figure 3.20: Horizontal slice of the 3-D model of Vs at a depth of 100 km.

3.6.5 Lithospheric Structure of the Japanese Islands Region

The lithology of mantle xenoliths varies from locality to locality, reflecting different tectonic situations and formation environments. The Japanese Islands existed from a complex tectonic situation dominated by subduction plates, accretion, backarc spreading, and arc-arc collision.

The Japanese Islands are geologically divided into northeastern Japan (North Honshu and Western Hokkaido) and southwest Japan (Western half of Honshu, Shikoku, and Kyushu). The Kanto tectonic line (KTL) can be seen separating the southwest of Japan from the northeast of Japan.

There are two tectonic provinces to consider: 1- They have a high density, a relatively low temperature, and a high s-wave velocity in the Pacific Ocean and to the northeast of Japan. 2- The southwest of Japan and the Eurasian plate's margin, with low density, high temperature, and low s-wave density. Intensive Serpentinization in SW of japan caused the upper mantle's Pn velocity has about 0.2 km/s smaller than the surrounding.

3.7   Conclusion

The study aims to obtain a more reliable model of the lithospheric structure of the Japanese Islands and Northwest Pacific Ocean, using geophysical and petrological constraints, and to conclude the processes operating during the formation and inversion of this margin. My study presents a self-consistent model using satellite gravity gradient data, seismic tomography models, Isostasy, and thermodynamic modeling to infer the thickness, density, and temperature of the crust and lithosphere beneath the Japanese Islands. The integration between the various data sets results in a higher robustness model compared with modeling them separately. The modeling approach is computationally intensive, so it is impossible to quantify the uncertainty of all individual geophysical properties. My Moho depth map provides high-resolution details for areas with poor or nonexistent seismic station coverage. The crust is thinning in the oceanic regions while thickening in the continental regions. The geophysical measurements are combined with geological and petrological constraints to produce a robust and self-consistent model of the Lithosphere under the Japanese Islands. The upper mantle's temperature, density, and seismic velocity as a function of pressure, temperature, and petrology composition are the outputs of this modeling to differentiate between the different tectonic domains. The model's output can explain the geophysical, geodetic, and seismic data obtained in the area. The model illustrates and explores the lower crust and upper mantle structure. The mechanics and evolution of the lithosphere are yet unclear. The next research step will be integrated research using geodynamic and numerical modeling and combined integration of gravity data with

seismological data in a Bayesian way to evaluate several hypotheses of Japanese island evolution.
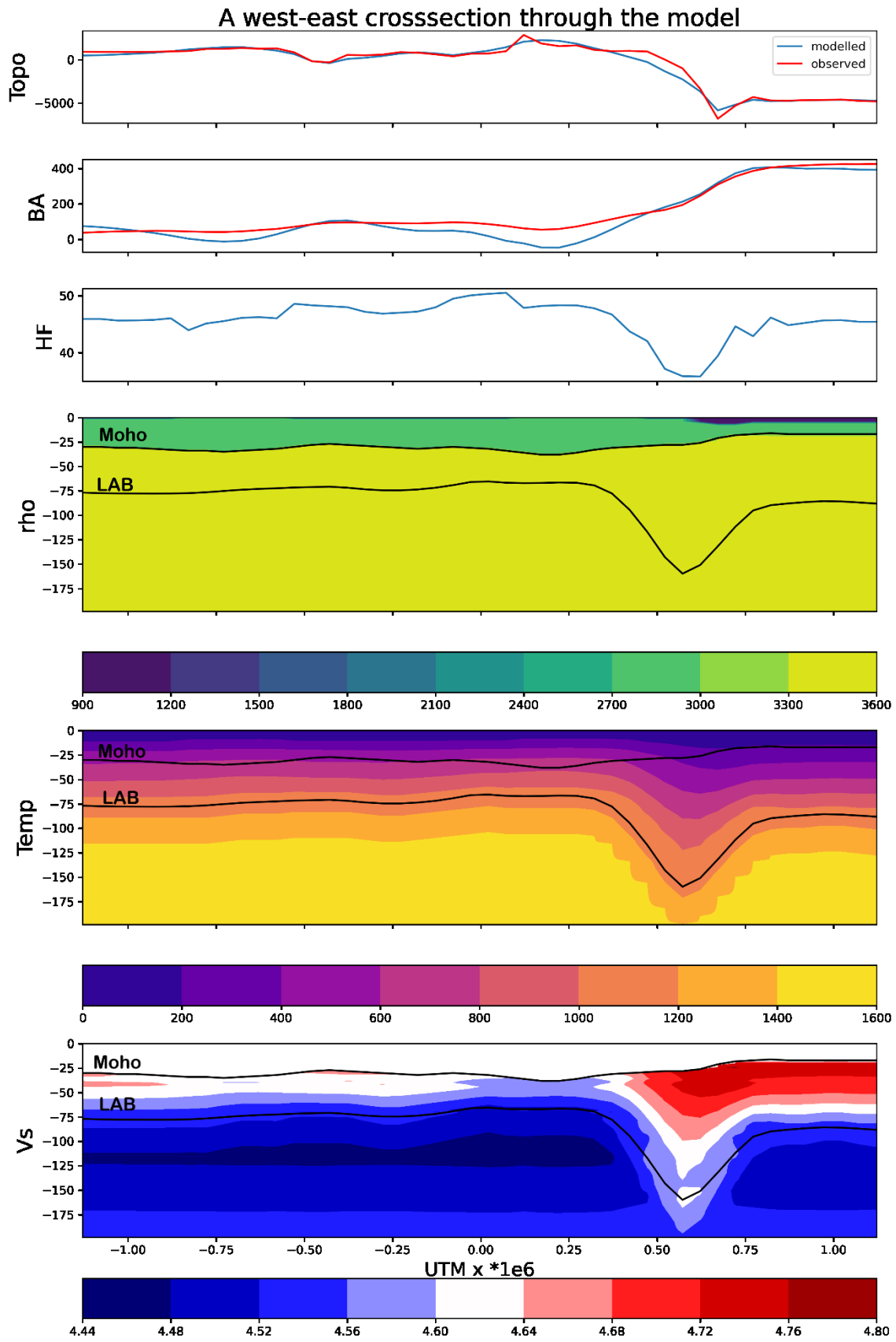
Figure 3.21: a) 2-D cross-section for the Japan Trench (continued)
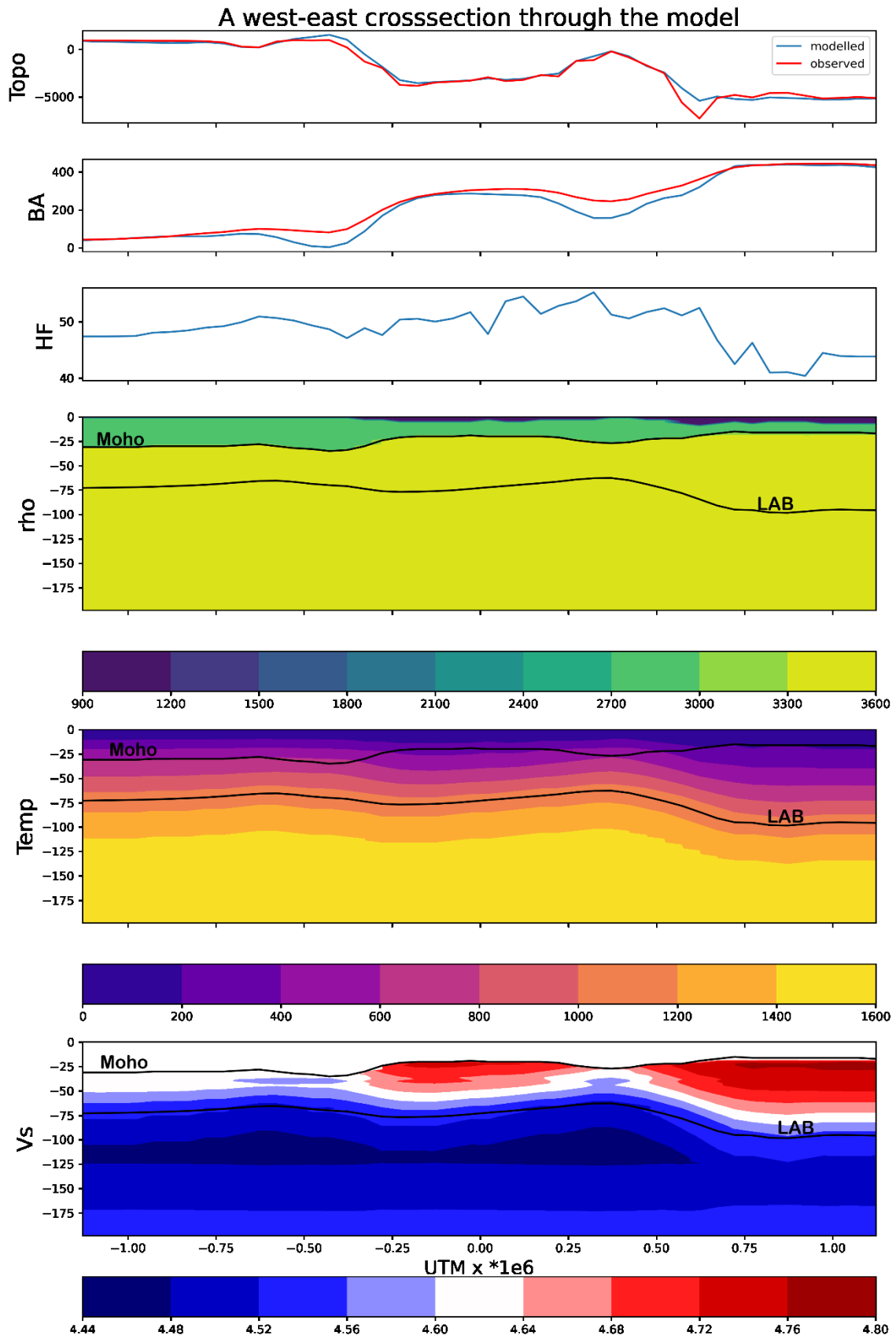
Figure 3.21: b) 2-D cross-section for the Nankai Trough.
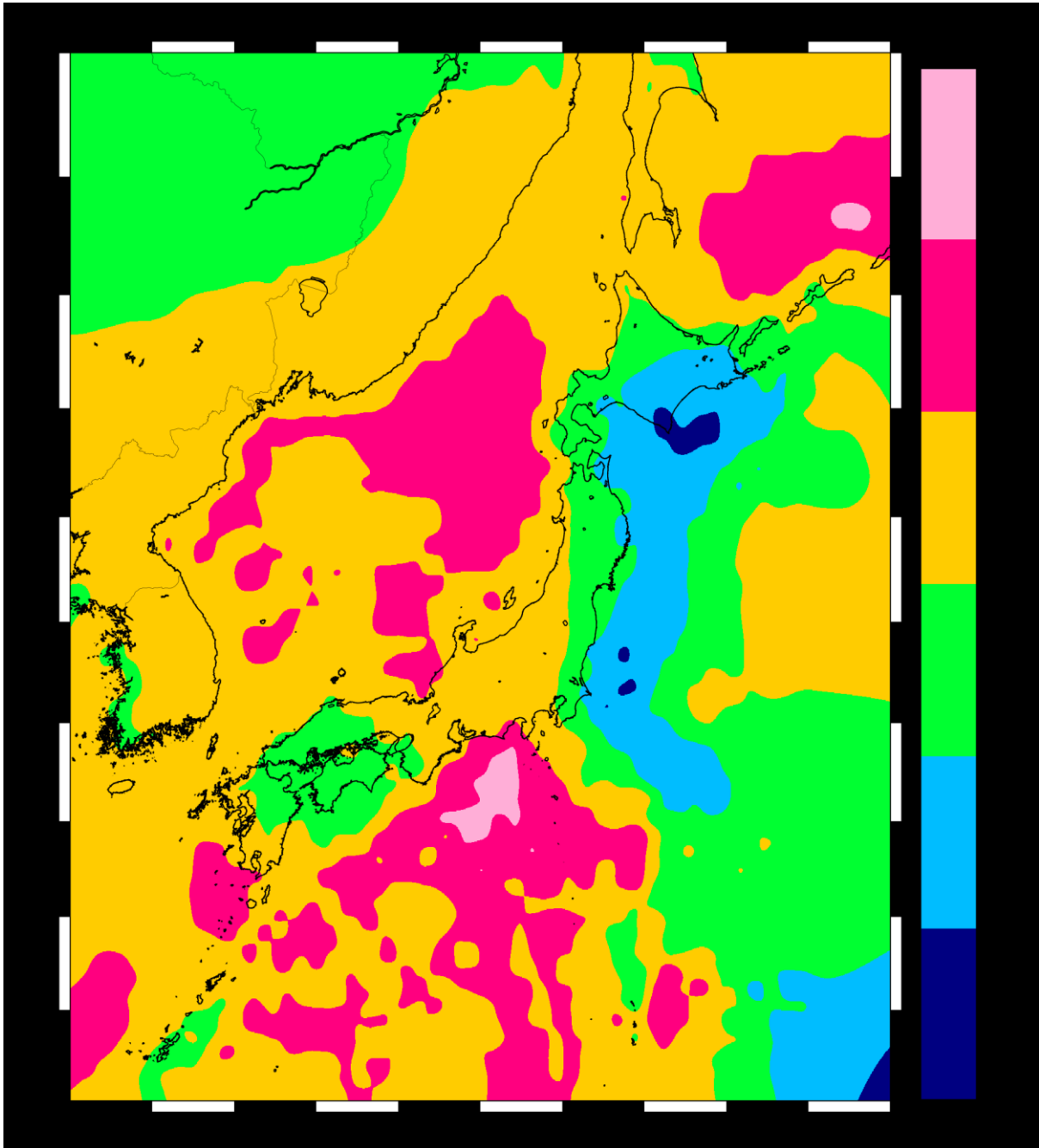
Figure 3.22: The output model of the surface heat flow in the area of the Japanese Islands.

Chapter 4

Conclusions and Outlook

4.1 Summary of the thesis

The Northwestern Pacific Ocean Plate has a complicated tectonic history. Because of the tectonic activity, the study of Lithospheric structures and up- per mantle is one of the most difficult geology subjects. The heterogeneous crust and structures result from the collision of the Pacific Ocean plate, the Philippines Sea plate with the Okhotsk Plate and the Eurasian plate. The area's complex tectonic and geodynamic environment has resulted in intricate Lithosphere geometry. I offer an integration of the geophysical observations (seismic tomography, gravity gradients), topography data, geoid heights, surface temperature, and the prior knowledge of Petrology analysis of mantle xenoliths in this work. To model the depth to Moho on a wide scale, I used the satellite gravity gradients of the latest model of the GOCE mission (GOCO06s) to overcome the deficiency of the data. The steps of the study began with researching the area's tectonic history, collecting and managing accessible data sets, and using 3-D gravity gradients inversion to simulate the density distribution, crustal thickness, and Moho depth in the area. The developed non-linear gravity inversion approach is based on Bott's method and the regularization of Tikhonov. Two models were developed in this thesis. Both of them look at the structure and geometry of Moho and Lab layers. I integrated interdisciplinary data sets to overcome the uncertainty and ambiguity in geophysics interpretations.

In the first model, the input data were gravity gradients of GOCO06s, topography data of the ETopo1 model, Moho depths from previous Receiver functions studies, range of density contrast, and range of regularization parameters. The output result is a 3-D density distribution model, crust thickness model, and Moho depth map. I used CRUST 1.0 and Litho1.0 models to constrain the layers' thickness. The Moho depths of Receiver functions studies were used to constrain and compare the Moho depths of my model. I used the Slab2 model to constrain the shape and geometry of the stagnant slabs. Comparing the estimated Moho depths model with the regional and global models shows good agreement and high levels of consistency. The Oceanic parts have high density, low Crust thickness, and shallow Moho depths in contrast with the Continental parts, characterized by low density with high crustal thickness and deep Moho layer. That corresponds to the tectonic situation of the Northwest Pacific Ocean. Comparing my Moho depth map with the depths of Moho of the Airy's theory of Isostasy

shows identical similarities with disparity visible in the trench and high mountainous areas. Trenches zones are marked by low topography, lowest crust thickness, and low Moho depth.

The motivation of the second model is to model the temperature, heat flow, density, and seismic velocities controlled by pressure, temperature, and petrological composition of Mantle xenoliths. Depending on the primary data and internal options, the program can change the thicknesses or densities to achieve the best possible result/fit. The parameter uncertainties for 3-D inversion are several kilometers for the Moho depth, tens of kilometers for the LAB depth, and several kilograms per cubic meter for average crustal densities (Motavalli-Anbaran et al., 2013). The amount of prior information used also influences the level of uncertainty. Changes in crustal thickness can be offset in part by changes in LAB depth in the same direction (a thicker crust necessitates a thicker lithosphere). As a general rule, a 1 km thickening of the crust can be offset by a 10 km deepening of the LAB. As previously stated, gravity and geoid data were given precedence. The multidisciplinary integration can reduce uncertainty and ambiguity in the resulting temperature, heat flow, and density distribution models of the Lithosphere and Upper Mantle. My models display the Japanese Islands region from a different perspective and are integrated in a way that is compatible with geophysical, geological, and seismic tomography models.

Bibliography

Abe, Natsue, Shoji Arai, and Yasuhiro Saeki (1992): "Hydration processes in the arc mantle; petrology of the Megata peridotite xenoliths, the Northeast Japan arc", Journal of Mineralogy, Petrology and Economic Geology, 87(8), 305–317.

Afonso, J.C., Salajegheh, F., Szwillus, W., Ebbing, J. & Gaina, C. (2019): "A global reference model of the lithosphere and upper mantle from joint inversion and analysis of multiple data sets", *Geophysical Journal International*, **217(3)**, 1602–1628. ISSN: 0956-540X. DOI: 10.1093/gji/ggz094.

Afonso, J. C., Fernandez, M., Ranalli, G., Griffin, W. L., & Connolly, J. A. D. (2008): Integrated geophysical-petrological modeling of the lithosphere and sublithospheric upper mantle: Methodology and applications. Geochemistry, Geophysics, Geosystems, 9 (5).

Allen, P. A. and J. R. Allen (2005): Basin Analysis: Principles and Applications. WileyBlackwell

Amante, Christopher and Barry W. Eakins (2009): ETOPO1 1 arc-minute global relief model: procedures, data sources and analysis.
URL:https://www.ngdc.noaa.gov/mgg/global/relief/ETOPO1/docs/ETOPO1.pdf.

Anderson, Don L. (1995): "Lithosphere, asthenosphere, and perisphere", Reviews of Geophysics, 33 (1), 125. ISSN: 8755-1209. DOI: 10.1029/ 94RG02785.

Arai, Shoji (1986): "K/Na variation in phlogopite and amphibole of upper mantle peridotites due to fractionation of the metasomatizing fluids", The Journal of Geology, 94(3), 436–444.

Arai, Shoji, Natsue Abe, and Satoko Ishimaru (2007): "Mantle peridotites from the Western Pacific, Island Arcs: Past and Present", Gondwana Research, 11(1), 180–199. ISSN:1342-937X. DOI:https://doi.org/10.1016/j.gr.2006.04.004.

Arai, Shoji, Hisatoshi HIRAI, and Kozo UTO (2000): "Mantle peridotite xenoliths from the Southwest Japan arc: a model for the sub-arc upper mantle structure and composition of the Western Pacific rim", Journal of Mineralogical and Petrological Sciences, 95(4), 9–23. DOI:10.2465/jmps.95.9.

Artemieva, Irina M. (2009): "The continental lithosphere: Reconciling thermal, seismic, and petrologic data", Lithos Continental Lithospheric Mantle: The Petro-Geophysical

Approach, 109(1), 23–46.ISSN:0024-4937.

Bouman, J., Ebbing, J., Meekes, S., Abdul Fattah, R., Fuchs, M., Gradmann, S., Haagmans, R., et al. (2015): "GOCE gravity gradient data for lithospheric modeling", Int. J. Appl. Earth Obs., 35, 16-30. GOCE earth science applications and models (Based on the ESA GOCE solid earth workshop, 16-17 October 2012). ISSN: 0303-2434.

DOI: https://doi.org/10.1016/j.jag.2013.11.001.

Bouman, J., Ebbing, J., Fuchs, M., Sebera, J., Lieb, V., Szwillus, W., Haagmans, R., et al. (2016): "Satellite gravity gradient grids for Geophysics", Scientific Reports, 6, 21050.

Bowin, C. (2000): "Mass anomalies and the structure of the earth", Physics and Chemistry of the Earth, Part A: Solid Earth and Geodesy, 25(4), 343–353. ISSN:1464-1895. DOI: https://doi. org/10.1016/S1464-1895(00)00056-9.

Braitenberg, Carla (2015): "Exploration of tectonic structures with GOCE in Africa and across-continents", International Journal of Applied Earth Observation and Geoinformation, 35, 88–95. GOCE earth science applications and models(Based on the ESA GOCE solid earth workshop, 16-17 October 2012) ISSN: 0303-2434. DOI:https ://doi.org/10.1016/j.jag.2014.01.013.

Braitenberg, Carla, Mariani. Patrizia, and Tommaso. Pivetta (2011): "GOCE observations in exploration geophysics", Ouwehand, L. (ed), Proceedings of 4th Int GOCE User Workshop, ESA SP-696.

URL:https://earth.esa.int/eogateway/documents/20142/37627/p35 _braite.pdf.

Chattopadhaya, S., Ghosh, B., Morishita, T., Nandy, S., Tamura, A. & Bandyopadhyay, D. (2017): "Reaction microtextures in entrapped xenoliths in alkali basalts from the Deccan large igneous province, India: Implications to the origin and evolution", Journal of AsianEarth Sciences, 138, 291–305.

Christensen, Nikolas I. and Walter D. Mooney (1995): "Seismic velocity structure and composition of the continental crust: A global view", Journal of Geophysical Research: Solid Earth, 100(B6), 9761–9788. ISSN: 01480227. DOI: 10.1029/95JB00259. URL: http://doi.wiley. com/10.1029/95JB00259.

Cooper, G.R.J. and D.R. Cowan (2006): "Enhancing potential field data using filters based on the local phase", Computers & Geosciences, 32(10), 1585–1591. ISSN: 00983004. DOI: 10.1016/j.cageo.2006.02.016.

Connolly, J. A. D. (2005). "Computation of phase equilibria by linear programming: A tool for geodynamic modeling and its application to subduction zone decarbonation". In: Earth and Planetary Science Letters 236.1, pp. 524 –541. ISSN: 0012-821X. DOI: https://doi.org/10.1016/j.epsl.2005.04.033.

Duesterhoeft, E., Quinteros, J., Oberhänsli, R., Bousquet, R. & Capitani, C. de. (2014): "Relative impact of mantle densification and eclogitization of slabs on subduction dynamics: A numerical thermodynamic/thermokinematic investigation of metamorphic density evolution", Tectonophysics, 637, 20–29. ISSN:0040-1951.

Fischer, K.M., Ford, H.A., Abt, D.L. & Rychert, C.A. (2010): "The Lithosphere-Asthenosphere Boundary", Annual Review of Earth and Planetary Sciences, 38 (1), 551–575. ISSN: 0084-6597.

Fitch, Thomas J. (1972): "Plate convergence, transcurrent faults, and internal deformation adjacent to Southeast Asia and the western Pacific", Journal of Geophysical Research, 77(23), 4432–4460.ISSN:01480227. DOI: 10.1029/JB077i023p04432.

Floberghagen, R., Fehringer, M., Lamarre, D., Muzi, D., Frommknecht, B., Steiger, C., Piñeiro, J., et al. (2011): "Mission design, operation and exploitation of the gravity field and steady-state ocean circulation explorer mission", Journal of Geodesy, 85(11), 749–758. ISSN: 0949-7714. DOI: 10.1007/s00190-011-0498-3.

Fu, Guangyu and Yawen She (2017): "Gravity anomalies and isostasy deduced from new dense gravimetry around the Tsangpo Gorge, Tibet", Geophysical Research Letters, 44(20), 10–233.

Fu, G., Gao, S., Freymueller, J.T., Zhang, G., Zhu, Y. & Yang, G. (2014): "Bouguer gravity anomaly and isostasy at western Sichuan Basin revealed by new gravity surveys", Journal of Geophysical Research: Solid Earth, 119(4), 3925–3938.

Fukao, Yoshio and Masayuki Obayashi (2013): "Subducted slabs stagnant above, penetrating through, and trapped below the 660 km discontinuity", Journal of Geophysical Research: Solid Earth, 118(11), 5920–5938.ISSN:21699313.

Fullea, J., Afonso, J. C., Connolly, J. A. D., Fernandez, M., García-Castellanos, D., & Zeyen, H. (2009). LitMod3D: An interactive 3-D software to model the thermal, compositional, density, seismological, and rheological structure of the lithosphere and sublithospheric upper mantle. Geochemistry, Geophysics, Geosystems, 10(8).

Fullea Urchulutegui, Javier, Manel Ferna`ndez, and Hermann Zeyen (2006): "Lithospheric structure in the Atlantic–Mediterranean transition zone (southern Spain, northern Morocco): a simple approach from regional elevation and geoid data", Comptes Rendus Geoscience, Quelques développements récents sur la géodynamique du Maghreb, 338(1), 140–151. ISSN:1631-0713. DOI:https://doi.org/10.1016/j.crte.2005.11.004.

Green, D.H., Hibberson, W.O., Kovács, I. & Rosenthal, A. (2010): "Water and its influence on the lithosphere-asthenosphere boundary", Nature, 467 (7314), 448–451. ISSN: 0028-0836. DOI: 10.1038/nature09369.

Geological Survey of Japan (1992): Geological Atlas of Japan. Tech. rep. Tokyo: Asakura Shoten. 2nd ed, 22 map sheets, Geological Survey of Japan, (in Japanese).

Globig, J., Fernàndez, M., Torne, M., Vergés, J., Robert, A. & Faccenna, C. (2016): "New insights into the crust and lithospheric mantle structure of Africa from elevation, geoid, and thermal analysis", Journal of Geophysical Research: Solid Earth, 121(7), 5389–5424. DOI: 10.1002/2016JB012972.

Goudie, Andrew (2004): Encyclopedia of Geomorphology, Routledge. doi:10.4324/9780203381137

Griffin, W.L., O'Reilly, S.Y., Afonso, J.C. & Begg, G.C. (2009): "The Composition and Evolution of Lithospheric Mantle: a Re-evaluation and its Tectonic Implications", Journal of Petrology, 50(7),1185–1204.ISSN:0022-3530.

Griffin, W.., O'Reilly, S.., Abe, N., Aulbach, S., Davies, R.., Pearson, N.., Doyle, B.., et al. (2003): "The origin and evolution of Archean lithospheric mantle", Precambrian Research, 127(1-3), 19–41. ISSN: 03019268. DOI: 10.1016/S0301-9268(03)00180-3.

Guy, Alexandra, Nils Holzrichter, and Jo¨rg Ebbing (2017): "Moho depth model for the Central Asian Orogenic Belt from satellite gravity gradients", Journal of Geophysical Research: Solid Earth, 122(9), 7388–7407. ISSN: 21699313.

Hantschel, T. and A. I. Kauerauf (2009): Fundamentals of basin and petroleum systems modeling. Springer Science & Business Media.

Hao, T.-Y., XU, Y., XU, Y., SUH, M., LIU, J.-H., DAI, M.-G. & LI, Z.-W. (2006): "Some New Understandings on the Deep Structure in Yellow Sea and East China Sea", Chinese Journal of Geophysics, 49(2), 405–416.

Haxby, WF and DL Turcotte (1978): "On isostatic geoid anomalies", Journal of Geophysical Research: Solid Earth, 83(B11), 5473–5478.

Hayes, G.P., Moore, G.L., Portner, D.E., Hearne, M., Flamme, H., Furtney, M. & Smoczyk, G.M. (2018): "Slab2, a comprehensive subduction zone geometry model", Science, 362(6410), 58–61. DOI: 10.1126/ science.aat4723.

Hees, GL Strang van (2000): "Some elementary relations between mass distributions inside the Earth and the geoid and gravity field", Journal of Geodynamics, 29(1-2), 111–123.

Hirose Fuyuki, Junichi Nakajima and Akira Hasegawa (2008): "Three-dimensional seismic velocity structure and configuration of the Philippine Sea slab in southwestern Japan estimated by double-difference tomography", Journal of Geophysical Research: Solid Earth, 113(B09315), 1-26.

Hirschmann, Marc M. (2010): "Partial melt in the oceanic low velocity zone", Physics of the Earth and Planetary Interiors, 179(1), 60–71. ISSN: 0031-9201.

Hirth, Greg and David L. Kohlstedt (1996): "Water in the oceanic upper mantle: implications for rheology, melt extraction and the evolution of the lithosphere", Earth and Planetary Science Letters, 144(1), 93–108. ISSN: 0012-821X. DOI: https://doi.org/10.1016/0012- 821X(96)00154-9.

Hofmeister, A. M. (1999): Mantle values of thermal conductivity and the geotherm from phonon life times, Science, 283, 1699–1706.

Hosse, M., Pail, R., Horwath, M., Holzrichter, N. & Gutknecht, B.D. (2014): "Combined regional gravity model of the Andean convergent subduction zone and its application to crustal density modeling in active plate margins", Surveys in Geophysics, 35(6), 1393–1415.

Huang, Jinli and Dapeng Zhao (2006): "High-resolution mantle tomography of China and surrounding regions", Journal of Geophysical Research, 111(B9). DOI: 10.1029/2005jb004066.

Huzita, Kazuo (1968): "Rokko Movements and its Appearance: Intersecting Structural Patterns of Southwest Japan and Quaternary Crustal Movements", The Quaternary Research (Daiyonki-Kenkyu), 7(4), 248–260. ISSN: 1881-8129. DOI:10.4116/jaqua.7.248.

Igarashi, Toshihiro, Takashi Iidaka, and Sawako Miyabayashi (2011): "Crustal Structure in the Japanese Islands Inferred from Receiver Function Analysis", Zisin (Journal of the

Seismological Society of Japan. 2nd ser.), 63(3), 139–151. ISSN:1883-9029. DOI:10.4294/zisin.63.139.

Iidaka, T., Takeda, T., Kurashimo, E., Kawamura, T., Kaneda, Y. & Iwasaki, T. (2004): "Configuration of subducting Philippine Sea plate and crustal structure in the central Japan region". In: Tectonophysics 388.1-4, pp. 7–20. ISSN: 00401951. DOI: 10.1016/j.tecto.2004.07.002.

Ince, E.S., Barthelmes, F., Reißland, S., Elger, K., Förste, C., Flechtner, F. & Schuh, H. (2019): "ICGEM – 15 years of successful collection and distribution of global gravitational models, associated services, and future plans", Earth System Science Data, 11(2), 647–674. ISSN: 1866-3516. DOI: 10.5194/essd-11-647-2019.

Isozaki, Yukio (1997): "Contrasting two types of orogen in Permo-Triassic Japan: Accretionary versus collisional", The Island Arc, 6(1), 2–24. ISSN: 1038-4871. DOI:10.1111/j.1440-1738.1997.tb00038.x.

Iwasaki, Takaya and Hiroshi Sato (2009): "Crust and Upper mantle Structure of Island Arc Being Elucidated from Seismic Profiling with Controlled Sources in Japan", Zisin (Journal of the Seismological Society of Japan. 2nd ser.), 61, 165–176. ISSN: 0037-1114. DOI: 10.4294/zisin.61.165.

Iwasaki, T., Yoshii, T., Ito, T., Sato, H. & Hirata, N. (2002): "Seismological features of island arc crust as inferred from recent seismic expeditions in Japan", Tectonophysics, 355(1-4), 53–66. ISSN: 00401951. DOI: 10.1016/S0040-1951(02) 00134-8.

Kaczmarek, M.-A., Bodinier, J.-L., Bosch, D., Tommasi, A., Dautria, J.-M. & Kechid, S.A. (2016): "Metasomatized mantle xenoliths as a record of the lithospheric mantle evolution of the northern edge of the Ahaggar Swell, in Teria (Algeria)", Journal of Petrology, 57(2), 345–382.

Kaizuka, S. (1975): "A tectonic model for the morphology of arc-trench systems, especially for the echelon ridges and mid-arc faults", Jpn. J. Geol. Geogr., 45, 9–28.

Karato, Shunichiro (2012): "On the origin of the asthenosphere", Earth and Planetary Science Letters, 321-322, 95–103. ISSN:0012-821X. DOI: https://doi.org/10. 016/j.epsl.2012.01.001.

Katsui, Y., Yamamoto, M., Nemoto, S. & Niida, K. (1979): "Genesis of Calc-Alkalic Andesites from Oshima-Ōshima and Ichinomegata Volcanoes, North Japan", Faculty of Science,

Hokkaido University,19(1-2),157–168.

Katsumata, Akio (2010): "Depth of the Moho discontinuity beneath the Japanese islands estimated by traveltime analysis", Journal of Geophysical Research, 115(B4), B04303. ISSN:0148-0227. DOI:10.1029/2008JB005864.

Kimura, Masaaki (1985): "Back-arc rifting in the Okinawa Trough", Marine and Petroleum Geology, 2(3), 222–240. ISSN: 02648172. DOI:10.1016/0264-8172(85)90012-1.

Kodama, Kazuto, Hitoshi Tashiro, and Tohru Takeuchi (1995): "Quaternary counterclockwise rotation of south Kyushu, southwest Japan", Geology, 23(9), 823. ISSN:0091-7613. DOI:10.1130/0091-7613(1995)023<0823:QCROSK>2.3.CO;2.

Kuno, Hisashi (1960): "High-alumina Basalt", Journal of Petrology, 1(1), 121–145. ISSN:0022-3530. DOI:10.1093/petrology/1.1.121.

Kuno, Hisashi (1966): "Lateral variation of basalt magma type across continental margins and Island Arcs", Bulletin Volcanologique, 29(1),195–222.ISSN: 0258-8900. DOI: 10.1007/BF02597153.

Kuno, Hisashi (1967): "Mafic and ultramafic nodules from Itinomegata, Japan", Wiley, P. J. ed. ultra-mafic and related rocks, 337–342.

Kvas, A., Brockmann, J.M., Krauss, S., Schubert, T., Gruber, T., Meyer, U., Mayer-Gürr, T., et al. (2021): "GOCO06s – a satellite-only global gravity field model", Earth System Science Data, 13(1), 99–118. DOI: 10.5194/essd-13-99-2021.

Kvas, A., Mayer-Gürr, T., Krauss, S., Brockmann, J.M., Schubert, T., Schuh, W.-D., Pail, R., et al. (2019): "The satellite-only gravity field model GOCO06s", GFZ Data Serv.

Laske, G., Masters, G., Ma, Z. and Pasyanos, M. (2013): "Update on CRUST1.0 - A 1-degree global model of Earth's crust", Abstract of EGU2013-2658 presented at 2013 Geophys. Res., 15, 2658.

Li, Xiong and Hans-Jürgen Götze (2001): "Ellipsoid, geoid, gravity, geodesy, and geophysics", Geophysics, 66(6), 1660–1668. ISSN: 0016-8033. DOI: 10.1190/1.1487109.

Liu, X., Zhao, D., Li, S. & Wei, W. (2017): "Age of the subducting Pacific slab beneath East Asia and its geodynamic implications", Earth and Planetary Science Letters, 464, 166–174. ISSN:0012821X. DOI:10.1016/j.epsl.2017.02.024.

Maaløe, Sven and Ken-ichiro Aoki (1977): "The major element composition of the upper mantle estimated from the composition of lherzolites", Contributions to Mineralogy and

Petrology, 63(2), 161–173.

Martinec, Zdeněk (2014): "Mass-density Green's functions for the gravitational gradient tensor at different heights", Geophysical Journal International, 196(3), 1455–1465. ISSN: 0956-540X. DOI: 10. 1093/gji/ggt495.

Matsubara, Makoto and Kazushige Obara (2011): "The 2011 off the Pacific coast of Tohoku Earthquake related to a strong velocity gradient with the Pacific plate", Earth, Planets and Space, 63(7), 663–667.

Matsubara, M., Sato, H., Ishiyama, T. & Horne, A. Van. (2017a): "Configuration of the Moho discontinuity beneath the Japanese Islands derived from three-dimensional seismic tomography", Tectonophysics, 710-711, 97–107. ISSN:00401951.

DOI: 10.1016/j.tecto.2016.11.025.

Matsubara, Makoto et al. (2017b): "Seismic Velocity Structure in and around the Japanese Island Arc Derived from Seismic Tomography Including NIED MOWLAS Hi-net and S-net Data", Seismic Waves - Probing Earth System. IntechOpen. DOI:10.5772/intechopen.86936.

Mckenzie, D. and M. J. Bickle (1988): "The Volume and Composition of Melt Generated by Extension of the Lithosphere", Journal of Petrology, 29(3), 625–679. ISSN: 0022-3530. DOI: 10.1093/petrology/29.3.625.

Miyashiro, Akiho (1986): "Hot regions and the origin of marginal basins in the western Pacific", Tectonophysics, 122(3), 195–216. ISSN:0040-1951.

Montenbruck, Oliver and Eberhard Gill (2000): Satellite Orbits. Springer Berlin Heidelberg. ISBN:978-3-540-67280-7.

Motavalli-Anbaran, S. H., Zeyen, H., and Ardestani, V. E. (2013). 3D joint inversion modeling of the lithospheric density structure based on gravity, geoid and topography data—Application to the Alborz Mountains (Iran) and South Caspian Basin region. Tectonophysics, 586, 192-205.

Nakajima, Junichi and Akira Hasegawa (2007a): "Subduction of the Philippine Sea plate beneath southwestern Japan: Slab geometry and its relationship to arc magmatism", Journal of Geophysical Research, 112 (B8), B08306. ISSN: 0148-0227. DOI: 10.1029/2006JB004770.

Nakajima, Junichi and Akira Hasegawa (2007b): "Tomographic evidence for the mantle

upwelling beneath southwestern Japan and its implications for arc magmatism", Earth and Planetary Science Letters, 254(1), 90–105. ISSN: 0012-821X. DOI: https://doi.org/10.1016/j.psl.2006.11.024.

Nakajima, Junichi, Toru Matsuzawa, and Akira Hasegawa (2002): "Moho depth variation in the central part of northeastern Japan estimated from reflected and converted waves", Physics of the Earth and Planetary Interiors, 130(1-2), 31–47. ISSN: 00319201. DOI: 10.1016/S0031-9201(01)00307-7.

Nakamura, H., Iwamori, H., Nakagawa, M., Shibata, T., Kimura, J.-I., Miyazaki, T., Chang, Q., et al. (2019): "Geochemical mapping of slab-derived fluid and source mantle along Japan arcs", Gondwana Research, 70, 36–49. ISSN: 1342-937X. DOI:https://doi.org/10.1016/j.gr.2019.01.007.

Nakamura, K. (1983): "Possible nascent trench along the eastern Japan Sea as the convergent boundary between Eurasian and North American plates", Bulletin of the Earthquake Research Institute, University of Tokyo, 58, 711–722.

Nixon, P. H. (1987): Mantle xenoliths. United States. URL: https://www.osti.gov/biblio/5699888.

Okamura, Y., Watanabe, M., Morijiri, R. and Satoh, M. (1995): "Rifting and basin inversion in the eastern margin of the Japan Sea", The Island Arc, 4(3), 166–181. ISSN: 1038-4871. DOI: 10.1111/j.1440-1738.1995.tb00141.x.

O'Reilly, Suzanne Y. and W.L. Griffin (2013): "Moho vs crust–mantle boundary: Evolution of an idea", Tectonophysics, 609, 535–546. ISSN: 00401951. DOI: 10.1016/j.tecto.2012.12.031.

O'Reilly, S.Y. and W.L. Griffin (2006): "Imaging global chemical and thermal heterogeneity in the subcontinental lithospheric mantle with garnets and xenoliths: Geophysical implications", Tectonophysics, 416 (1-4), 289–309. ISSN: 00401951. DOI: 10.1016/j.tecto.2005.11.014.

Otofuji, Yo-ichiro and Takaaki Matsuda (1984): "Timing of rotational motion of Southwest Japan inferred from paleomagnetism", Earth and Planetary Science Letters, 70(2), 373–382.

Otofuji, Yo-ichiro, Takaaki Matsuda, and Susumu Nohda (1985): "Paleomagnetic evidence for the Miocene counter-clockwise rotation of Northeast Japan—rifting process of the Japan Arc", Earth and Planetary Science Letters, 75(2-3), 265–277.

O'Reilly, Suzanne Y. and W. L. Griffin (2010): "Rates of magma ascent: Constraints from mantle-derived xenoliths", Timescales of magmatic processes: From core to atmosphere, 1803799613, 116–124.

Park, J.-O., Tokuyama, H., Shinohara, M., Suyehiro, K. and Taira, A. (1998): "Seismic record of tectonic evolution and backarc rifting in the southern Ryukyu island arc system", Tectonophysics, 294(1-2), 21–42. ISSN: 00401951. DOI: 10.1016/S0040-1951(98)00150-4.

Perinelli, C., Bosi, F., Andreozzi, G.B., Conte, A.M. & Armienti, P. (2014): "Geothermometric study of Cr-spinels of peridotite mantle xenoliths from northern Victoria Land (Antarctica)", American Mineralogist, 99(4), 839–846.

Rabbel, Wolfgang, Mikhail Kaban, and Magdala Tesauro (2013): "Contrasts of seismic velocity, density and strength across the Moho", Tectonophysics, 609, 437–455. ISSN: 00401951. DOI: 10.1016/j.tecto.2013.06.020.

Rathnayake, S., Tenzer, R., Chen, W., Eshagh, M. & Pitoňák, M. (2021): "Comparison of Different Methods for a Moho Modeling Under Oceans and Marginal Seas: A Case Study for the Indian Ocean", Surveys in Geophysics, 42(4), 839–897. ISSN: 0169-3298. DOI: 10.1007/s10712-021-09648-2.

Reguzzoni, M., Sampietro D. , and Sanso`, F. (2013): "Global Moho from the combination of the CRUST2.0 model and GOCE data", Geophysical Journal International, 195(1), 222–237. ISSN: 0956-540X. DOI: 10.1093/gji/ggt247.

Reguzzoni, Mirko and Sampietro, Daniele (2012): "Moho Estimation Using GOCE Data: A Numerical Simulation", Geodesy for Planet Earth. Ed. by Steve Kenyon, Maria Christina Pacino, and Urs Marti. Berlin, Heidelberg, Springer Berlin Heidelberg, 205–214. ISBN: 978-3-642-20338-1.

Rummel, R., Balmino, G., Johannessen, J., Visser, P. & Woodworth, P. (2002): "Dedicated gravity field missions—principles and aims", Journal of Geodynamics, 33(1-2), 3–20.

Sakuyama, Masanori (1977): "Lateral variation of phenocryst assemblages in volcanic rocks of the Japanese islands", Nature, 269 (5624), 134–134. ISSN: 0028-0836. DOI: 10.1038/269134a0.

Sakuyama, Masanori (1979): "Lateral variations of H2O contents in quaternary magmas of

Northeastern Japan", Earth and Planetary Science Letters, 43(1), 103–111. ISSN:0012821X. DOI:10.1016/0012-821X(79)90159-6.

Sampietro, Daniele, Mirko Reguzzoni, and Carla Braitenberg (2014): The GOCE Estimated Moho beneath the Tibetan Plateau and Himalaya. Berlin, Heidelberg, Springer Berlin Heidelberg, 391–397. ISBN: 978-3-642-37222-3.

Sato, Hiroshi (1994): "The relationship between Late Cenozoic tectonic events and stress field and basin development in northeast Japan", Journal of Geophysical Research: Solid Earth, 99(B11), 22261–22274. ISSN: 01480227. DOI: 10.1029/94JB00854.

Satsukawa, T., Godard, M., Demouchy, S., Michibayashi, K. & Ildefonse, B. (2017): "Chemical interactions in the subduction factory: New insights from an in situ trace element and hydrogen study of the Ichinomegata and Oki-Dogo mantle xenoliths (Japan)", Geochimica et Cosmochimica Acta, 208, 234–267.

Sebera, J., Šprlák, M., Novák, P., Bezděk, A., & Vaľko, M. (2014): Iterative spherical downward continuation applied to magnetic and gravitational data from satellite. Surveys in Geophysics, 35(4), 941-958.

Shin, Young Hong et al. (2007): "Moho undulations beneath Tibet from GRACE-integrated gravity data", Geophysical Journal International, 170(3), 971–985.

Shiomi, Katsuhiko, Kazushige Obara, and Haruo Sato (2006): "Moho depth variation beneath southwestern Japan revealed from the velocity structure based on receiver function inversion", Tectonophysics, 420(1-2), 205–221. ISSN: 00401951. DOI: 10.1016/j.tecto.2006. 01.017.

Sibuet, J. C., Deffontaines, B., Hsu, S. K., Thareau, N., Le Formal, J. P., & Liu, C. S. (1998). Okinawa trough backarc basin: Early tectonic and magmatic evolution. Journal of Geophysical Research: Solid Earth, 103(B12), 30245-30267.

Silva, J. B. C., D. F. Santos, and K. P. Gomes (2014): "Fast basement relief inversion", Geophysics, 79(5), 79–91.

Sobh, M., Ebbing, J., Mansi, A. H., G̈otze, H., Emry, E. L., and Abdelsalam, M. G. (2020): The Lithospheric Structure of the Saharan Metacraton From 3-D Integrated Geophysical-Petrological Modeling. Journal of Geophysical Research: Solid Earth, 125(8).

Sobh, M., Ebbing, J., Mansi, A. H., and G̈otze, H.-J. (2019): Inverse and 3D forward gravity modelling for the estimation of the crustal thickness of Egypt. Tectonophysics,

752:52–67.

Song, T. A. (2003): "Large Trench-Parallel Gravity Variations Predict Seismogenic Behavior in Subduction Zones", Science, 301(5633), 630–633. ISSN: 0036-8075.

Steffen, Rebekka, Holger Steffen, and Gerhard Jentzsch (2011a): "A three-dimensional Moho depth model for the Tien Shan from EGM2008 gravity data", Tectonics, 30(5).

Sugimura, A. and S. Uyeda (2013): Island Arcs: Japan and Its Environs, Amsterdam: Elsevier Science, 256. ISBN: 1483256936, 9781483256931.

Sugiyama, Y. (1994): "Neotectonics of southwest Japan due to the right-oblique subduction of the Philippine Sea plate", Geofisica Internacional, 33, 53–76.

Szwillus, Wolfgang, Jö¨rg Ebbing, and Nils Holzrichter (2016a): "Importance of far-field topographic and isostatic corrections for regional density modeling", Geophysical Journal International, 207(1), 274–287. ISSN: 0956-540X. DOI: 10.1093/gji/ggw270.

Taira, Asahiko (2001): "Tectonic Evolution of the Japanese Island Arc System", Annual Review of Earth and Planetary Sciences, 29(1), 109–134. ISSN: 0084-6597.

Takahashi, E. (Dec. 1978): "Petrologic model of the crust and upper mantle of the Japanese Island arcs", Bulletin Volcanologique, 41(4), 529–547. ISSN: 0258-8900.

Takahashi, Eiichi (1975): "Finding of spinel-Lherzolite Inclusions in Oki-Dogo Island, Japan", The Journal of the Geological Society of Japan, 81(2), 81–83. DOI: 10.5575/geosoc.81.81.

Takahashi, M (1999): "Large felsic magmatism of the Miocene outerzone of southwest Japan", Earth Monit. Spec., 23, 160–168.

Takahashi, Masaki (2006a): "Tectonic boundary between Northeast and Southwest Japan Arcs during Japan Sea opening", The Journal of the Geological Society of Japan, 112(1), 14–32. DOI: https://doi. org/10.5575/geosoc.112.14.

Takahashi, Masaki (2006b): "Tectonic development of the Japanese Islands controlled by Philippine Sea Plate motion", Journal of Geography (Chigaku Zasshi), 115(1), 116–123. DOI: https://doi.org/10.5026/jgeography.115.116.

Tamaki, Kensaku and Eiichi Honza (1985): "Incipient subduction and deduction along the eastern margin of the Japan Sea", Tectonophysics, 119(1-4), 381–406. ISSN: 00401951. DOI: 10.1016/0040-1951(85)90047-2.

Tamaki, K., Suyehiro, K., Allan, J., Ingle, J. C., & Pisciotto, K. A. (1992). 83. Tectonic synthesis and implications of Japan Sea ODP drilling. In Proceedings of the Ocean Drilling Program, scientific results (No. part 2, pp. 1333-1348).

Tenzer, Robert and Wenjin Chen (2019): "Mantle and sub-lithosphere mantle gravity maps from the LITHO1.0 global lithospheric model", Earth-Science Reviews, 194, 38–56. ISSN:0012-8252.

Tenzer, Robert, K. Hamayun, and Peter Vajda (2009): "Global maps of the CRUST 2.0 crustal components stripped gravity disturbances", Journal of Geophysical Research, 114(B5), B05408. ISSN:0148-0227. DOI:10.1029/2008JB006016.

Tenzer, R., Chen, W., Tsoulis, D., Bagherbandi, M., Sj¨oberg, L. E., Nov´ak, P., and Jin, S. (2015). Analysis of the Refined CRUST1.0 Crustal Model and its Gravity Field. Surveys in Geophysics, 36(1):139–165.

Tsuchiya, N (1990): "Middle Miocene back-arc rift magmatism of basalt in the NE Japan arc", Chishitsu Chosajo Geppo (Bulletin of the Geological Survey of Japan);(in Japanese), 41(9), 73－505.

Tsuru, T., Park, J.-O., Takahashi, N., Kodaira, S., Kido, Y., Kaneda, Y., and Kono, Y. (2000). Tectonic features of the Japan Trench convergent margin off Sanriku, northeastern Japan, revealed by multichannel seismic reflection data. Journal of Geophysical Research: Solid Earth, 105(B7):16403–16413.

Tugume, F., Nyblade, A. A., Julia, J., and van der Meijde, M. (2013). Crustal shear wave velocity structure and thickness for archean and proterozoic terranes in africa and arabia from modeling receiver functions, surface wave dispersion, and satellite gravity data. Tectonophysics, 609:250–266.

Uieda, Leonardo and Vale´ria C. F. Barbosa (2016): "Fast nonlinear gravity inversion in spherical coordinates with application to the South American Moho", Geophysical Journal International, 208(1), 162–176. ISSN: 0956-540X.

van der Meijde, M., Pail, R., Bingham, R., and Floberghagen, R. (2015). Goce data, models, and applications: A review. International Journal of Applied Earth Observation and Geoinformation, 35:4–15. GOCE earth science applications and models(Based on the ESA GOCE solid earth workshop, 16-17 October 2012).

Van Horne, Anne, Hiroshi Sato, and Tatsuya Ishiyama (2017): "Evolution of the Sea of Japan

back-arc and some unsolved issues", Tectonophysics, 710-711, 6–20. ISSN: 00401951. DOI: 10.1016/j.tecto.2016.08.020.

Von Huene, R. and S. Lallemand (1990): "Tectonic erosion along the Japan and Peru convergent margins", Geological Society of America Bulletin, 102(6), 704–720. ISSN: 00167606.

Wei, Dongping and Tetsuzo Seno (1998): "Determination of the Amurian plate motion", Mantle Dynamics and Plate Interactions in East Asia, Geodyn. Ser., ed. SL Flower, C Chung, T Lee, American Geophysical Union, 337–346. DOI: 10.1029/GD027p0337.

Wei, W., Xu, J., Zhao, D., and Shi, Y. (2012). East Asia mantle tomography: New insight into plate subduction and intraplate volcanism. Journalof Asian Earth Sciences, 60:88–103.

Wood, B and S Banno (1973): "Garnet-orthopyroxene and orthopyroxene-clinopyroxene relationships in simple and complex systems." Contr. Mineral. and Petrol., 42(2), 109–124, https://doi.org/10.1007/BF00371501.

Xuan, Songbai, Shuanggen Jin, and Yong Chen (2020). "Determination of the isostatic and gravity Moho in the East China Sea and its implications", Journal of Asian Earth Sciences, 187, 104098. ISSN: 1367-9120.

Yao, Y., Huang, D., Yu, X., and Chai, B. (2016). Edge interpretation of potential field data with the normalized enhanced analytic signal.Acta Geodaetica et Geophysica, 51(1):125–136.

Zhao, Dapeng (2015): "The 2011 Tohoku earthquake (Mw 9.0) sequence and subduction dynamics in Western Pacific and East Asia", Journal of Asian Earth Sciences, 98, 26–49. ISSN:13679120. DOI:10.1016/ j.jseaes.2014.10.022.

Zhao, Dapeng (2021). "Seismic imaging of Northwest Pacific and East Asia: New insight into volcanism, seismogenesis and geodynamics", Earth-Science Reviews, 214, 103507. ISSN:0012-8252.